In compliance with the
Canadian Privacy Legislation
some supporting forms
may have been removed from
this dissertation.

While these forms may be included
in the document page count,
their removal does not represent
any loss of content from the dissertation.

The propagation and failure mechanism of gaseous detonations: experiments in porous-walled tubes

by
Matei I Radulescu

Department of Mechanical Engineering
McGill University
Montreal, Quebec, Canada

February 2003

A thesis submitted to the
Faculty of Graduate Studies and Research
In partial fulfillment of the requirements for the degree of
Doctor of Philosophy
in
Mechanical Engineering

Your file Votre référence
ISBN: 0-612-88563-1
Our file Notre référence
ISBN: 0-612-88563-1

Abstract

In order to elucidate the propagation mechanism of detonations, the failure mechanism of detonations propagating in tubes with porous walls is investigated experimentally. Two distinct failure mechanisms were identified depending on the type of detonating mixture. Experiments in mixtures characterized by piecewise laminar reaction zone structures with weak three-dimensional effects revealed that the attenuation and failure is caused by the global mass divergence to the porous, permeable walls. The limits observed in these mixtures agreed very well with the theoretical limiting conditions for the existence of curved ZND detonations subjected to lateral expansions.

Experiments were also conducted in a second class of mixtures, characterized by irregular cellular structures and turbulent reactions zones. When detonations in this class of mixtures are attenuated, transverse waves re-amplify from local instabilities in the reaction zone. This re-amplification permits the detonation wave to continue to propagate and overcome the effects of global mass divergence and transverse wave attenuation at the porous walls. Ultimately, when the rate of transverse wave re-generation is surpassed by the rate of transverse wave damping at the walls, the detonation can no longer be self-sustained and fails. The limits obtained in these irregular structure mixtures were found significantly wider than predicted by the ZND formulation, thus further confirming the important role of the three-dimensional turbulent structure in these detonations in providing a more efficient mechanism of gas ignition and propagation than detonations that exhibit a regular structure.

The implications of the present study are that the ZND model is not valid in describing the reaction zone structure, the ignition mechanism and thus the propagation mechanism in these turbulent detonations. In these mixtures, the ignition mechanism is a combination of the classical mechanism of adiabatic shock compression leading to ignition as well as the intense turbulent mechanism usually attributed to deflagrations only.

Résumé

Afin d'élucider le mécanisme de propagation des détonations gazeuses, nous avons étudié le mécanisme d'atténuation et extinction des détonations se propageant dans des tubes dont le mur est poreux. Deux différents mécanismes ont été identifiés. Dans les mélanges caractérisés par des zones de réaction laminaires et des effets tri-dimensionnels faibles, l'extinction est due aux expansions globales engendrées par le mur perméable. Les limites déterminées expérimentalement sont en excellent accord avec les limites théoriques qui permettent l'existence de détonations de type ZND courbées.

Pendant l'atténuation des détonations caractérisées par des zones de réaction turbulentes, des ondes de choc transversales provenant des instabilités dans la zone de réaction se re-amplifient continuellement, permettant de nier l'effet des expansions globales et de l'atténuation des ondes transversales par le mur poreux. Quand le taux d'atténuation des ondes transversales devient supérieur à celui de re-amplification, la détonation ne peut plus être entretenue et s'éteint. Les limites obtenues dans ces mélanges sont beaucoup plus larges que les prédictions basées sur le modèle ZND, ce qui confirme le rôle important de la turbulence qui permet un mécanisme d'allumage plus efficace.

Les implications de mes travaux sont donc que le modèle ZND n'est pas valide pour la description de la zone de réaction, du mode d'allumage et donc du mécanisme de propagation des détonations turbulentes. Dans ces mélanges, le mécanisme d'allumage est une combinaison du mécanisme classique d'auto-allumage par la compression des ondes de choc frontales (de type ZND) et du mécanisme de transport turbulent attribué normalement aux déflagrations seulement.

Acknowledgements

I would like to thank my thesis supervisor John Lee for his guidance, interest and encouragements during my degree. I would also like to thank Andrew Higgins for his continuous interest in my research, useful discussions and for meticulously proofreading my manuscript. The following people, whom I would like to thank, also contributed directly or indirectly to the completion of my thesis:

my family for their continuous support,

Hoi Dick Ng for discussions on detonation wave stability and help with the numerical aspects of this work,

Vincent Tanguay for continuous discussions, valuable criticisms, insights and suggestions on all the aspects of my work, and for teaching me the fundamentals of poker,

Aena Santella for the thesis survival kit and continuous support during the last stages of the thesis writing and re-writing,

Jenny Chao for proofreading preliminary versions of my manuscript,

Gary Sharpe, Shaun Lovejoy, and Laurent Mydlarski for related and apparently unrelated discussions,

Joseph Shepherd for his healthy skepticism,

Marianne Huot and Nils Tilton for their help with the damping experiments and schlieren visualization set-up,

the entire Shock Wave Physics Group at McGill for their continuous support and encouragements,

and the Fonds de Recherche FCAR for financial support during the course of my degree and NSERC for supporting fundamental research in detonation physics.

Lastly, I would like to thank Professors Forman Williams, David Frost, Laurent Mydlarski, Andrew Higgins, Meyer Nahon, Harry Lam, Luca Cortelezzi and James Nemes for serving as examiners on my thesis committees and making very useful suggestions.

Table of contents

List of figures

List of tables

Chapter 1 Introduction

1.1 Overview

It is well known that real detonation waves in general exhibit a complex three-dimensional cellular structure. The multi-dimensional effects manifest themselves as a complex of transverse shocks interacting with the leading shocks, shear layers and combustion regions near the triple point interactions (Lee, 1984). However, the various physical mechanisms of gas ignition and the origin and self-sustenance of the three-dimensional shock structure are poorly understood and lack a theoretical treatment. This is due primarily to the complexity of the phenomenon and to the great difficulty in conducting measurements in such a transient reaction structure, where three-dimensional gasdynamic effects are strongly coupled with the fast chemical kinetics.

In the present thesis, the objective is to contribute to the understanding of the various mechanisms that are responsible for the cellular structure of gas detonations, and in particular to address the question why gas detonations display such a complicated three-dimensional structure.

Since the cellular structure of the detonation waves was discovered in the late 50's (Voitsekhovskii et al., 1958), it became clear that more insight on the detonation propagation mechanism can be gained by studying the response of the detonation wave to strong perturbations of its cellular structure (e.g., Mitrofanov & Soloukhin, 1965, Strehlow & Salm, 1976). Direct measurements of undisturbed detonations remain very difficult to conduct even with modern experimental diagnostics (Shepherd et al., 2002) and are usually limited to the analysis of the gross features appearing on soot foils (Schelkin & Troshin, 1965, Strehlow & Biller, 1969, Shepherd et al. 2002). In general, external perturbations to the detonations are best studied experimentally by observing how the detonation structure disintegrates near the failure limits or is formed under favorable initiation conditions. Near the failure or the initiation limits, the dynamics of the disintegration or formation of the detonation wave can operate on larger spatial scales than usually encountered in detonations propagating far from the limit (Radulescu et al., 2002, Lee et al., 1995). Thus, observation of the wave

dynamics near the failure limit or under critical initiation conditions provides an experimental "magnifying glass" for studying the underlying mechanisms of detonation propagation. Furthermore, when a detonation is brought to marginal near-failure or initiation conditions, it is the most vulnerable to external stimuli and thus most easily studied. For these reasons, we anticipate that the complexity of the detonation propagation mechanism can be reduced near its limits, since the wave would only survive quenching or initiate under the most severe conditions via its most efficient propagation mechanism.

The methodology of this thesis follows this strategy of systematically studying the failure and initiation of gas detonations. Since meaningful conclusions can only be achieved if the external effects which bring the detonation close to its failure or initiation conditions are easily quantifiable, the present study uses porous wall tubes, which permit evaluation of the losses originating from the mass leakage through the wall of the permeable tubes. This boundary condition permits determination of the global rate of mass divergence leading to net mass, momentum and energy deficits in the reaction zone and the rate of attenuation of transverse shocks reflecting on the porous structure. These quantifiable losses permit further analytical modeling, so as to complement the conclusions reached from experimental observations.

1.2 Previous studies on detonation failure and limits

1.2.1 Limits in smooth tubes

Much work has been devoted to the study of marginal detonations and detonability limits in smooth wall detonation tubes, which arise when the tube diameter becomes comparable with the average characteristic transverse wave spacing of the mixture λ (Manson et al., 1963, Dupré et al., 1986, Edwards & Morgan, 1977, Saint-Cloud et al, 1972, Lee et al, 1995, Manzhalei, 1992). As the limits are approached, say for the same mixture propagating in tubes with smaller diameters, transverse waves become increasingly stronger (Edwards & Morgan, 1977) and the detonation wave in general exhibits increasing instabilities, broadening by more than an order of magnitude the spectrum of length scales

characterizing the detonation wave dynamics (Lee et al., 1995). The detonability limits were found to scale well with the average transverse wave spacing (Dupré et al., 1986, 1991).

At the limits in smooth tubes, galloping detonations are observed: the detonation wave quasi-periodically re-amplifies from local instabilities and further disintegrates into a fast turbulent flame due its inability to sustain its growing cell structure in narrow tubes (Edwards & Morgan, 1977). The onset of the acceleration phase is marked by a fine-scale pattern of interacting transverse waves, which later grows and decays in the narrow tubes. These observations indicate that the fine-scale three-dimensional transverse wave structure may play an important role in the re-initiation of detonations near marginal conditions.

However, it was also found that detonations diluted by an inert gas, such as argon or helium, which display much more regular cell structures with weak three-dimensional effects (Strehlow et al., 1967), do not exhibit any galloping regime in smooth tubes (Haloua et al., 2000, Lee et al., 1995, Edwards & Morgan, 1977). The detonation limits in such mixtures characterized by regular cell structures are also significantly narrower than in mixtures where a galloping regime is possible (Dupré et al., 1991). These experimental observations suggest that the galloping regime, and the associated three-dimensional small-scale activity during the re-amplification stages of the galloping cycle, permit the detonation wave self-sustenance under more stringent conditions. This also indirectly suggests that the cell regularity and strength of the three-dimensional structure can be influential on the failure and re-initiation mechanism of detonations near the limits in smooth tube walls.

Although much insight can be gained from such near-limit detonation experiments in smooth tubes, the study of the wave dynamics becomes difficult since very small and/or extremely long tubes are required to observe the pulsating phenomena (Haloua et al., 2000, Manzhalei, 1992). These pulsations are usually recorded by microwave interferometry methods, which measure the dynamics of the entire combustion front across the cross-section of the tube (Edwards & Morgan, 1977, Lee et al., 1995, Haloua et al., 2000). Hence the resolution is

limited only to the large pulsations of the wave occurring on sufficiently long length scales. Due to the difficulty in observing these detonations over typical lengths of thousands of tube diameters, photographic observations are also very difficult to implement.

Furthermore, since the limits are usually observed when there is less than a detonation cell across the tube, the influence of the walls, apart from not permitting a self-sustained cell structure to "fit" in the tube, are also likely to introduce mass, momentum and heat losses due to the walls boundary layers (Fay, 1959). The boundary layers also permit dissipation of turbulent acoustic energy by the interaction of pressure waves in the reaction zone with the denser gas near the walls. These further complications cannot be neglected from any theoretical treatment of the problem. For this reason, experiments on near-critical behavior in narrow, smooth tubes only provide limited answers on the propagation mechanism of detonations.

1.2.2 The critical tube diameter

The failure of detonation waves has also been extensively studied by perturbing the detonation as it encounters an abrupt area change (Mitrofanov and Soloukhin, 1965, Edwards et al., 1979, Lee 1996), i.e., the so-called "critical tube diameter" problem. A recent comprehensive survey of the phenomenon can be found in (Lee, 1996). Close inspection of the cellular structure measured via smoke foils or open shutter photographs revealed that detonation cellular structure disintegrates at the abrupt area divergence due to the combined action of gasdynamic expansions originating from the unconfined sides and the absence of inward running transverse waves, which can no longer maintain the cellular structure. An open-shutter photograph taken by Vasil'ev (Lee, 1996) in the two-dimensional analog of the critical tube diameter problem illustrating this process is shown in Fig. 1.1. This photograph records the trajectory of the luminous triple points (intersections between transverse waves and leading shock front), as the detonation propagates from left to right. At criticality, following the lateral expansions and attenuation of the cellular structure, a few re-initiation centers originate from weakened triple points and re-establish the detonation wave.

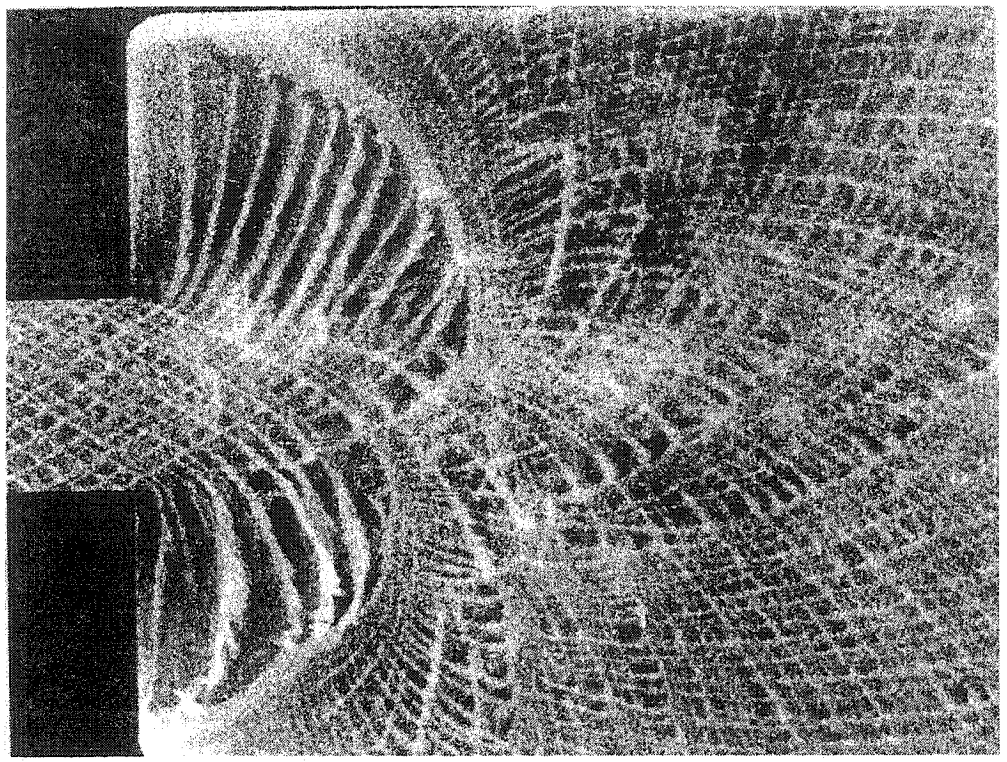

Fig. 1.1 Critical flowfield for diffraction of a $C_2H_2 + 2.5O_2$ detonation (from Lee, 1996)

Since successful or unsuccessful transmissions at a sudden area change are unambiguously determined, much work was conducted in a wide variety of detonation systems for determining the critical conditions for failure (e.g., Knystautas et al., 1982). For typical systems, a unique correlation was found relating the critical tube diameter d_{CT} to the average transverse wave spacing, or *cell size*, λ, yielding $d_{CT} \approx 13\lambda$ (Lee, 1984). These observations, although not yet validated by a theoretical treatment, indicate that the cell spacing provides a unified scaling in various mixtures, implying the importance of the cellular structure dynamics in detonations.

However, it was found that this universal correlation for the diffraction problem breaks down for detonations displaying regular cellular structures and weak transverse waves (Moen et al., 1986, Shepherd et al. 1986, Desbordes et al., 1993). In these special cases, the limit is found to be approximately 2 to 3 times higher (i.e., $d_{CT} \approx 30\lambda$). The flow field observed experimentally during the

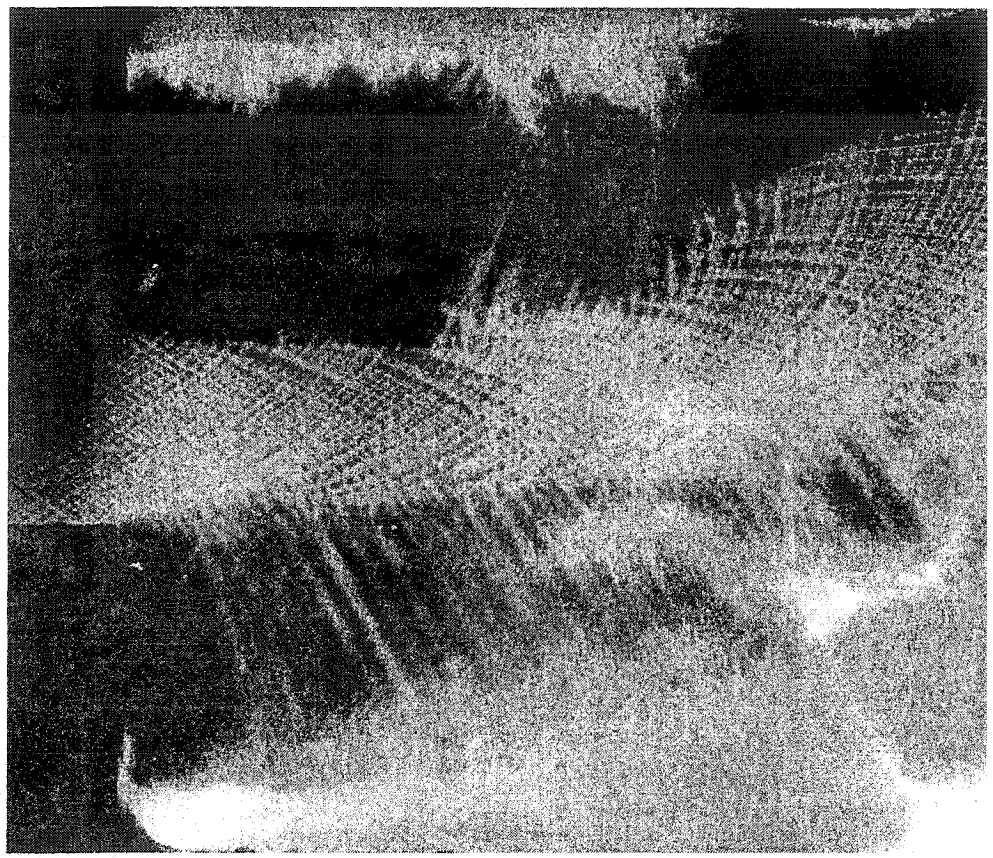

Fig. 1.2 Critical flowfield for diffraction of a C_2H_2 + $2.5O_2$ + 85% Ar detonation (from Lee, 1996)

diffraction process in the two-dimensional channel geometry is also substantially different than for the irregular structure detonations (Lee, 1996). An example is shown in Fig. 1.2, obtained for oxy-acetylene detonations diluted with 85% argon. The open shutter photograph shown in Fig. 1.2 indicates that the attenuation process is more gradual and devoid of the local re-amplifications of transverse waves observed for the undiluted mixture (Fig. 1.1). The cellular structure gradually increases near the core while the rest of the wave is extinguished. These observations led Lee (1996) to conclude that the weaker transverse waves in such diluted systems do not actively participate during the attenuation process, and the detonations fail mainly from lateral expansions, which impart a slowly evolving curvature to the leading front.

It thus appears that differences in the failure mechanism of detonations in the critical tube problem can be correlated with the regularity in the cell structure,

as was also observed for detonability limits in smooth tubes. Although at present there is no clear explanation for these observations, the diffraction experiments appear to shed further light on the failure mechanism of detonations for regular and irregular detonation structures.

1.2.3 Limits in deformable or permeable tubes

To further elucidate the response of detonation waves to perturbations in its structure, experiments were also conducted in deformable tubes, where the degree of net lateral divergence of the flow can be controlled by the choice of the confining material (Dabora et al., 1965, Murray & Lee, 1984, 1986, Vasil'ev et al., 1972). In principle, such experiments permit the study of detonations in quasi-steady attenuated states over length scales more appropriate for detailed investigations of their dynamics. However, previous studies only concentrated in determining the limits between propagating and failing detonations and in empirically correlating the observed limits with the magnitude of area divergence (Murray & Lee, 1986). Murray, for example, attempted to correlate the detonation limits obtained in thin-walled plastic tubes with the magnitude of the area divergence. He used the quasi-one-dimensional Fay-Dabora model for weakly divergent detonations, which relates the lateral mass divergence, or nozzle flow, with the detonation velocity deficit and the detonation thickness (Fay, 1959, Dabora et al., 1965). Assuming an arbitrary critical velocity deficit below which reactions are quenched and taking the cell size λ as the characteristic reaction thickness, he obtained relative success in correlating his experimental limits and velocity deficits with the model's predictions. However, little insight was gained from only comparing the predictions of a highly empirical model with the experimental limits obtained in deformable tubes, where the lateral losses also depend in a non-trivial way on the thickness and dynamic properties of the confining material (Murray and Lee, 1984, Dabora et al., 1965, Dabora & Broda, 1993).

Further experiments of Dupré (Dupré et al., 1988) performed in porous wall tubes permitted an alternate means of controlling the lateral losses. The porous wall tube permits to control both the mass divergence through the

permeable wall pores and the attenuation of the transverse shocks reflecting on it. In the experiments, a short section of the tube was lined by a porous material, such as multiple layers of metallic wire mesh. However, the authors did not attempt to measure the details of the attenuation process nor the structure of the attenuated waves and only sought the critical conditions under which the detonation is damped inside the porous wall section. They found a unique correlation for critical damping relating the porous wall tube diameter d^* to the transverse wave spacing λ of the detonable mixtures, yielding approximately $d^* / \lambda \approx 4$ in various hydrocarbon-oxygen detonations with some discrepancies in hydrogen-oxygen mixtures. These limits are much larger than in smooth tube walls, thus revealing the great ability of the porous walls in damping detonations.

Less extensive studies with porous wall tubes were carried out by Teodorczyk & Lee (1995), Vasil'ev (1994) and Guo et al. (2002) in round and square tubes with relatively short attenuation sections of a few tube diameters. In the square tube geometry, two transparent opposing walls were used in order to visualize the attenuation process by the Schlieren technique. However, due to the large distance between the two transparent walls (a few detonation cells), the visualization of the attenuation process was masked by integrating through the three-dimensional details of the reaction zone structure and did not permit the flow field to be clarified.

Although the experimental technique of using a porous wall tube is promising, the previous studies completely neglected the effect of net lateral mass divergence that arises from the leaky boundary condition. Instead, only the transverse wave attenuation mechanism from porous tube walls was considered in their interpretation of their results, and the damping results were solely interpreted in view of this assumed mechanism. This lead to the conclusion that transverse waves are essential to the detonation wave propagation, since detonations failed when the transverse waves were removed. However, the validity of the conclusions is questionable since the global mass divergence mechanism could give rise to detonation failure even in the hypothetical limit of ZND-type detonations devoid of any transverse waves. In fact, it would be impossible to

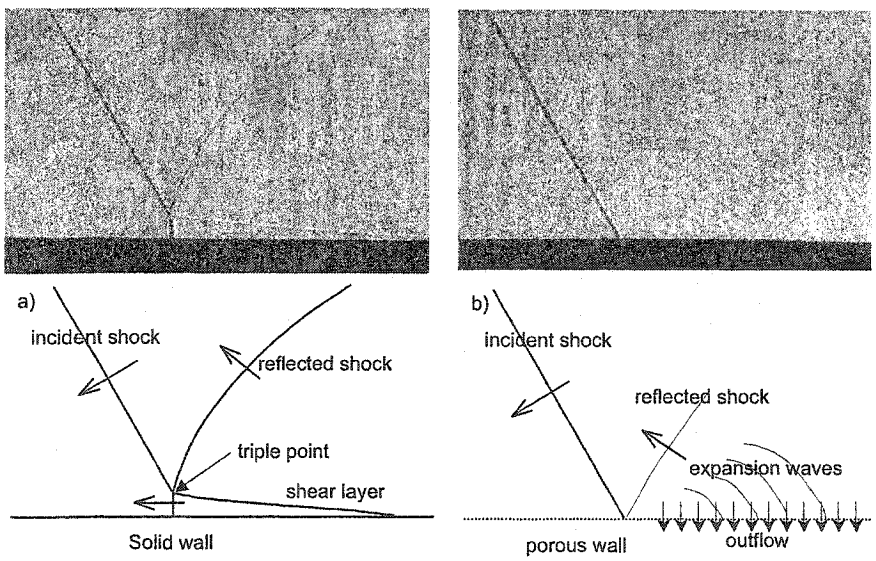

Fig. 1.3 Photographs illustrating the reflection of an incident oblique shock (a), on a solid wall, and (b), on a porous foam wall, taken from (Kobayashi et al., 1993)

isolate the transverse wave attenuation mechanism only, since it is exactly the fact that mass can leak through the pores of the tube that leads to weaker reflected shocks and damping of the detonation's triple point shock interactions. For example, Fig.1.3 shows the reflection of an oblique shock in air on solid and porous walls (Kobayashi et al., 1993). The mass sink at the porous wall leads to lower pressures behind the reflected shock, which is now weaker, and to the disappearance of the triple point configuration. The same mechanism is likely to operate in detonations alike, where the triple points are attenuated and incident pressure waves are weakened.

However, in the hypothetical one-dimensional limit, when triple point interactions are not present, global mass leakage leads to mass, momentum and energy transport out of the reaction zone, would generate expansion waves penetrating in the reaction zone. If the amount of mass divergence, and hence the magnitude of the expansions are too severe, the detonations can quench. This scenario thus approaches Vasil'ev's and Murray's interpretations (Vasil'ev et al. 1972, Murray & Lee, 1986) for their yielding confinement experiments where failure is accounted for by global mass divergence only.

In reality, both the attenuation of transverse waves and the global net mass divergence are likely to operate simultaneously in both the porous wall experiments and yielding confinement experiments of Murray. For meaningful conclusions to be reached, a careful examination of the various phenomena is thus required, which can only be achieved through careful examination of the different assumptions and flowfields during the attenuation process. Hence, for meaningful conclusions to be obtained, the respective roles of the global mass divergence and transverse wave attenuation mechanisms need to be carefully re-evaluated.

1.3 Outline of the present study

The porous wall technique appears to be the most practical and suitable technique to monitor the changes in the detonation structure due to losses at the tube boundaries and hence study the propagation mechanism of detonations. Although the transverse wave attenuation mechanism and the global mass divergence mechanism are linked, the porous walls yield quantifiable boundary conditions, through the known porosity of the walls, and offer an effective means to attenuate detonation waves. This is unlike the deformable wall experiments, where the limited material deformation leads to significantly less attenuation (Vasil'ev, 1994). Also, experiments in long porous-walled tubes provide the possibility to study attenuated detonations propagating at a steady velocity deficit. This is unlike the "critical tube diameter" diffraction experiments, where the attenuation and failure is a highly transient phenomenon. Experiments in porous walled tubes would thus permit to treat the attenuated detonations as stationary: it would permit to model theoretically the detonation attenuation in porous walled tubes with steady state models of attenuated reaction zone structures.

Hence, the present study presents a detailed investigation of the attenuation or failure of detonations propagating in long sections of porous walled tubes, such that the detonation dynamics can be monitored. Anticipating that transverse wave strength and cell regularity may play an influential role in the failure mechanism of detonations in porous wall tubes, as indirectly indicated by the previous near-limit experiments discussed above, a wide range of mixtures are investigated displaying different levels of cell regularity, ranging from "excellent"

such in oxy-hydrogen-argon mixtures to "highly irregular" mixtures such as oxy-propane or oxy-methane (Strehlow, 1969). To overcome difficulties encountered in the two-dimensional square-channel configuration, the majority of the tests are performed in circular tubes lined with porous material. The attenuation process inside the porous walled section of the tube is monitored via streak photography. These experiments are presented in Chapter 2. Tests are also performed in rectangular cross section tubes with porous walls placed only on two opposing sides, the two other walls permitting flow visualization (schlieren and open shutter photographs) of the flow field during the attenuation process. These results are presented in Chapter 3. Different aspect ratios of the rectangular cross-section are investigated in order to study the importance of the inherent three-dimensional detonation wave structure in the two-dimensional attenuation geometry.

In Chapter 4, the attenuation and failure results are compared to a theoretical model where only the effect of mass divergence is included. Under the simplifying assumptions of steadiness and one-dimensionality of the wave, exact relations can be derived involving the critical wave curvature induced by lateral mass divergence that will permit self-sustenance of a curved ZND wave (see Klein, 1994 for review). This will thus permit the validity of the simplifying assumption to be verified and thus gauge the importance of the transverse wave structure in the various detonation systems investigated. The results of this theoretical treatment are presented in Chapter 4, followed by discussions on detonations wave stability, conclusions on the actual mechanism of propagation of real detonations and a tentative answer to the rather naïve original questions "*how detonations work*?" and "*why do detonation waves display such a complex system of interacting transverse waves*?"

Chapter 2 Failure of detonations in porous wall tubes

2.1 Overview

In the present chapter are reported the experimental results on the failure of detonations propagating in tubes with porous walls. Following the entrance of a fully developed detonation wave into a porous wall section of the tube, the dynamics of the detonation wave are monitored via self-luminous streak photography and the critical conditions for detonation damping are determined for a wide range of mixtures characterized by a broad range of cellular regularity.

2.2 Experimental set-up

The tube experiments were performed in a 4.8-m-long acrylic round tube, 51 mm internal diameter. A sketch of the experimental set-up is shown in Figure 2.1. The mixtures were ignited by a 1-J electric spark from the discharge of a capacitor bank. A 0.5-m long wire spiral placed near the igniter was used to promote the rapid formation of a self-sustained detonation. The damping section was always located approximately 3 meters downstream of the end of the spiral. Four different damping sections were used. They consisted of a single porous wall tube or a bundle of multiple porous-wall tubes of smaller diameter. The porous-walled sections were introduced inside the smooth wall tube (see Fig. 2.1). The configurations of the porous wall sections are shown in Fig. 2.2. The experiments performed in the multiple porous wall tube bundles permitted generalizing the conclusions to porous wall tubes of different diameters. The porous tube walls were made of 14 layers of tightly rolled steel mesh. This number of layers was chosen after ensuring that the damping limits separating successful transmission and detonation failure were independent of the number of layers of the tube wall, provided that at least 10 layers were used.

The steel mesh used had 4 wires per millimeter, each wire of a diameter of 0.114 mm. The resulting open area ratio of the walls was 30%. This same porous material was used throughout the experiments. The configuration where most of the results were obtained was the single porous wall tube configuration. This permitted the highest resolution for the experimental measurements inside the

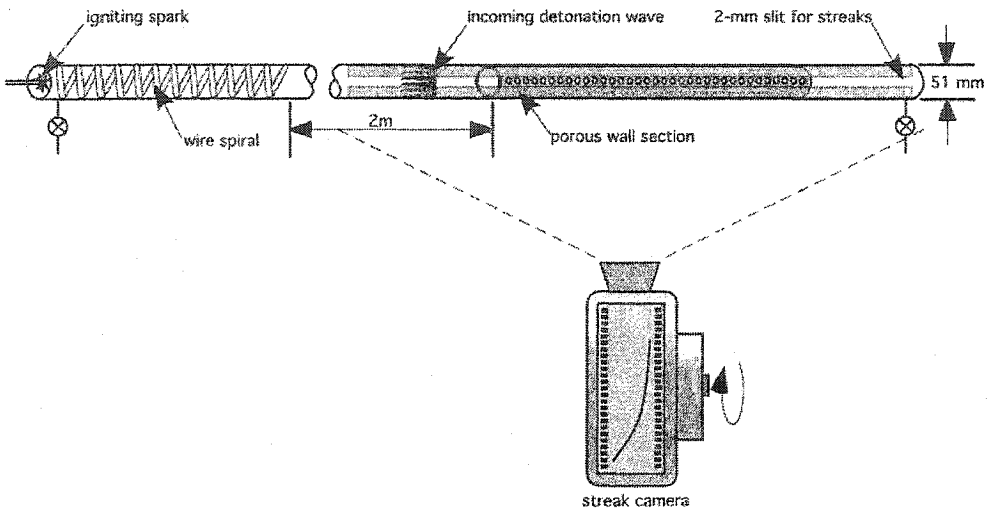

Fig. 2.1 Schematic of experimental set-up for detonation damping in porous-walled tubes

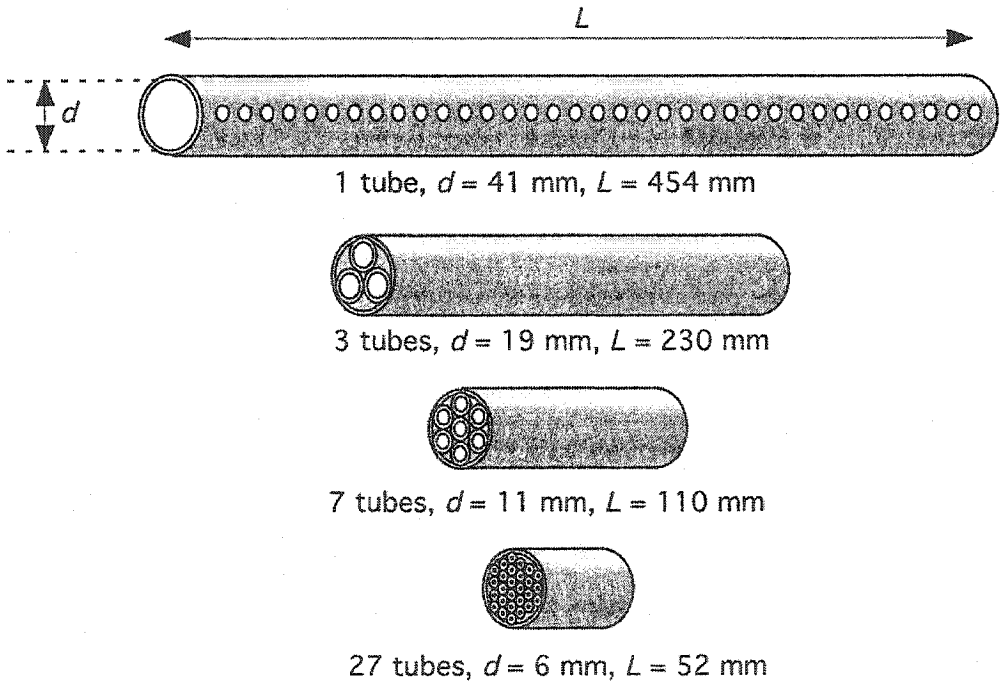

Fig 2.2 Different configurations of the porous-walled damping section

porous wall tube. In order to detect light emission inside the porous wall tube and hence permit high-speed photography of the combustion wave propagation, 2 mm holes equally spaced at 5 mm intervals were drilled through the porous wall (see Fig. 2.2). Preliminary tests with and without the visualization holes determined

that their presence did not alter the observed limits. The experiments were monitored by streak photographs of the luminous detonation. This permitted recording the velocity of the detonation (or deflagration) inside the damping section, and in the smooth tube sections before and after the damping section. A rotating drum streak camera was used with a constant film velocity of approximately 80 m/s. Kodak T-Max 400 film was used for the streak photographs. The streak photographs were digitally scanned and processed through an image analysis software. The velocity measurements from the streak photographs were estimated with ~2% accuracy. In certain experiments, a Mylar sheet coated with soot was also placed at the end of the smooth tube to record the cellular structure of the detonation. For these experiments, the porous wall section was removed. In all experiments, a piezoelectric PCB pressure transducer (113A31) with a typical rise time of 1 μsec was placed before the damping section as to record the pressure signature of the incoming self-sustained detonation to ensure that a fully established CJ detonation was obtained.

The fuels investigated were hydrogen (H_2), propane (C_3H_8), methane (CH_4) and acetylene (C_2H_2). Various dilutions with argon (Ar) or nitrogen (N_2) were investigated in the acetylene-oxygen and hydrogen-oxygen systems. This

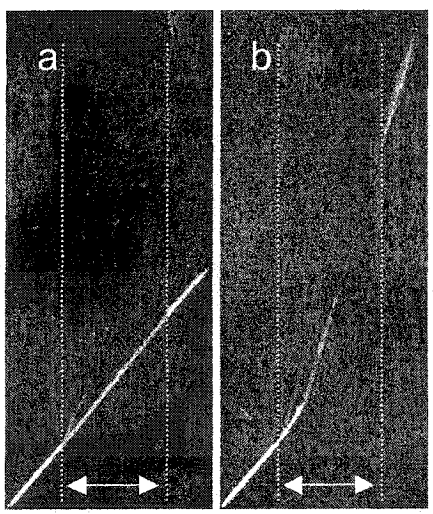

Fig. 2.3 Self-luminous streak photographs of a C_2H_2 + $2.5O_2$ detonation attenuation in the d = 41 mm porous walled section: *a*), P_o = 2.5 kPa, and *b*) P_o =1.7 kPa; time axis is vertical increasing upwards, arrow indicates length of porous walled section

permitted investigating mixtures characterized by large differences of cell regularity. The methane and propane mixtures are characterized by very irregular cell structures (Strehlow, 1969). Undiluted acetylene mixtures exhibit irregular cell structures, with increasing regularity with increasing argon dilution (Shepherd et al., 1986, Vandermeiren & Van Tiggelen, 1984). The argon-diluted hydrogen detonations offer the best regularity, with a slight loss of regularity for undiluted and nitrogen diluted mixtures (Strehlow, 1969). The gases were obtained from commercial cylinders. The desired mixture was prepared before an experiment in a separate vessel. The gases were allowed to mix for a minimum of 24 hours. The detonation tube was evacuated before an experiment to pressures less than 0.07 kPa, and the mixture was introduced through both ends of the tube at the desired initial pressure. The sensitivity of a given mixture composition was controlled via the initial pressure (rather than mixture composition), with an accuracy of 0.05 kPa. The concentrations of the various gases were determined by the method of partial pressures.

2.3 Results in acetylene-oxygen-argon detonations

2.3.1 Failure limits

Typical streak photographs obtained in a mixture of stoichiometric acetylene-oxygen are shown in Figure 2.3. These streak records can be interpreted as an *x-t* diagram, the vertical axis representing time. The reciprocal of the slope of the trajectory of the luminous combustion front represents its average wave velocity. In the first streak record shown, one can see that the incoming detonation is only slightly attenuated in the test section to a lower velocity and re-covers its original velocity upon exit in the smooth wall section. Below a critical pressure, the detonation wave fails in the porous wall tube. This is unambiguously seen on the streak records, such as Fig 2.3b, where the abrupt failure of the detonation wave to approximately 40% of its original velocity occurs inside the porous wall section.

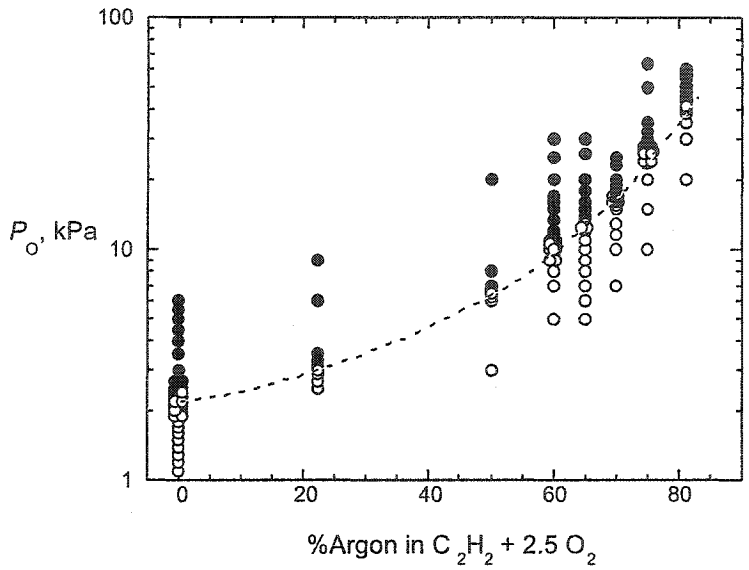

Fig 2.4 Summary of successful transmission experiments (●) and detonation failure experiments (○) in C_2H_2 + 2.5O_2 + %Ar in the 41-mm porous-walled tube

A summary of the critical pressures separating successful transmission from failure in the porous wall tubes in acetylene-oxygen mixtures with various amounts of argon dilution is shown in Fig. 2.4. Repeat experiments are shown to provide a measure of the reproducibility of the results. It is however more instructive to present the same results as a function of a parameter representing mixture sensitivity. To this effect, following convention, the experimentally measured cell size λ is used (Lee, 1984). The variation of λ with initial pressure for the different argon dilutions is shown in Fig. 2.5. The resulting power-law best-fit correlations between cell size and initial pressure are given in Table 2.1 for the data shown in Fig. 2.5. Values of λ are taken from the literature (Desbordes et al., 1986, 1988, 1993, Edwards et al., 1978, Manzhalei et al., 1974, Laberge et al., 1993, Knystautas et al., 1982, Strehlow et al., 1967), with the exception of the mixtures diluted with 60, 65, and 70 % argon, which were measured in the present study by the smoke foil technique in separate experiments in the solid wall tube. Since the relevant length scale governing the magnitude of

Table 2.1 Cell size correlations for $C_2H_2 + 2.5O_2 + \%Ar$ as a function of argon dilution given by $\lambda[\text{mm}] = C(P_o\,[\text{kPa}])^{-\alpha}$

$C_2H_2 + 2.5O_2 + \%Ar$	C	α
0% Ar	28.7	1.26
22% Ar	39.6	1.21
50% Ar	61.5	1.12
60% Ar	75.3	1.22
65% Ar	93.1	1.20
70% Ar	113.8	1.20
75% Ar	152.0	1.15
81% Ar	367	1.23

the side losses is the porous tube diameter *d*, we chose the non-dimensional parameter (d / λ) as the measure of the sensitivity of the mixture with respect to the magnitude of the attenuating conditions. This parameter represents the competition between the fast energy release rate at the detonation front, characterized by λ, to the losses to the tube walls, governed by the tube diameter *d*.

Figure 2.6 shows the variation of the critical damping limit (d / λ)* for oxy-acetylene detonations as a function of the argon dilution. For the undiluted mixture, a critical value of (d / λ)* $\approx$ 4 is achieved. For large argon dilutions, the limits approach a much higher value of approximately (d / λ)* $\approx$ 11. It is also interesting to note that the dependence of the limits on the amount of argon dilution is a not a smoothly increasing function, but instead displays a distinctive step-like transition near approximately 60% argon dilution. It is interesting to note however that the limit pressure changes smoothly with argon dilution (Fig. 2.4). The step transition in (d / λ)* is thus due to changes of the cell size λ with argon dilution. Whether this change is due to dynamic or kinetic effects, and the implication of this observation is further discussed in Chapter 5.

To further verify the validity of our scaling failure criterion (d / λ)* for a given argon dilution, supplementary experiments in various porous tube sizes

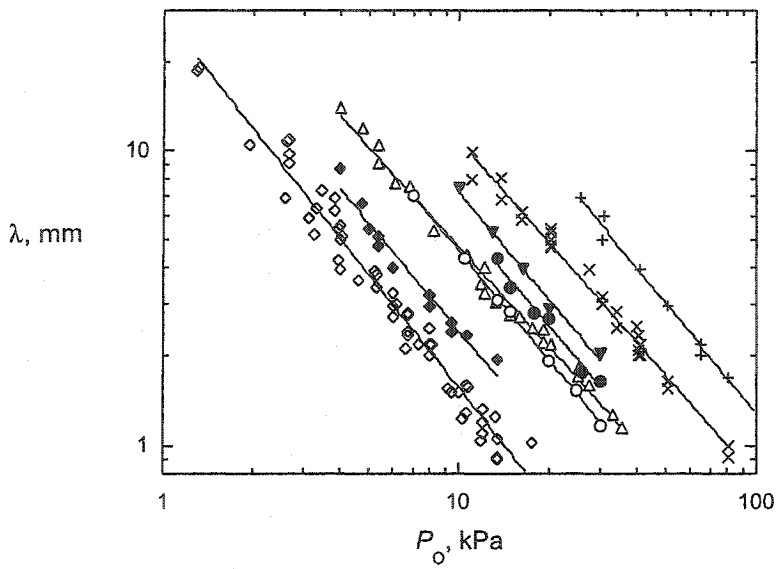

Fig 2.5 Cell width variation in $C_2H_2 + 2.5O_2 + \%Ar$ with initial pressure for 0%Ar (◇), 22%Ar (◆), 50%Ar (△), 60%Ar (○), 65%Ar (●), 70%Ar (▼), 75%Ar (×), and 81% Ar (+) (see text for references)

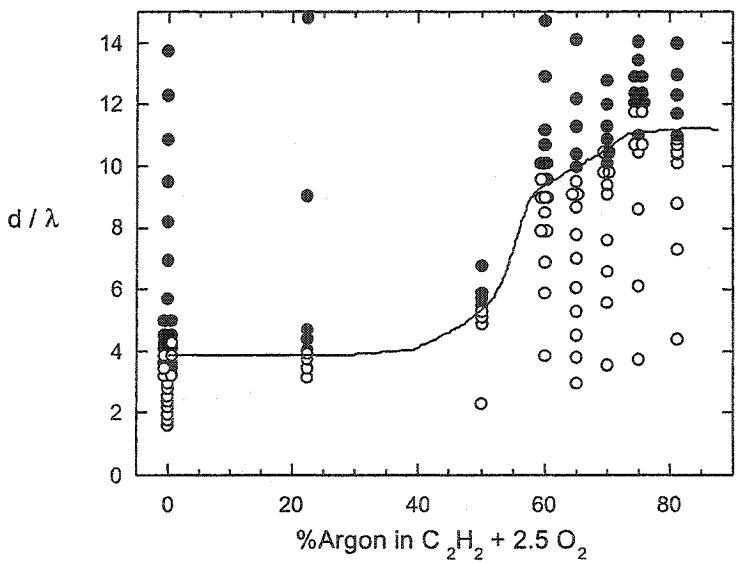

Fig 2.6 Summary of successful transmission experiments (●) and failure experiments (○) in $C_2H_2 + 2.5O_2 + \%Ar$ in the 41-mm porous-walled tube in terms of (d / λ)

were carried out. The tubes were such that the length to diameter ratio was

maintained at the same value. The results obtained for two representative mixtures, namely undiluted and 75% argon diluted acetylene-oxygen detonations, are shown in Fig. 2.7. Clearly, the limits $(d / \lambda)^*$ do not change with geometry scaling (tube diameter), thus confirming the validity of our scaling criterion for each respective mixture.

The large increase in the damping limit for high argon dilutions suggests that these detonations are more susceptible to failure in the porous wall tubes for the same mixture sensitivity (same cell size λ). This is in accord with diffraction and direct initiation experiments, which revealed that the limits are significantly higher for argon-diluted acetylene-oxygen detonations (Desbordes et al., 1993). It is also interesting to note that the critical argon dilution separating the two limits (~60%Ar) corresponds to the limit between regular and irregular cell structures. Highly regular cells were observed above ~60% argon (Shepherd et al., 1986, Vandermeiren & Van Tiggelen, 1984), while detonations below this argon dilution exhibited irregular cells. It is thus tempting to make the correlation between the irregularity in the detonation structure and the different damping limits observed. As previously noted by Moen and Lee, detonations characterized by a more irregular cell structure and stronger transverse waves are more robust and difficult to damp than regular structure detonations with weak transverse waves.

2.3.2 Detonation velocity dependence on attenuation

The streak photographs also permitted to gain further quantitative insight into the failure mechanism of the different mixtures in the porous wall tubes. The velocity of the incoming detonation waves in the smooth section (V_{smooth}), the velocity of the attenuated detonation, and the velocity of the failed detonation wave were all measured from the streak records. The velocity of the detonations in the smooth tube sections were found to agree within experimental accuracy to the Chapman-Jouguet (CJ) detonation velocity, computed with the CEA chemical equilibrium code (Gordon & McBride, 1994). The velocities of the attenuated detonations in the porous wall tube section were measured once they acquired a steady velocity inside the porous wall section. The velocity of the failed

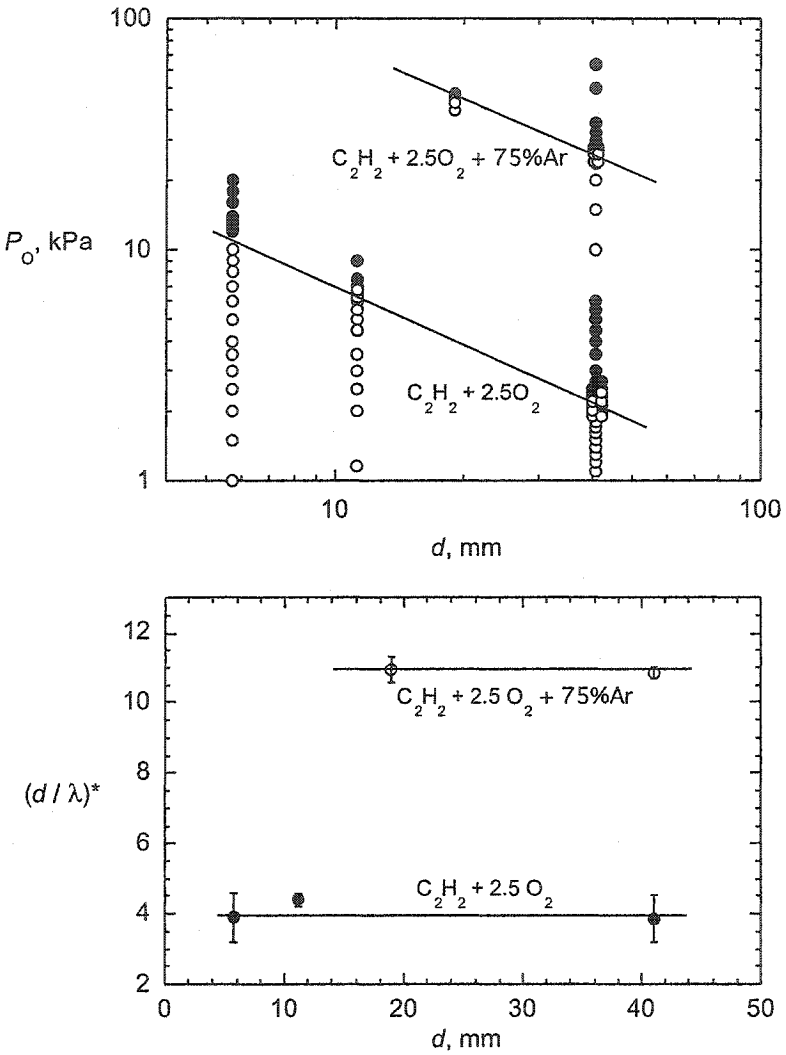

Fig. 2.7 Summary of successful transmission experiments (●) and failure experiments (O) in $C_2H_2 + 2.5O_2$ and $C_2H_2 + 2.5O_2$+ 75%Ar as a function of porous wall tube diameter (*a*), and variation of the critical damping limit $(d / \lambda)^*$ in the two mixtures (*b*)

detonation was more difficult to measure in some cases, due to the lower luminosity of the deflagration wave. This was especially the case for the mixtures diluted with a significant amount of argon. In these cases, the deflagration was estimated by tracking the point where detonation fails and the point where the

luminous front corresponding to the combustion products exits the porous wall section. The so-obtained velocities of the attenuated steady detonations or deflagrations propagating in the 41-mm porous wall tube are shown in Fig. 2.8, normalized by the measured velocity in the smooth section of the tube.

The general trend obtained from the velocity deficits shown in Fig. 2.8 is that as limits are approached (smaller d / λ), the influence of the losses to the porous wall tubes is more significant and the velocity deficit increases. At criticality, a velocity deficit of approximately 20% is observed. However, one can observe two different diameter dependences as a function of argon dilution. For dilutions greater than approximately 60% argon, it appears that the velocity deficits are significant even far from the limits. On the other hand, undiluted and 22% argon dilutions experiments reveal a very small velocity deficit away from the limits. As a quantitative criterion, the velocity deficit measured at twice the limit (i.e. $(d / \lambda) = 2\ (d / \lambda)^*$) is approximately 1-2% for the low dilution mixtures and greater than 10% for the dilutions above 60%. These results indicate that detonations diluted with argon are more influenced by the attenuating conditions near the walls, while the undiluted mixtures are not. Similar trends were observed by Moen et al. (1986) in their study of the dependence of the detonation velocity on the diameter of smooth tubes for regular and irregular structure mixtures. It thus appears that mixtures characterized by irregular cell structures are more robust and permit the detonation to overcome the attenuating effects of the porous walls.

2.3.3 Attenuation rates

The streak photographs also provide some interesting observations regarding the dynamics of the detonation waves inside the porous wall section of the tube. It was found that for the mixtures diluted with large amount of argon dilution, the attenuation rate inside the porous wall section was significantly slower than in the non-diluted mixtures. Figure 2.9 shows two typical photographs obtained near the limits for an undiluted and 75% argon diluted oxy-acetylene mixture. For the 75% argon diluted mixtures shown, one can note the long transient before the wave fails just before the exit of the porous wall section.

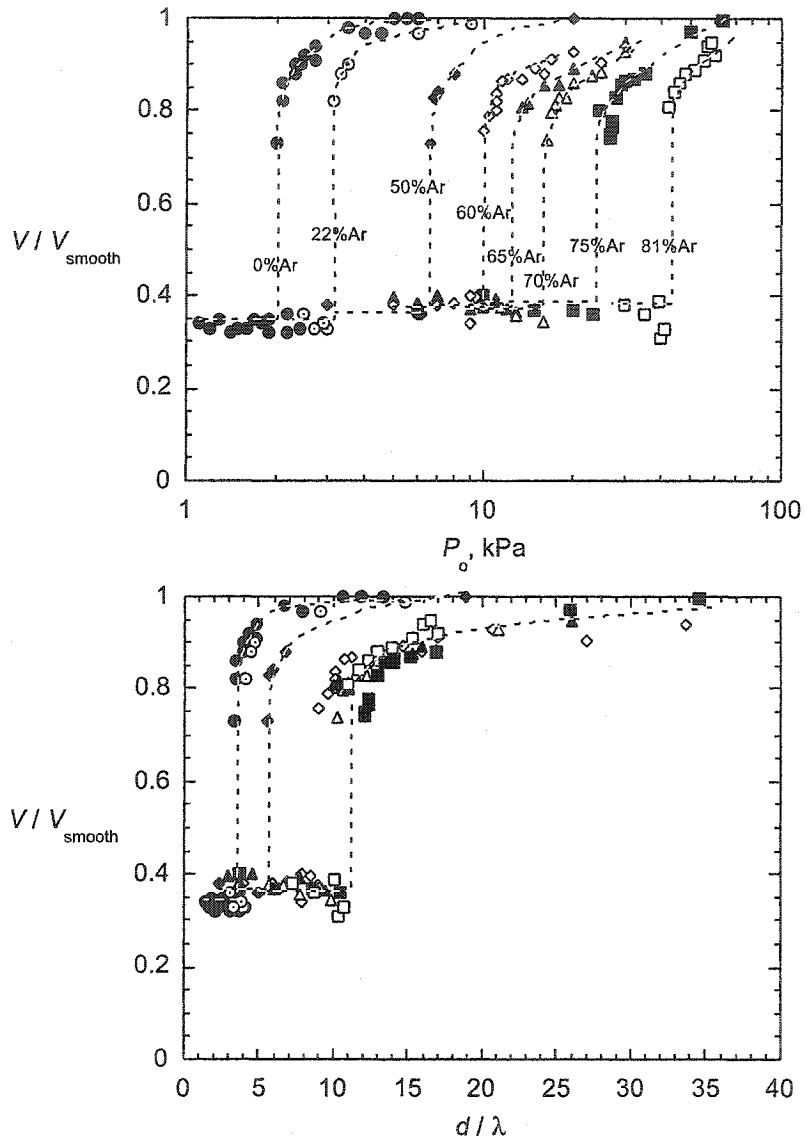

Fig. 2.8 Detonation wave velocity deficits in the 41-mm porous wall tubes in $C_2H_2 + 2.5O_2 +$ %Ar mixtures as a function of *a*), initial mixture pressure, and *b*), as a function of (d / λ)

On the other hand, for the undiluted mixture, failure occurs very rapidly, within approximately two tube diameters. This failure length provides a measure of the characteristic decay rate of the detonation inside the porous wall section. Measurements of the failure length, as obtained from the streak photographs, are

shown in Figure 2.10, as obtained from the experiments in the 41-mm porous wall tube. For a more accurate representation of the real attenuation length scale that leads to failure of the detonations, the failure length x_f is measured from the point where the first expansion wave reaches the tube axis (i.e.,

$$x_e = \frac{V_{CJ}}{a_{CJ}} \frac{d}{2} \approx d \qquad 2.1$$

where V_{CJ} is the CJ detonation velocity and a_{CJ} is the sonic velocity in the detonation products) to the point where the wave fails. This failure distance is indicative of the real distance the detonation wave travels after the presence of the attenuating walls is first "felt" at the tube axis. The results are normalized by λ, and shown in terms of the parameter (d / λ) to measure the proximity to the damping limit.

From the results of Fig. 2.10, it can be seen that the failure length in argon diluted detonations is a strong (exponential) function on (d / λ). As the losses are alleviated by increasing (d / λ), the effect of the attenuating walls takes significantly more time to damp the detonations, suggesting a mechanism that operates slowly on long time scales.

On the other hand, for the undiluted and low dilution mixtures, the failure length is approximately a constant value of approximately 3-7λ. However, some deviations from the constant value of 3-7λ are observed close to the limits for the undiluted mixtures. Close inspection of the streak photographs near failure for the undiluted mixtures reveals that the wave undergoes a series of quasi-periodic pulsations before failure. A typical streak photograph displaying this phenomenon is shown in Fig. 2.11. The number of pulsations was in general non-reproducible, ranging from only one or two to several pulsations observed over the entire propagation of the detonation in the porous wall section. The average velocity of these near limit pulsating detonations before failure was approximately $0.75V_{CJ}$. These pulsations were not observed in the mixtures diluted with large amounts of argon.

The differences in attenuation rates observed experimentally are very similar to the differences noted by Lee for detonation diffraction experiments in

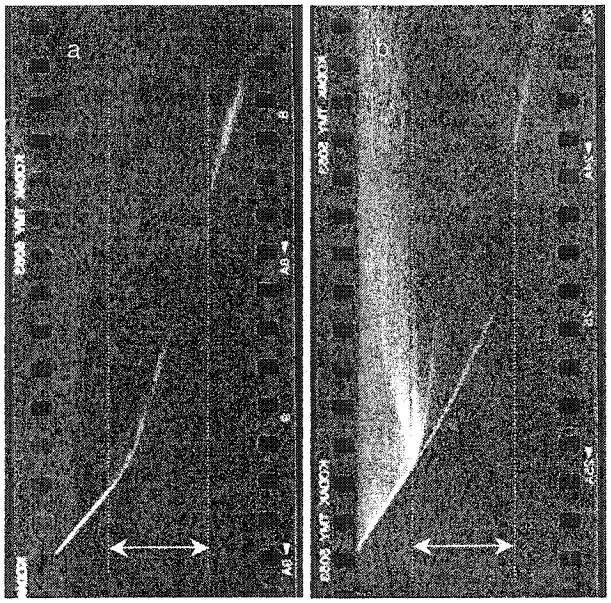

Fig. 2.9 Streak photographs illustrating detonation damping in *a*), $C_2H_2 + 2.5O_2$, 2.2kPa, and *b*) $C_2H_2 + 2.5O_2 + 75\%Ar$, 24kPa

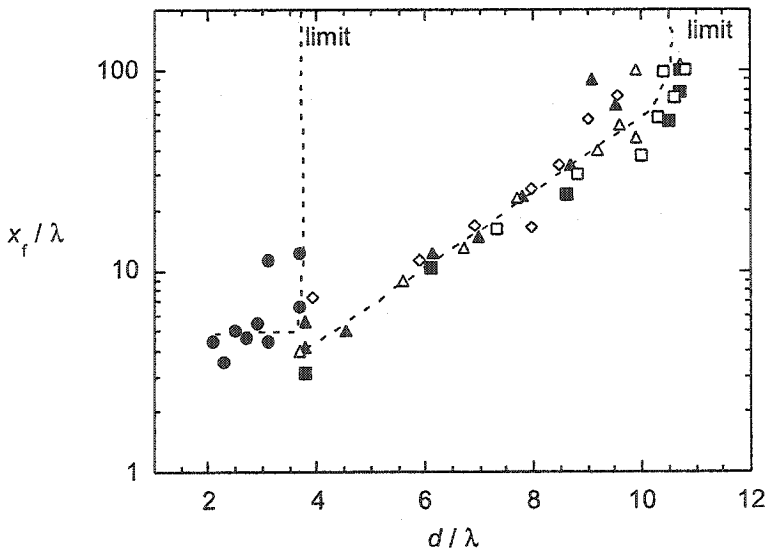

Fig 2.10 Normalized failure length for $C_2H_2 + 2.5O_2 + \%Ar$ detonations in the 41-mm porous-walled tube (symbols same as Fig. 2.8)

undiluted and highly argon diluted acetylene-oxygen detonations (Lee, 1996), as

discussed in the Introduction. Similar to the diffraction experiments, it thus appears that the attenuation of the highly argon diluted mixtures follows a global phenomenon involving the slow distribution of the frontal wave curvature, imposed by the global expansions generated by the mass divergence into the porous walls. This long transient is consistent with the theoretical predictions of Bdzil & Stewart (1986) for the penetration of the failure wave into a ZND detonation subjected to lateral mass divergence.

The failure of the undiluted detonations is however much more rapid, and thus is more closely governed to local quenching of the detonation structure. The mechanism suggested in (Dupré et al., 1988) of transverse wave attenuation near the porous wall can be a plausible cause of the sudden failure in these irregular cell mixtures. However, these interpretations remain to be verified through further experiments elucidating the flowfield details of the attenuation process.

2.4 Propane and methane detonations

The same tests were also performed in stoichiometric oxy-methane and oxy-propane mixtures. These mixtures are characterized by very irregular cell structure (Strehlow, 1969). The velocity deficits measured from the streak photographs in the 41-mm tube for these two mixtures are shown in Figure 2.12. To express the limiting pressures in terms of the scaling parameter (d / λ), the cell measurements of (Pedley et al., 1988, Knystautas et al., 1982, Laberge et al., 1993) were used, shown in Fig. 2.13. The cell size correlations with initial mixture pressure for oxy-propane and oxy-methane mixtures are respectively

$$\lambda[\text{mm}] \cong 230(P_o[\text{kPa}])^{-1.27} \qquad 2.2$$

$$\lambda[\text{mm}] \cong 996(P_o[\text{kPa}])^{-1.28} \qquad 2.3$$

The normalized velocities of the detonations in the porous wall tubes are shown in terms of the scaling ratio (d / λ) in Fig. 2.14. The first conclusion that can be reached is that the limits in both mixtures is $(d / \lambda)^* \approx 4$, the same as obtained in the acetylene-oxygen mixture. Furthermore, the velocity deficits far from the limits are small, similar to the conclusion obtained from the undiluted acetylene-oxygen mixtures. The critical velocity deficit observed in both mixtures is approximately 30%. For these near-critical waves obtained close to the

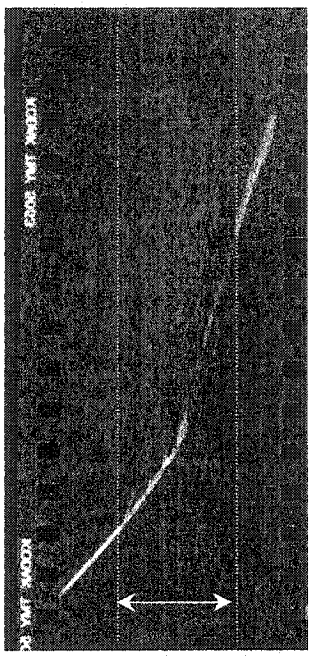

Fig 2.11 Near-limit pulsating phenomena in $C_2H_2 + 2.5O_2$ detonations in the 41-mm porous walled tube, $P_o = 1.9$kPa

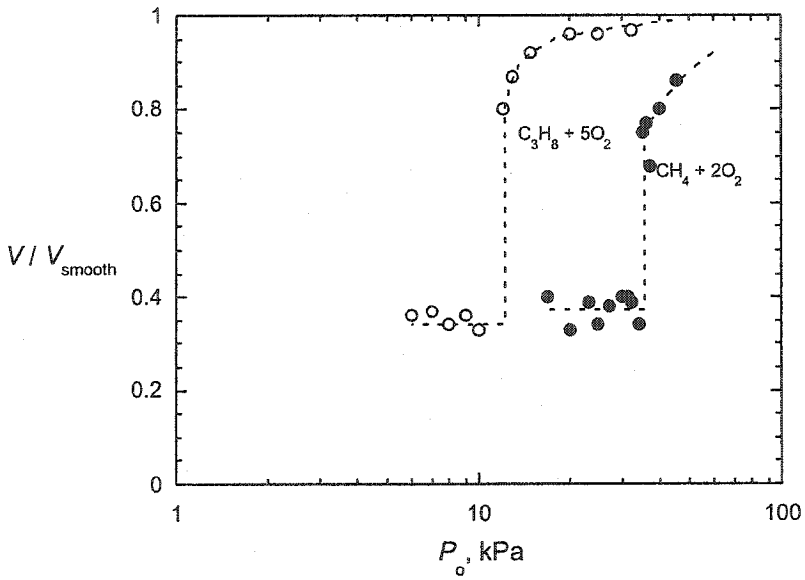

Fig 2.12 Detonation wave velocity deficits in the 41-mm porous wall tubes in $C_3H_8 + 5O_2$ and $CH_4 + 2O_2$ detonations as a function of initial mixture pressure

damping limit, a pulsating wave is observed in the streak photographs, as shown

in Figure 2.15 for a near-limit oxy-methane mixture. The pulsations are quasi-periodic and occur approximately every 7λ, as was observed for the acetylene-oxygen mixtures. However, they are more pronounced for methane mixtures, where the streaks indicate quasi-periodic failure and re-initiation of the detonation wave.

For the mixtures that failed in the porous wall tube, the failure length was also measured as outlined above. The results for these two mixtures are shown in Figure 2.16. Also shown for comparison are the results obtained above for stoichiometric oxy-acetylene. The same failure length is observed for all three mixtures, approximately 4 to 7λ.

In conclusion, the attenuation and failure mechanism in propane and methane mixtures is very similar to what was observed for oxy-acetylene mixtures above. The same limit of $(d / \lambda)^* \approx 4$ is observed, the failure length is a constant of approximately 4 to 7λ, which also corresponds to the length of pulsations observed near criticality. Similarly to the acetylene-oxygen mixtures, and unlike the highly argon diluted ones, the velocity deficits far from the limits are small, suggesting the ability of these detonations to negate the losses at the tube walls.

2.5 Hydrogen-oxygen-argon-nitrogen mixtures

Similar tests were also performed in the stoichiometric hydrogen-oxygen mixtures, undiluted or diluted with 40% argon or 25% nitrogen. These mixtures are characterized by weak transverse waves and regular cell patterns (Strehlow, 1969, Shepherd et al., 2002). For these mixtures, it was found that the visible self-emission was significantly lower than in the hydrocarbon systems. For this reason, only the detonations could be unambiguously monitored inside the porous wall section via self-luminous streak photographs.

The velocity deficits obtained in undiluted stoichiometric oxy-hydrogen and oxy-hydrogen diluted by 25%N_2 or 40%Ar are shown in Figure 2.17. To reduce the velocity dependence on the scaling parameter (d / λ), the cell size data of (Kaneshige, 1999, Barthel, 1974, Knystautas et al., 1982, Manzhalei et al.,

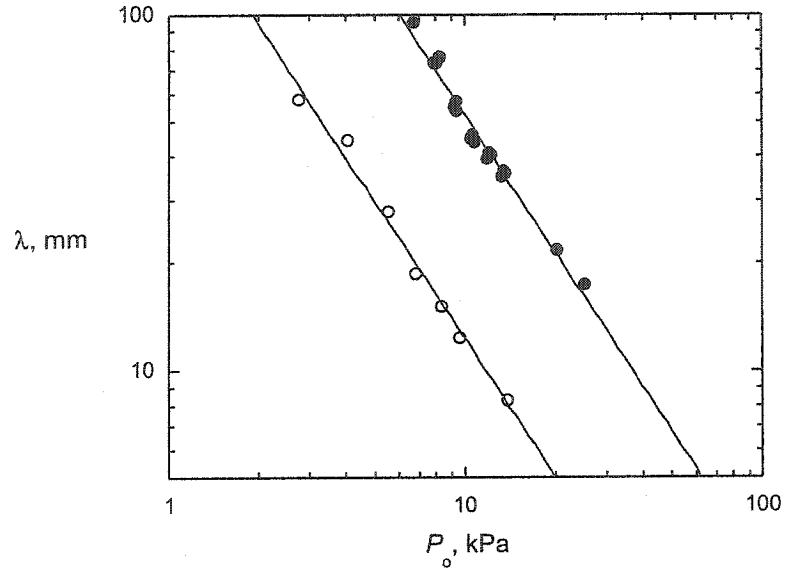

Fig 2.13 Cell width variation in with initial pressure for $C_3H_8 + 5O_2$ (O) and $CH_4 + 2\ O_2$ (●) (see text for references)

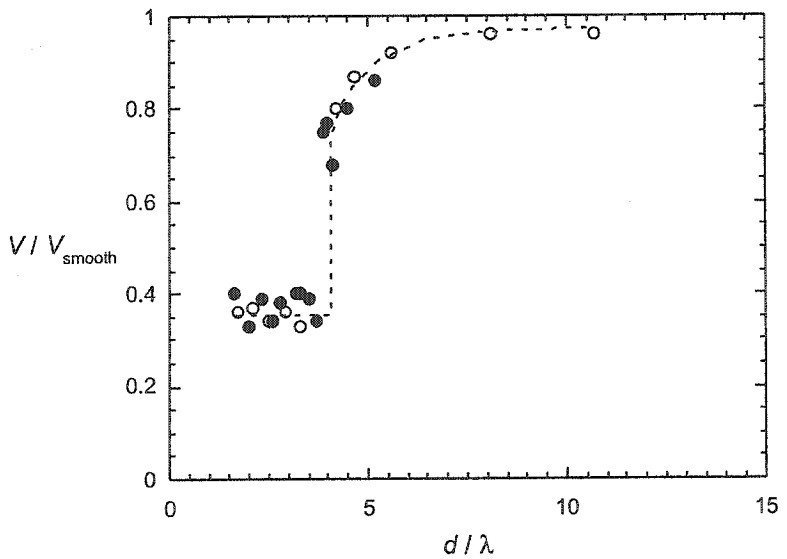

Fig 2.14 Detonation wave velocity deficits in the 41-mm porous wall tubes in $C_3H_8 + 5O_2$ and $CH_4 + 2O_2$ detonations as a function of (d / λ) (symbols same as Fig. 2.12)

1974) (shown in Figure 2.18) was used. The re-scaled velocity deficits are shown

in Figure 2.19. Firstly, it can be observed that the limits do not vary significantly with the argon or nitrogen dilutions investigated. A unique limit of approximately $(d / \lambda)^* \approx 7$ is observed for all three mixtures. A similar value for the limit was observed by Dupré in her experiments in porous wall tubes (Dupré et al., 1988).

At the limits, all three mixtures display a unique velocity deficit of approximately 15%. It is also interesting to note that far from the limits, these mixtures display a large velocity deficit, similar to the behavior in acetylene-oxygen mixtures diluted with large amounts of argon. At twice the limit, the velocity deficit is ~ 10%. Furthermore, the near-limit pulsations observed in the undiluted hydrocarbon mixtures were not observed for these hydrogen mixtures. In conclusion, it appears that these mixtures behave like the oxy-acetylene mixtures diluted with large amounts of argon. Since both mixtures display regular cell patterns and weak transverse waves, the similar attenuation and failure characteristics could be linked with cell regularity effects. Nonetheless, the limiting damping value in the hydrogen and acetylene-oxygen-argon mixtures is not unique. This raises the question of the validity of choosing the average transverse wave spacing λ as sensitivity length scale for these mixtures, and hence questions the relevance of the transverse wave structure in these mixtures characterized by weak three-dimensional effects.

2.6 Summary of observations on detonation failure

The results obtained in the porous wall tubes suggest two different classes of attenuation and failure mechanism. For undiluted hydrocarbon detonations, a unique failure limit was found, namely $(d / \lambda)^* \approx 4$. These mixtures were found to exhibit a weak dependence on the porous tube diameter far from the limit, with negligible velocity deficits. The failure of these mixtures in the porous wall section was very rapid. Complete failure was observed after approximately 4-7λ after the first expansion waves reached the tube axis. Near failure, an oscillatory detonation wave was observed with large velocity pulsations. Although the present technique could not resolve the magnitude of these pulsations, the period of oscillation was found to correspond approximately to 5-7λ.

Fig. 2.15 Near-limit pulsating phenomena in $CH_4 + 2O_2$ detonations in the 41-mm porous walled tube, $P_o = 35$kPa

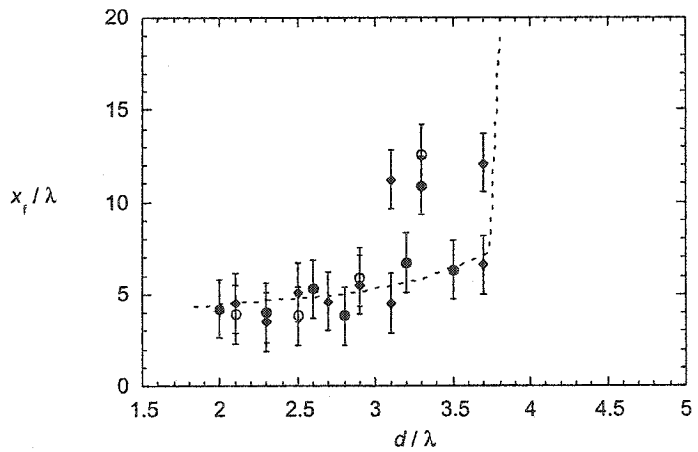

Fig 2.16 Normalized failure length for $C_2H_2 + 2.5O_2$ (◆), $CH_4 + 2O_2$ (●), and $C_3H_8 + 5O_2$ (O) in the 41-mm porous-walled tube

The detonation failure for acetylene-oxygen mixtures diluted with more than 60% Argon, and in hydrogen-oxygen-diluent mixtures investigated revealed large departures from the observations made for the undiluted hydrocarbon-oxygen mixtures. The attenuation of the hydrogen mixtures and the acetylene-oxygen-argon mixtures in the porous wall tubes were found to be strongly dependent on the attenuating boundary condition. Far from the limit, large velocity deficits were observed. When these detonations failed in the porous wall

section, the length to failure was also significantly longer. This failure length was not a constant value, but depended strongly on the tube diameter. The failure limits in these regular cell detonations were also found to differ from the constant value of $(d / \lambda)^* \approx 4$ observed for the three undiluted hydrocarbon-oxygen detonations, although a common value was not found. For oxy-acetylene mixtures diluted with large amount of argon, the limit $(d / \lambda)^* \approx 11$ was found, while for the hydrogen-oxygen mixtures, the limit $(d / \lambda)^* \approx 6$ - 8 was found. These results suggest that the cell size λ does not provide a unifying scaling length scale in correlating the failure limit in the argon diluted hydrocarbon mixtures and in the hydrogen-oxygen mixtures. The reason for these differences are further examined in the following chapters, where the flowfield is investigated more closely and the attenuation is treated theoretically in order to elucidate the failure limit dependence on the thermo-chemical properties of the mixtures.

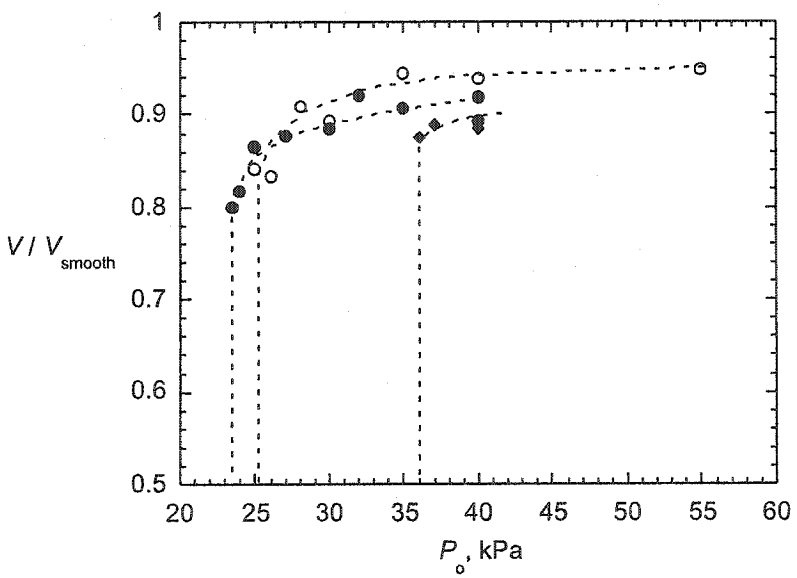

Fig 2.17 Detonation wave velocity deficits in the 41-mm porous wall tubes in $2H_2 + O_2$ (●), $2H_2 + O_2 + 2Ar$ (○), and $2H_2 + O_2 + N_2$ (◆) as a function of initial mixture pressure

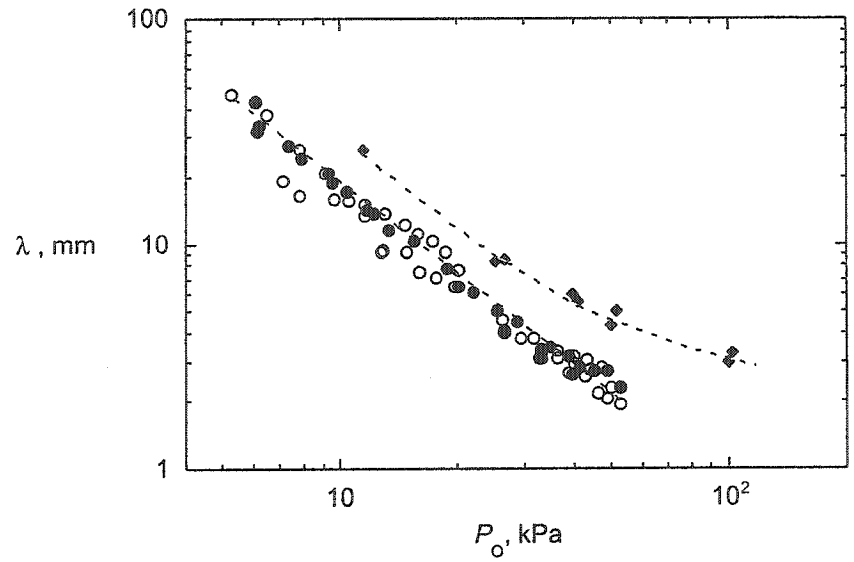

Fig 2.18 Cell width variation with initial pressure in $2H_2 + O_2$ (○), $2H_2 + O_2 + 2Ar$ (●), and $2H_2 + O_2 + N_2$ (◆) (see text for references)

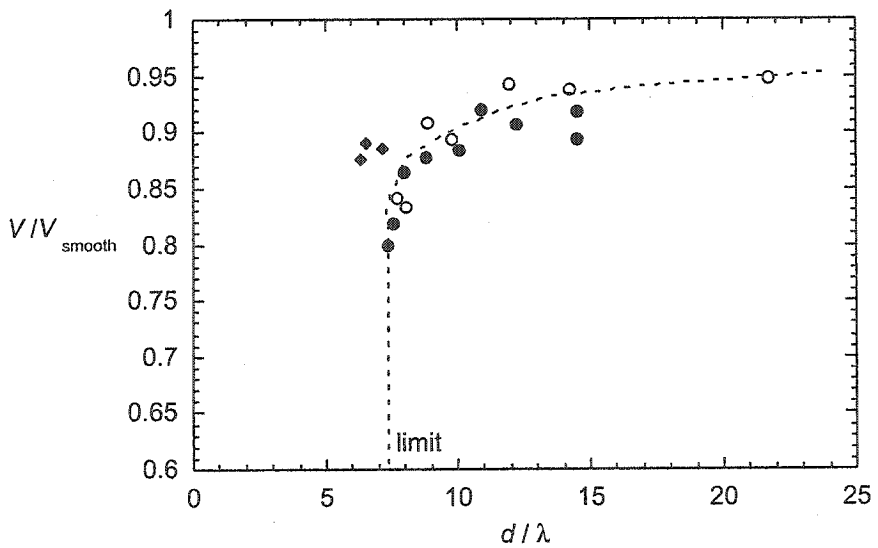

Fig 2.19 Detonation wave velocity deficits in the 41-mm porous wall tubes in $2H_2 + O_2$ (●), $2H_2 + O_2 + 2Ar$ (○), and $2H_2 + O_2 + N_2$ (◆) as a function of (d / λ)

Chapter 3 Attenuation and failure of detonations in two-dimensional porous wall channels

3.1 Overview

To gain further insight into the failure mechanism of detonations propagating in porous wall tubes, further experiments were conducted in two-dimensional channels lined with porous walls. The aspect ratio of the channel cross-section was systematically varied in order to control the mode of cellular propagation (two dimensional in thin channels and three dimensional in wide channels). This permitted meaningful conclusions to be drawn regarding the importance of the cellular structure of detonation waves during the attenuation of the detonations by the porous walls. The two-dimensional geometry also permitted to implement different flow visualization techniques across the third dimension and study the different flow fields during the attenuation process.

3.2 Experimental set-up

Most of the experiments were performed in thin rectangular channels, 1-m long, 10 cm in height and 4 mm in width (see Fig. 3.1a). The thin rectangular tube was separated into 2, 3 or 4 smaller channels, 40, 25.4 and 16 mm in height (d) and constant width of $w = 4$ mm. In general, the thin channel configuration of small aspect ratio (w / d) permitted to obtain detonation waves propagating in a planar mode, with cell evolution in two dimensions only (Strehlow, 1968). The length of the damping section in each of the mini-channels was always greater than 10 channel heights. The same porous material used in the circular tube experiments presented in Chapter 2 was used in the channel experiments. Different experiments were also performed in a two-dimensional configuration of larger aspect ratios of (w / d) = 0.61 and 6.1. The dimensions and configuration of the porous channels is shown in Figures 3.1b and 3.1c.

For the experiments in channels with aspect ratio (w / d) less than unity (Figs 3.1a and 3.1b), one entire sidewall of the channel was glass, as to permit the visualization of the flow field. The principal diagnostic for these thin channel experiments were streak and open shutter photography of the self-emission

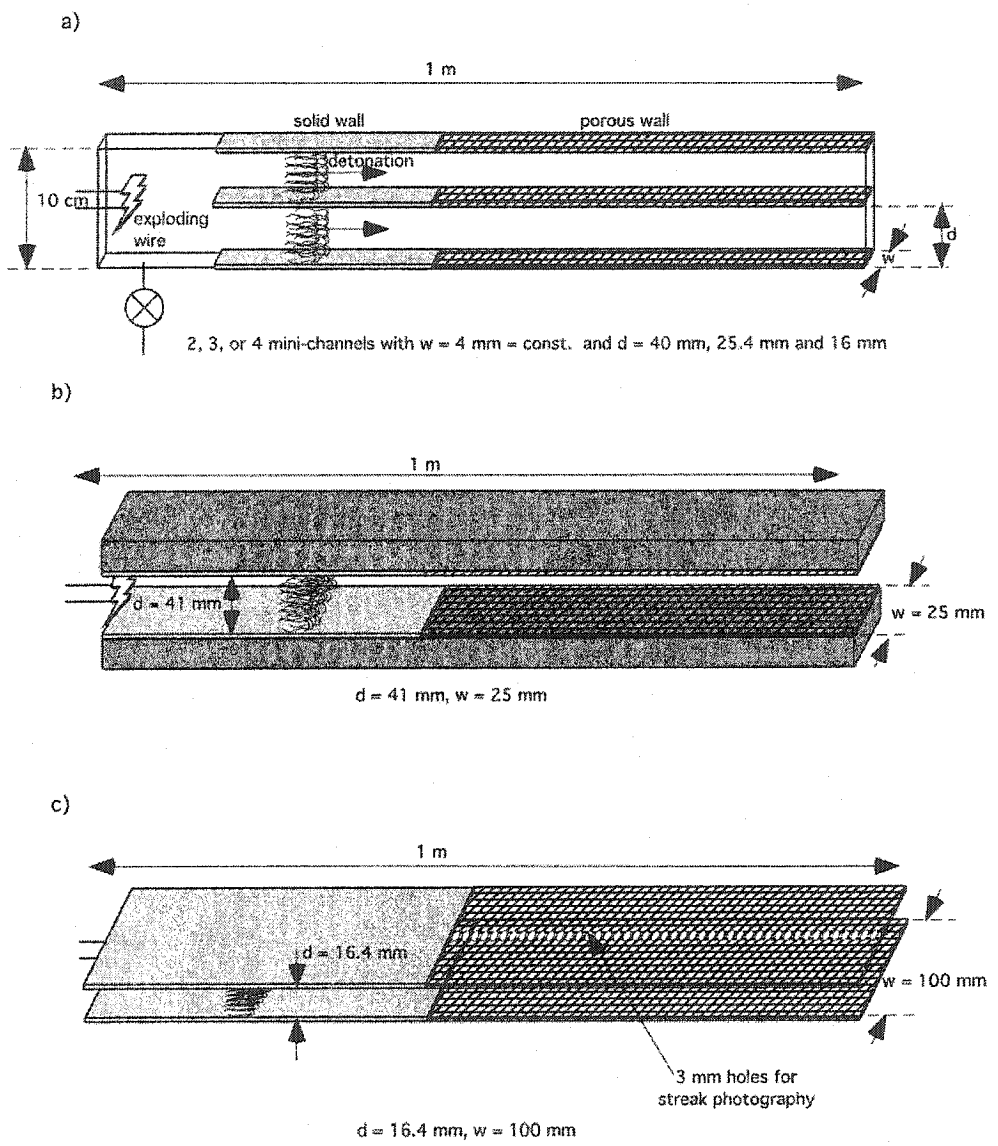

Fig. 3.1 Schematic of experimental set-up in the channel geometry

luminosity. For the experiments with large aspect ratio (Fig. 3.1c), the detonation waves inside the porous wall section were monitored by streak photography. To this effect, 2 mm diameter holes were drilled every 5 mm along a line. This permitted light detection inside the porous wall section.

Larger scale experiments were also conducted in a channel 1-m long, 10cm height and 2.5 cm thick, in which both opposite walls were optical quality glass. The last 46 cm of the 2.5cm-wide-walls were made of the same porous

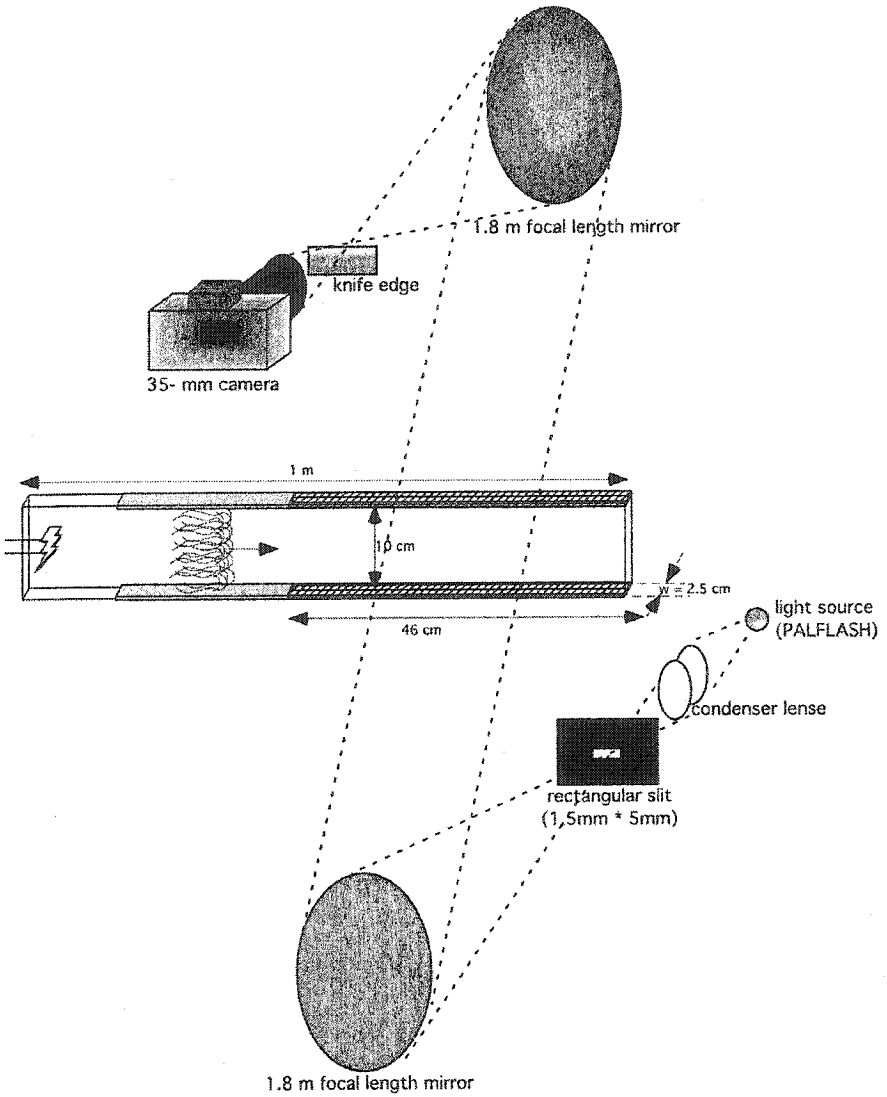

Fig. 3.2 Schlieren set-up in the channel experiments

material as above. A schematic is shown in Figure 3.2. This set-up was used to perform visualization of the density-gradient field by the schlieren technique and study the reaction zone structure. A typical single pass Z set-up was used (Settles, 2001). A single argon spark gap flash unit was used as light source (Pal Flash 500, manufactured by OPTIKON), with a flash intensity of 6 Joules and duration of less than approximately 1 microsecond. By controlling the delay time of the light flash, single individual frames of the detonation wave structure could be

obtained at various locations of the channel in either the solid wall or the porous wall sections.

In all tests, the mixtures were prepared in advance by the method of partial pressures in separate containers, as described in Chapter 2. The detonation channel was evacuated to pressures less than 50 Pa, and the mixture was introduced in the channel at ambient pressure. The pressure was than reduced to the desired initial pressure. The sensitivity of a given mixture was controlled via the initial pressure, with an accuracy of 50 Pa. In all the experiments, the detonations were directly initiated by a 25 kV electric discharge through an exploding wire, with nominal energy of ~ 100 Joules.

3.3 Attenuation and failure of acetylene-oxygen-argon detonations

3.3.1 Open shutter pictures in C_2H_2+2.5O_2 detonations

Typical open shutter photographs illustrating the details of the attenuation and failure process for stoichiometric oxy-acetylene in the thin porous wall channels ($w / d = 0.16$, $d = 25.4$ mm) are shown in Figs. 3.3 and 3.4. The series of photographs shown illustrate the influence of the porous walls for successively less sensitive mixtures, i.e., for decreasing initial pressure. In the photographs, the detonations propagate from left to right. These time-integrated photographs are equivalent to smoke foil records, where the path of the intense combustion regions near the triple points can be recorded. With proper adjustment of the aperture, the intense combustion region can be isolated from the less luminous combustion products.

Fig. 3.3 illustrates the flowfield of the attenuated detonations that do not fail in the porous wall section. In the smooth wall section of the channel, the irregular structure of interacting transverse waves is clearly seen for this system. As the detonation enters the damping section, one can note the influence of the porous wall on the frontal transverse wave structure. As the transverse waves are damped upon reflection from the porous walls, the detonation cells are enlarged along a local failure wave originating from the walls and propagating towards the axis. However, after an initial transient of approximately 4 average cell lengths,

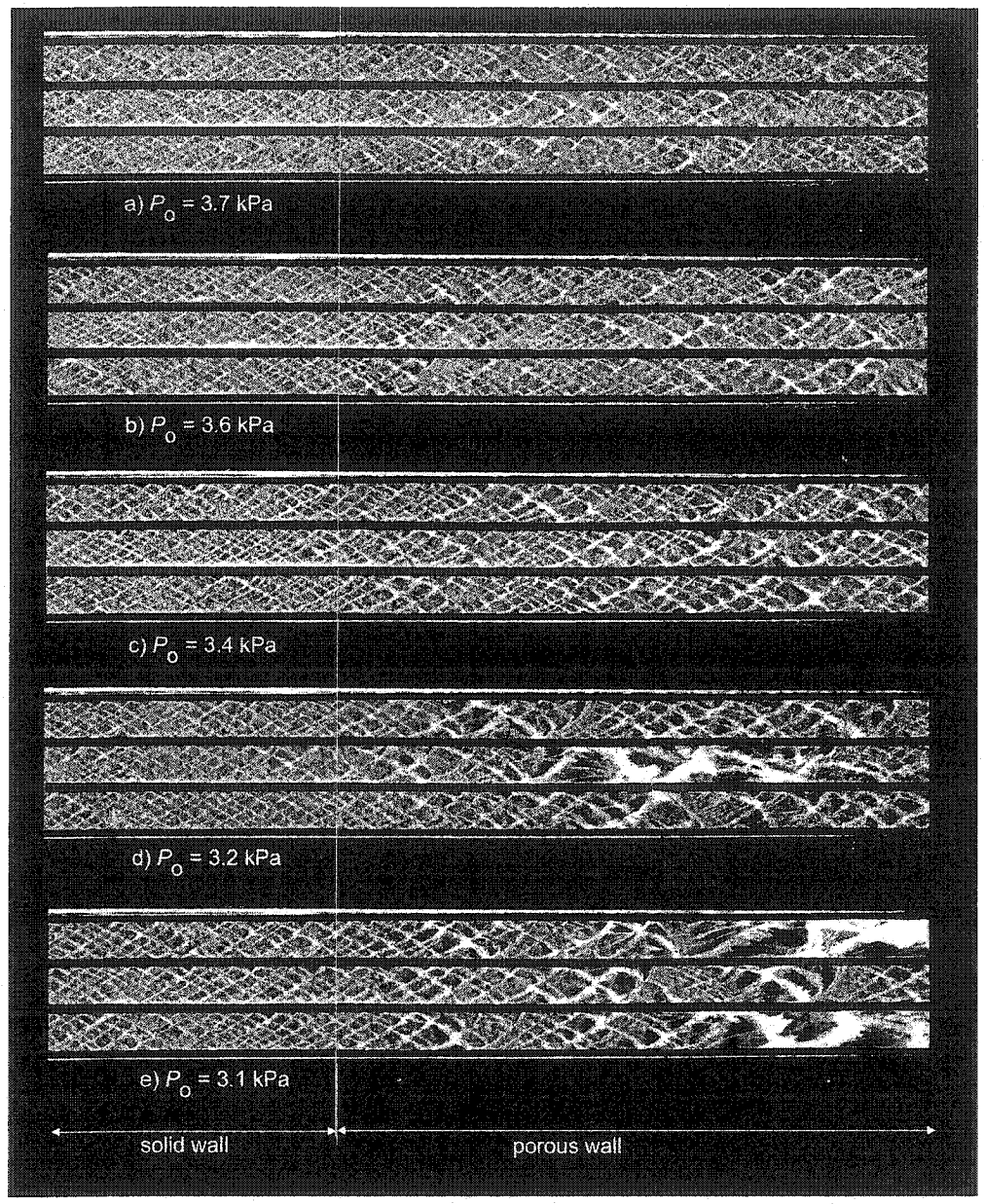

Fig. 3.3 Open shutter photographs illustrating the attenuation of $C_2H_2 + 2.5O_2$ detonations in the (d, w) = (25.4 mm, 4 mm) porous wall channels

the detonation wave recovers from the attenuation and regains its original irregular transverse wave structure. It is also interesting to note the subsequent ongoing competition between triple point weakening at the wall and the re-amplification of the new triple points across the detonation front, which becomes

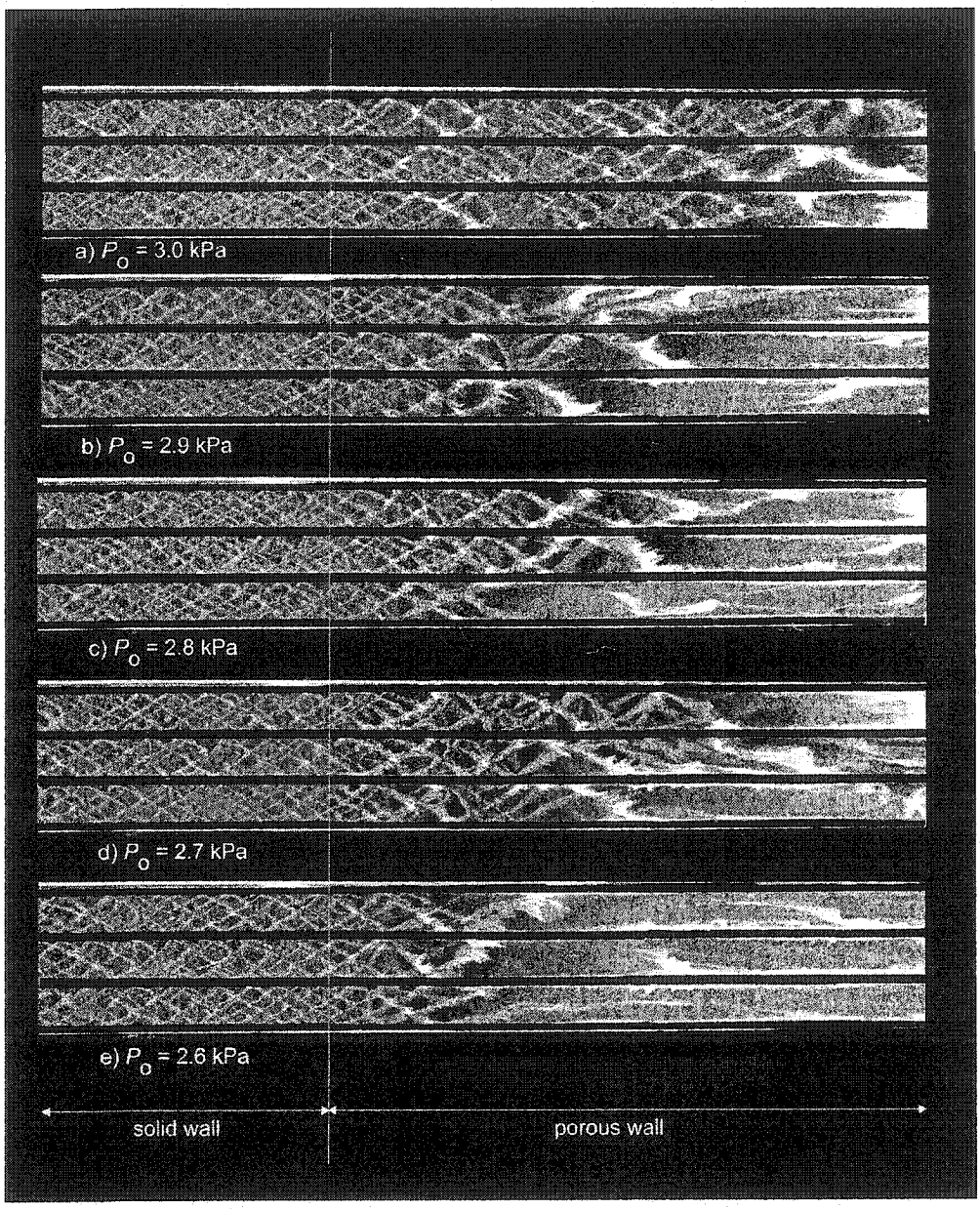

Fig. 3.4 Open shutter photographs illustrating the failure of $C_2H_2 + 2.5O_2$ detonations in the (d, w) = (25.4 mm, 4 mm) porous wall channels

more clear for less sensitive mixtures. Within the limited resolution of the photographs, the regeneration of new triple points for this mixture appears to be associated with the interaction of weakened triple points.

Above the damping limit, the velocity deficits of the detonations propagating in the porous wall section, as measured from streak photographs, was

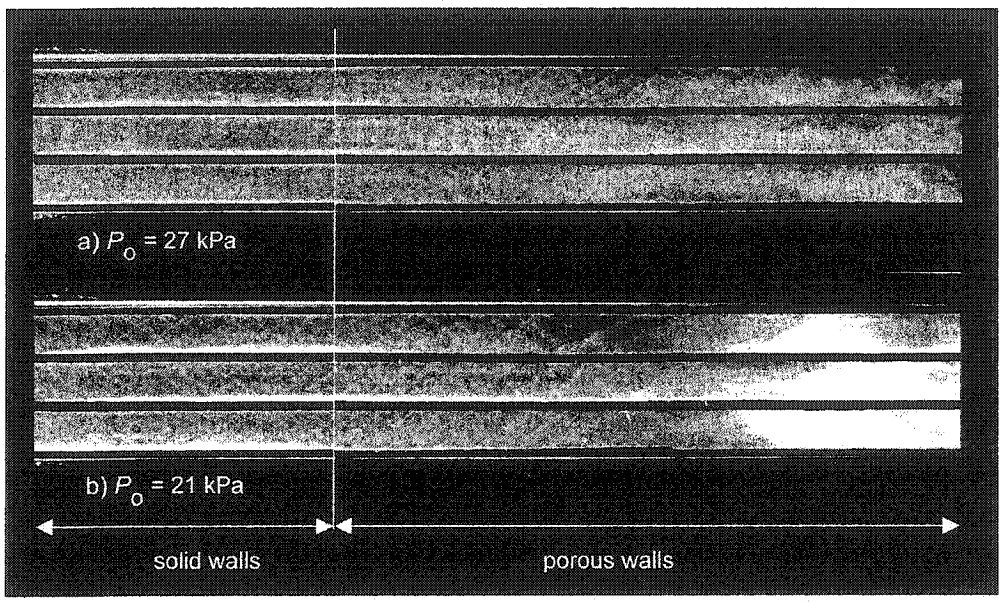

Fig. 3.5 Open shutter photographs illustrating the attenuation and failure of $C_2H_2 + 2.5O_2 + 75\%Ar$ detonations in the (d, w) = (25.4 mm, 4 mm) porous wall channels

found to be less than 2%. This is consistent with the results obtained for the same mixture in the porous wall tubes, as presented in Chapter 2. Based on the visual observations, it thus appears that the re-generation of transverse waves from local instabilities in the reaction zone allows the wave to propagate at near CJ velocities and to overcome the losses to the porous tube walls.

Near the critical conditions of damping in acetylene-oxygen detonations, complex wave phenomena are observed, as illustrated in Figure 3.3d and 3.3e. For these near-limit detonations, the detonation wave undergoes a series of successive local failures due to transverse waves attenuation, followed by the re-amplification of new triple points from weakened transverse shock interactions and from the turbulent reaction zones. These successive attempts to re-generate new transverse waves are best seen on the middle channel of Figures 3.3d and 3.3e. One can note that the length for each re-amplification phase before subsequent attenuation is approximately 4 to 8 λ, consistent with the oscillations observed from the streak records obtained for the same mixture in the tube experiments of Chapter 2. Since the same oscillations are observed in both the tube and channel experiments, the conclusion is that these near-limit pulsations

are intrinsic to the near-limit detonation dynamics. Furthermore, the average velocity of these highly unstable detonations is the same both in the tube and channel experiments, with a velocity deficit of approximately 30%. It can be speculated that the decrease in the average velocity is due to the more frequent and longer sub-CJ excursions during the pulsating phases.

Typical open shutter photographs illustrating the failure of such unstable detonations in the damping section are shown in Figure 3.4. As the detonation enters the porous wall section, one can note the weakening of the transverse wave structure as the triple points reflect from the porous walls, which leads to the subsequent failure of the entire detonation wave. This occurs when the re-amplification of triple points during their transverse motion from one wall to the other is not sufficiently fast. Streak photographs confirmed that the disappearance of the transverse waves corresponded to the wave failure to low velocities. It is also interesting to note that the dynamics of the detonation wave in the porous wall section follows quasi-periodical cycles before complete extinction. This is reminiscent of the galloping pulsations observed in the tube experiments. Before failure, a stochastic number of pulsations are observed, associated with successive attempts of re-initiation and attenuation of the re-generated triple points at the wall. Subsequent to the wave failure, some vestigial triple shock interactions remain visible on the photographs, but they are too weak to permit the re-establishment of a detonation wave. These open shutter photographs clearly illustrate that the intense combustion regions associated with the triple point interactions in undiluted acetylene-oxygen detonations are locally damped by the porous walls. This permits us to conclude that the failure for this mixture is dictated by the competition between weakening of transverse waves upon reflection on the porous walls and re-amplification of new transverse waves from the turbulent reaction zone.

3.3.2 Open shutter pictures in $C_2H_2 + 2.5O_2 + 75\%Ar$ detonations

The attenuation and failure processes for argon-diluted acetylene-oxygen detonations are fundamentally different from the undiluted detonations shown above. For highly argon diluted acetylene-oxygen mixtures, a very regular

cellular structure can be observed with much weaker transverse waves (Figures 3.5a and 3.5b). The luminosity of the triple points is significantly reduced, suggesting a significant decrease in local chemical activity near the triple points. Furthermore, the path of the triple points are close to straight lines, suggesting that the wave interactions are of the weak type (Fickett & Davis, 1979). Figure 3.5a illustrates the attenuation of such a stable wave when the detonation does not fail. In contrast to the undiluted detonations discussed above, a more gradual attenuation process is observed, indicated by the slow change in the detonation structure's morphology as it progresses inside the porous wall section. The detonation cells can be observed to continuously enlarge before attaining a steady state configuration near the end of the channel. For these conditions, the velocity deficits obtained from the streak photographs measurements are approximately 15%. These observations are indicative of a global attenuation mechanism where the time scales for the attenuation process and relaxation to a steady state are much longer. It is also interesting to note that unlike the undiluted waves discussed above, these argon-diluted detonations do not re-generate nor re-amplify any new transverse waves during the attenuation process. The long attenuation length scales are consistent with the experiments conducted in the tube geometry (Chapter 2) for the same mixture, or as observed by Lee (1996) for the diffraction experiments, thus confirming the universality of the phenomenon.

The case of failure for a less sensitive detonation is shown in Figure 3.5b. As the wave propagates in the porous wall section, one can note the progressive increase of the detonation cells, which we interpret as the gradual decrease in reaction rates and global attenuation of the entire detonation wave front. It is important to note that the eventual extinction of these waves occurs over the entire cross section of the front, whereas for the undiluted detonations discussed above, failure is due to local conditions where transverse waves cannot be re-generated from local instabilities.

3.3.3 Influence of channel aspect ratio on the damping limits

In order to study the influence of the channel aspect ratio on the damping limits, experiments in C_2H_2+2.5O_2 and C_2H_2+2.5O_2+75%Ar mixtures were

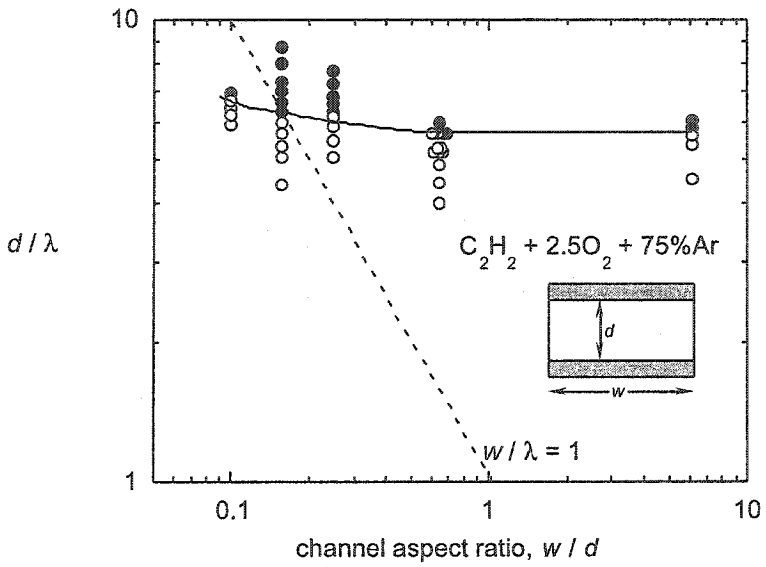

Fig. 3.6 Influence of channel aspect ratio on the damping limits $(d / \lambda)^*$ in $C_2H_2 + 2.5O_2 + 75\%Ar$; (●) successful propagation, (○) failure of detonation in the damping section

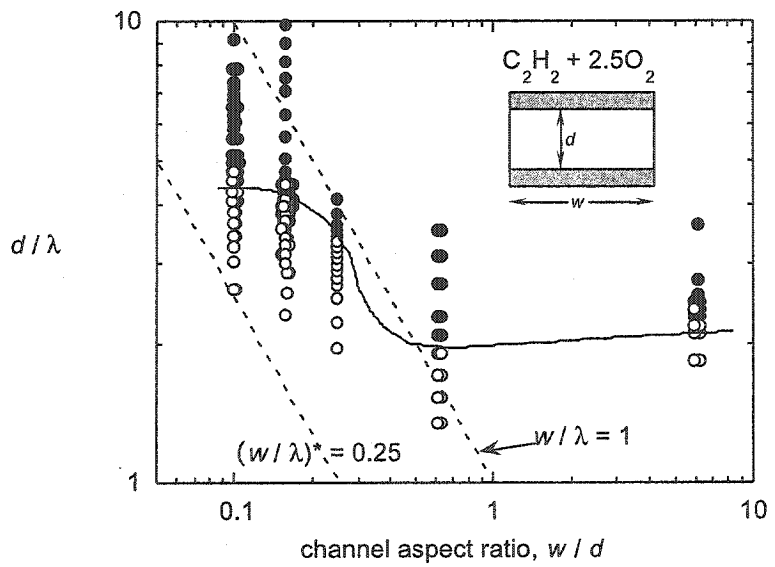

Fig. 3.7 Influence of channel aspect ratio on the damping limits $(d / \lambda)^*$ in $C_2H_2 + 2.5O_2$; (●) successful propagation, (○) failure of detonation in the damping section

performed for channels whose cross-sectional aspect ratios vary by two orders of magnitude (see Fig. 3.1). The critical pressure P_o^*, hence mixture sensitivity,

separating successful propagation and detonation damping was obtained from the photographic records. The results are tabulated in Table 3.1. Figure 3.6 shows graphically the dependence of the damping limit $(d / \lambda)^*$ for the argon diluted mixture. As can be seen, a unique limit of approximately $(d / \lambda)^* \approx 6$ is observed over the entire range of channel aspect ratios. The broken line shown in Fig. 3.5 shows the loci of the experimental conditions where only one cell exists across the channels width (i.e., $w / \lambda \approx 1$). The conclusion that can be reached is that the failure of these detonations does not dependent on the three-dimensional details of the wave. For $w < \lambda$, the cellular mode is constrained to only two dimensions, i.e. a planar mode of cellular dynamics (as can be deduced from Fig 3.5). This planar mode corresponds to transverse waves propagating mainly in the direction of the channel height. Yet, the damping limit observed for this situation is very close to the limiting condition obtained for very wide channels ($w / \lambda >> 1$) where cells are three dimensional and transverse waves evolve in all three dimensions. Hence the appearance of the transverse shocks in the w-direction does not influence the detonation failure.

For very narrow channels, however, the limit slightly increases by approximately 30%. This slight deviation can be attributed to the growing effect

Table 3.1 Critical conditions for damping of $C_2H_2 + 2.5O_2$ and $C_2H_2 + 2.5O_2 + 75\%Ar$ detonations in the various porous wall channels

Mixture	(d, w) mm, mm	w / d	P_o* kPa	λ mm	w / λ	(d / λ)*
$C_2H_2 + 2.5O_2$	(40,4)	0.1	2.45+0.25	9.1	0.4	4.4+11%
	(25.4, 4)	0.16	3.25+0.45	6.5	0.6	3.9+21%
	(16, 4)	0.25	4.25+0.5	4.7	0.9	3.4+1%
	(41, 25)	0.61	1.15+0.15	23.0	1.1	1.8+6%
	(16.4, 100)	6.1	3.05+0.15	7.1	14	2.3+8%
$C_2H_2 + 2.5O_2 + 10.5Ar$	(40,4)	0.1	16.5+0.5	6.0	0.7	6.7+4%
	(25.4, 4)	0.16	22.5+0.5	4.1	1.0	6.2+3%
	(16, 4)	0.25	33.5+0.5	2.5	1.6	6.3+3%
	(25, 16)	0.64	21.3+1	4.4	3.6	5.7+7%
	(16.4, 100)	6.1	30.5+.5	2.9	35	5.7+2%

of the boundary layers developing on the solid walls of the channel. Hence supplementary mass divergence to these boundary layers may slowly raise the limit for channels of smaller aspect ratios. Following Fay's analysis on the influence of the negative mass displacement due to boundary layers on solid walls (Fay, 1959), it can be shown (see Appendix 1) that the ratio ζ between the wave curvature due to the mass divergence in the boundary layers and the wave curvature generated by mass divergence to the porous walls in a channel geometry follows in the limit of small divergence:

$$\zeta \equiv \frac{\kappa_b}{\kappa_p} \approx 0.03\left(\frac{w}{d}\right)^{-1} \qquad 3.1$$

At a small aspect ratio (w / d) of 0.1, the curvature generated by the boundary layers is thus a third of the curvature generated by the porous walls and thus begins to play a sensible role in the limiting failure conditions in the experiments. This is consistent with the experimental findings of a slight increase in the damping limit (see Appendix 1 for a quantitative analysis).

Figure 3.7 shows the dependence of the damping limit (d / λ)* on channel aspect ratio (w / d) for undiluted C_2H_2+2.5O_2. A completely different behavior is observed in comparison with the argon diluted mixture (Fig. 3.6). For large aspect ratios, where the detonation structure is three-dimensional, a limit of (d / λ)* $\approx$ 2 is observed. However, a critical change of behavior is observed for channels containing less than a cell across their thickness (i.e., w < λ). The critical limit (d / λ)* approximately doubles and asymptotes to a value of approximately 4.3. This sudden change in the failure limit cannot be attributed to the effect of boundary layers in generating mass divergence, since this effect is expected to operate gradually (see Appendix 1). The sudden change of failure limit is attributed to the importance of the transverse wave structure in this mixture. When the detonation structure is planar and mainly two-dimensional (i.e., w < λ), interactions of transverse waves are present only in two-dimensions. In this case, the limit is approximately the same as in the tube experiments, suggesting that the attenuation mechanism is governed by the rate of attenuation of incident transverse waves on the porous walls, as governed by the distance

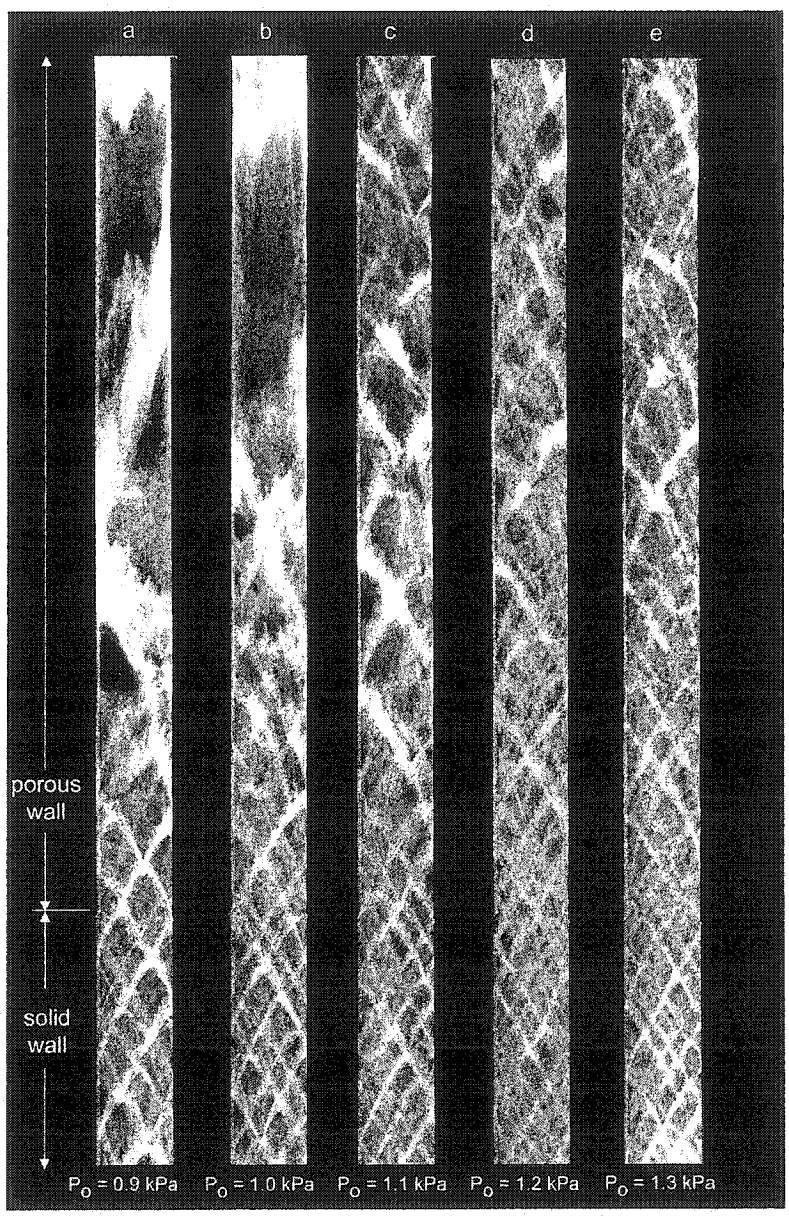

Fig. 3.8 Open shutter photographs illustrating the attenuation and failure of $C_2H_2 + 2.5O_2$ detonations in the (d, w) = (41 mm, 25 mm) porous wall channels

between porous walls. However, when the opposite family of transverse waves develops across the channel thickness, the detonation becomes three-dimensional and hence the transverse wave density doubles, it is twice as difficult to damp the transverse waves, hence the limit is lower by a factor of two.

These conclusions are further verified by the observations of the three-dimensional cellular dynamics in channel satisfying the condition $w > \lambda$. Figure 3.8 shows the structure of these three-dimensional detonation waves in the solid and porous wall parts of the channel for the case of an aspect ratio of $(w / d) = 0.6$. The details of the attenuation and regeneration of new transverse waves are three-dimensional, but the mechanisms of transverse wave attenuation at the walls and re-generation of new transverse waves are similar to the planar mode. In the solid part of the channel, multiple set of transverse waves appear overlapped, giving rise to a highly three-dimensional flowfield. This is to be compared with the planar mode observed for conditions such that $w < \lambda$ (Figure 3.3 and 3.4). When the detonations are only attenuated in the porous part of the channel (Figs. 3.8d and 3.8e), a highly turbulent flowfield appears, with continuous re-generation of interacting transverse waves in multi-dimensions. At the limit (Fig 3.8c), similar oscillations are observed as for the planar mode, although more complicated due to the new degree of freedom of oscillating transverse waves. Following the attenuation of transverse waves at the wall, new ones re-amplify from local instabilities and from mutual interactions. The damping of the detonation below the limit reveals that the same mechanism of transverse wave attenuation at the porous walls operates in these experiments.

It is also very interesting to note that the failure limits in Figure 3.7 show increasing statistical variability for narrow channels in undiluted detonations. These large fluctuations are less frequent for the large aspect ratios in the same mixture or for all experiments in the argon diluted detonations (Fig. 3.6). The reason for these large fluctuations can be attributed to the fact that local events of transverse wave attenuation at the walls and re-generation of new ones within the reaction zone govern the damping limit. Since these two effects are highly stochastic, due to the variability in strength of transverse waves and irregularity in the cellular structure, the limits observed vary in repeat experiments. It is also possible that for detonations in the planar mode, oscillations in the third dimension occurring at length scales less than the channel width may intermittently affect the transverse wave structure dynamics.

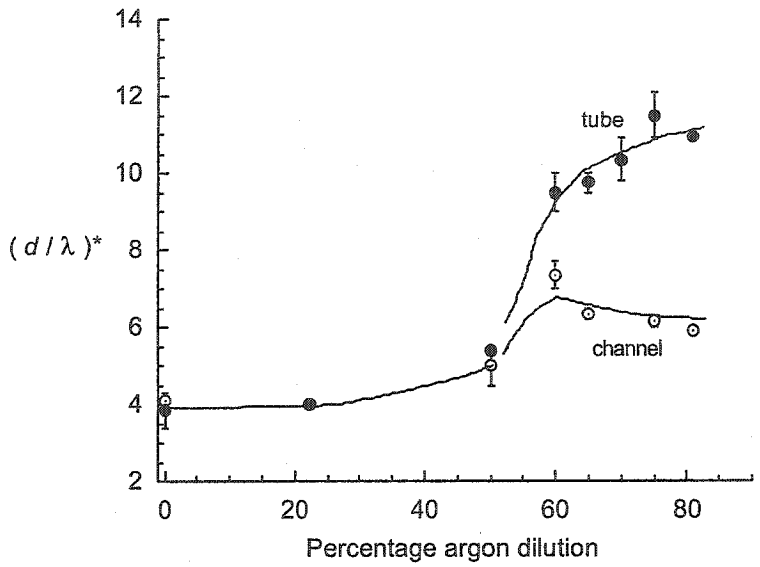

Fig. 3.9 Damping limit (d / λ)* obtained in the (d = 25.4 mm, w = 4 mm) channels (⊙), and in the tube geometry (●) in $C_2H_2 + 2.5O_2 +$ %Ar detonations

3.3.4 The transition between the two regimes in $C_2H_2/O_2/Ar$ detonations

From the above experiments, it can be concluded that a channel aspect ratio of (w / d)≈ 0.16 permits to study the porous wall influence on $C_2H_2/O_2/Ar$ planar mode detonations, where only transverse waves propagating in the direction incident to the porous wall are observed. For this reason, the influence of the amount of argon dilution was investigated for this particular geometry. Fig. 3.9 shows the evolution of (d / λ)* as a function of argon dilution. Also reproduced are the limits observed in the tube geometry, as determined in the previous chapter. The first conclusion that can be reached is that the critical value of (d / λ)* is not a monotonous function in terms of argon dilution in either the tube or the channel geometries, and indicates a discontinuous bifurcation at approximately 60% argon dilution. This discontinuity, suggesting two failure mechanisms, is further investigated in the discussions of Chapter 5.

The quantitative comparison between the limits obtained in the tube and channel geometry above and below the transitional argon dilution also provides

very interesting observations. For mixtures diluted with 50% argon and less, identical limits are observed in both the channel and tube experiments, with an asymptotic value of approximately $(d / \lambda)^* \approx 4$ for zero dilution. The uniqueness of the limits in both geometries suggests that the critical conditions near failure are governed uniquely by the distance between the porous walls and the characteristic transverse wave spacing λ. This is compatible with the observations that these mixtures fail by the attenuation of their transverse waves, and not due to the global mass divergence mechanism. Since the attenuation rate of transverse waves depends only on the distance between the porous walls, it follows that $(d / \lambda)^*$ should be the same for both the channel and tube experiments. This is precisely what is observed for the undiluted acetylene-oxygen detonations, for which the open shutter photographs indicate a competition between the rates of transverse wave generation from instabilities and the attenuation rate of transverse waves by the porous walls (e.g. Figs 3.3, 3.4 and 3.8).

For dilutions greater than 60% argon, the ratio of the limit observed in tubes to the limit in the two-dimensional channels asymptotes with increasing argon dilution to a constant value of 2. As already noted, the factor of two between the two limits is consistent with wave curvature arguments. If the detonation fails due to the global excess expansions generated by the porous walls, than the cylindrical curvature developed by the front in the channel experiments gives rise to an area divergence that is twice more severe than for the tube experiments, where the curvature is spherical and the area divergence in the reaction zone is three-dimensional instead of two-dimensional. A rigorous derivation of this result follows in Chapter 4.

3.4 Attenuation mechanism in hydrogen and propane detonations

The open shutter technique was found applicable to acetylene-oxygen mixtures only. In the other hydrocarbons and hydrogen mixtures, the background emission from the reaction zone was found significant and obscured the emission near the triple points. For this reason, the damping process in these mixtures was

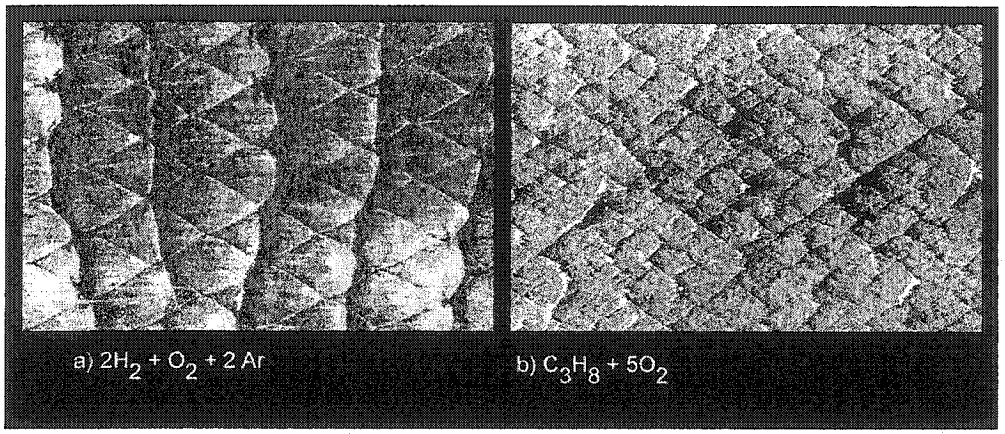

Fig. 3.10 Smoke foil records illustrating a), the regular structure in $2H_2 + O_2 + 2Ar$ (from Strehlow, 1969) and b), the irregular structure in $C_3H_8 + 5O_2$ (obtained in this study)

mainly studied by the schlieren technique. The experiments focused on two specific mixtures only, namely, stoichiometric propane-oxygen and stoichiometric hydrogen-oxygen diluted with 40% Argon. The choice of these mixtures was due to their very distinct cellular regularity characteristics, as shown in Fig. 3.10. The propane-oxygen mixture is characterized by very irregular cells and the formation of secondary fine triple-point structure superimposed on the main cellular pattern. On the other hand, the hydrogen-oxygen-argon system is well known for its excellent structural regularity. Hence, these mixtures can be treated as benchmark mixtures to further study the failure mechanism in regular and irregular mixtures, and hence extend our previous conclusions obtained for the C_2H_2-O_2-Ar system.

The experiments were performed in the larger scale channel (see Figure 3.2) for better visual resolution. From the entire duration of the light source (~1μsec), the motion blur is approximately 2 mm. A horizontal knife-edge was used in these experiments, permitting to detect density gradients in the transverse direction to the detonation propagation. For reference, positive vertical density gradients are lighter than the average in the schlieren photographs.

3.4.1 Experiments in $2H_2+O_2+2Ar$ detonations

Figure 3.11 shows the reaction zone structure in $2H_2+O_2+2Ar$ obtained in the smooth wall section of the channel at initial pressures of 13 kPa and 8kPa.

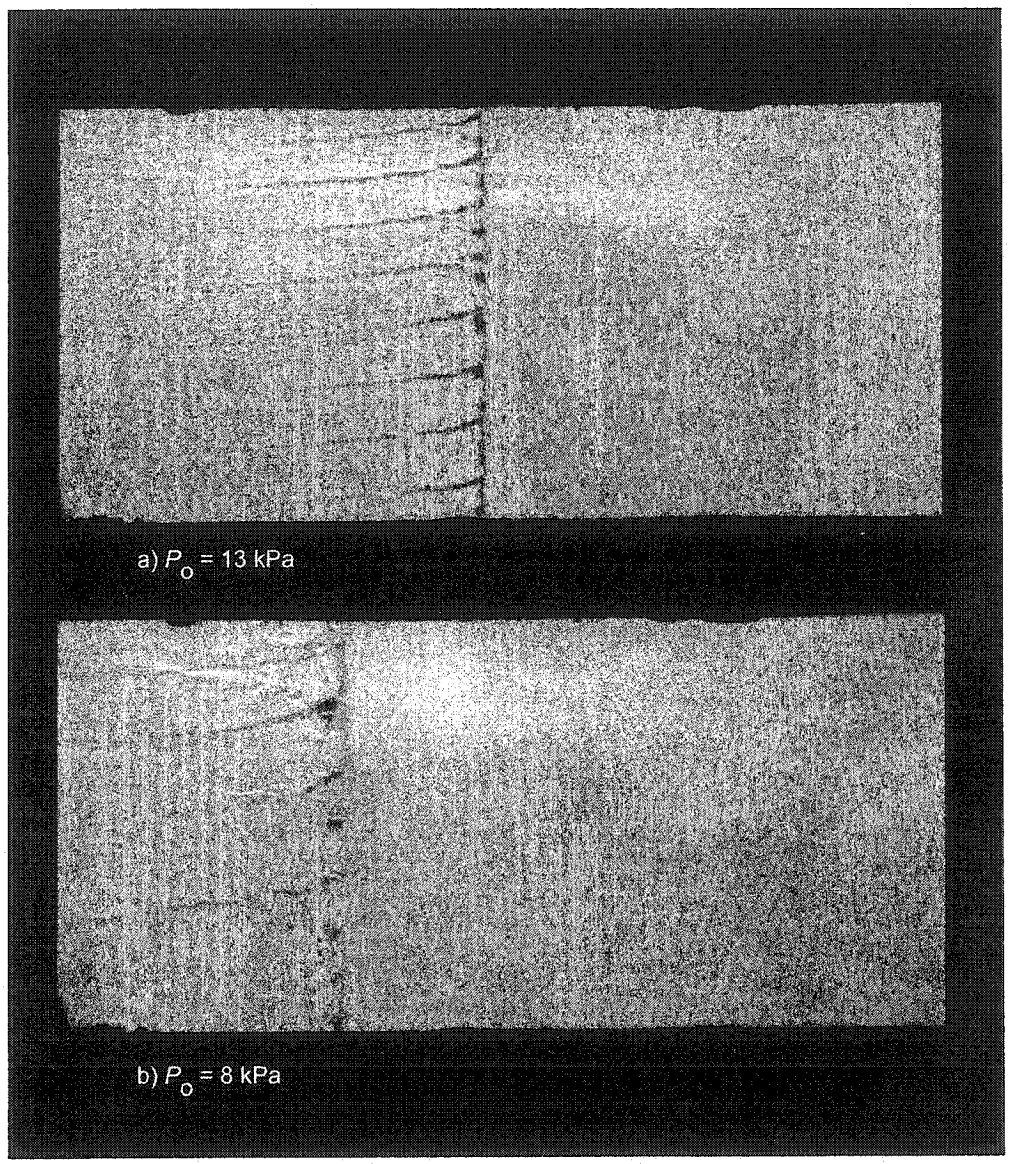

Fig. 3.11 Schlieren photographs in $2H_2 + O_2 + 2Ar$ in the solid wall section of the channel; a) P_o = 13 kPa, b) P_o = 8 kPa

Regularly spaced triple points are observed, separating laminar portions of the front (incident shocks and Mach stems). This is the classical picture of the reaction zone of gas detonations observed previously in similar regular-structure detonative systems (see for example Fickett & Davis, 1979 for review) and well reproduced in numerous numerical simulations (e.g. Oran et al., 1998). These photographs thus confirm that the combustion region is laminar, in that the gas is ignited uniformly behind the leading shock and Mach stems. This is consistent

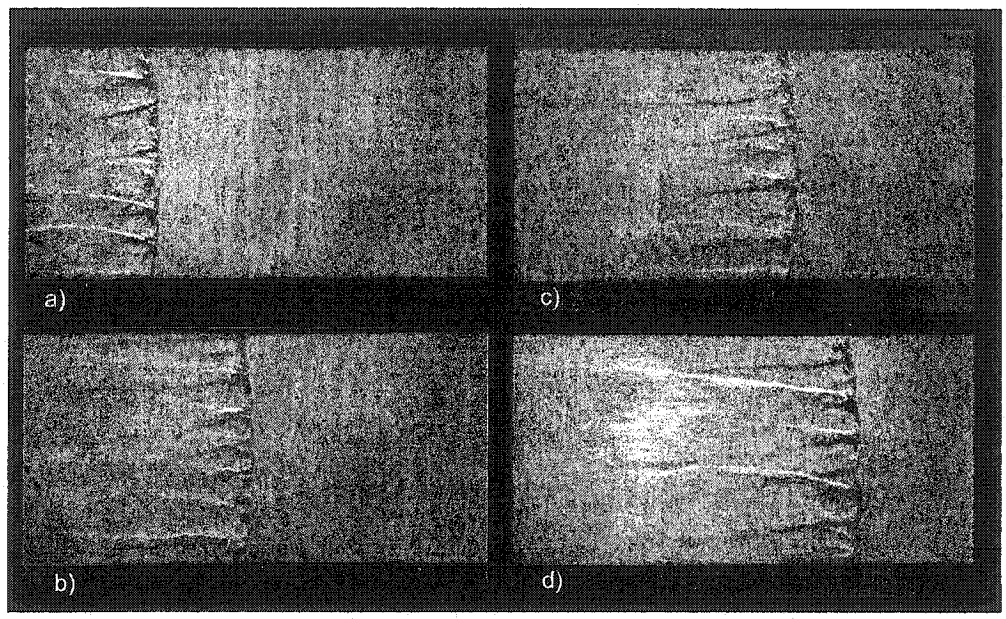

Fig. 3.12 Schlieren photographs in $2H_2 + O_2 + 2Ar$ detonations in the porous wall section of the channel taken at $P_o = 13$ kPa

with the very recent findings of (Shepherd et al. 2002) in the same mixture using the PLIF technique to visualize the OH radical concentrations in the reaction zone. In their study, they found that the gas is ignited uniformly behind the incident shocks and Mach stems. The transverse waves were found non-reactive and hence did not participate in the ignition mechanism.

Figure 3.12 shows the structure of the detonation front in the porous wall section for $P_o = 13$ kPa. The schlieren cut-off was increased in order to better resolve the density gradients in the reaction zone structure. The left side of the photographs correspond to ~1.5 d downstream of the start of the porous wall section. The different frames were taken from different experiments. It can be seen that the detonation wave becomes globally curved, with a curvature maintained over the entire travel of the detonation wave inside the porous wall section. Also noteworthy is that the average transverse wave spacing and the apparent thickness of the front both increase with respect to the un-attenuated detonations in Fig. 3.11*a*. This is indicative that the front becomes uniformly curved due to the mass divergence to the porous walls. The expansions generated by the porous walls lead to lower temperatures in the reaction zone, thus longer

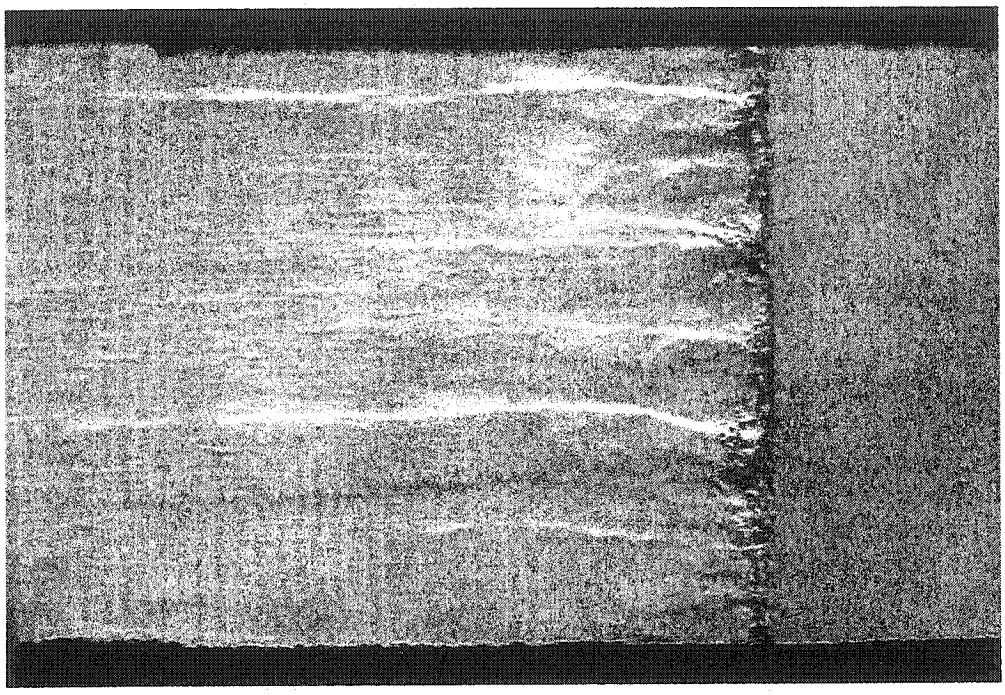

Fig. 3.13 Schlieren photograph in $C_3H_8 + 5O_2$ in the solid wall section of the channel, $P_o = 5.6$ kPa

reaction time and hence larger transverse wave spacings. Very similar schlieren photographs of the attenuation of hydrogen-oxygen-argon detonations in porous wall channels were previously obtained by Guo et al. (2002), although the significance of the results was then not recognized.

3.4.2 Experiments in $C_3H_8+5O_2$ detonations

The reaction zone structure observed in propane-oxygen detonations shows significant differences. Figure 3.13 shows the reaction zone structure of such detonations in the solid wall section of the channel for $P_o = 5.6$kPa. For this pressure, four cells fit across the channel height d and only one across the channel thickness w. The main front appears planar, but highly corrugated. The basic features of these photographs are the small-scale corrugations at the detonation front and the long tailed transversely moving shocks. The direction of propagation of these transverse waves can be determined from the luminosity: compression waves moving up are lighter, while downwards moving compression waves are darker. The transverse waves associated with the triple points forming

the main cellular structure decay appreciably in strength at a length scale of ~4 cell lengths, after which most of their energy is dissipated and their visual detection becomes difficult. At smaller scales, the structure of the detonation waves is highly turbulent. These fine scale bubbles appear in the pictures behind the main front, and extend approximately half a cell behind the main front. These bubbles are more frequent near the triple points. The large changes in luminosity across the bubbles' surfaces are indicative of large density gradients, which can only be associated with reaction zones. From the changes in luminosity, it can be concluded that these bubbles consist of higher density un-reacted or partly reacted gas engulfed in lower density gas that is closer to the termination of its oxidation process. It is likely that these small-scale reactive structures may be responsible for the small scale triple point structure observed on smoke foils. The delayed reaction of the various parcels of gas sets a series of interacting compression pulses. These can coalesce to form the intense transverse wave spectrum observed for these detonations.

To the author's knowledge, the spotty reaction zones observed in the present experiments was never previously observed with such clarity, since most of photographic investigations of detonation structure focused on detonations characterized by very regular systems (such Fig. 3.11). A worthy exception is the study of Subbotin who looked at the transverse wave structure of irregular detonations and concluded that a fine structure of un-reacted pockets trail behind the main detonation front (Subbotin, 1976). This is precisely what the photographs taken in the present study confirm.

Photographs taken in the porous wall section at the same initial conditions as above are shown in Figure 3.14. The view section was positioned such that the left of the photographs corresponds to ~1.5d downstream of the entrance in the porous wall section, as to focus on the initial transients of the attenuation process. For reference, a typical example of the flowfield obtained with the smoke foil technique is shown in Fig. 3.15 for the same $(d / \lambda) \approx 4$ condition in the smaller scale channels. The main features of this smoke foil record are as described above for acetylene-oxygen detonations: after the first expansion waves reach the

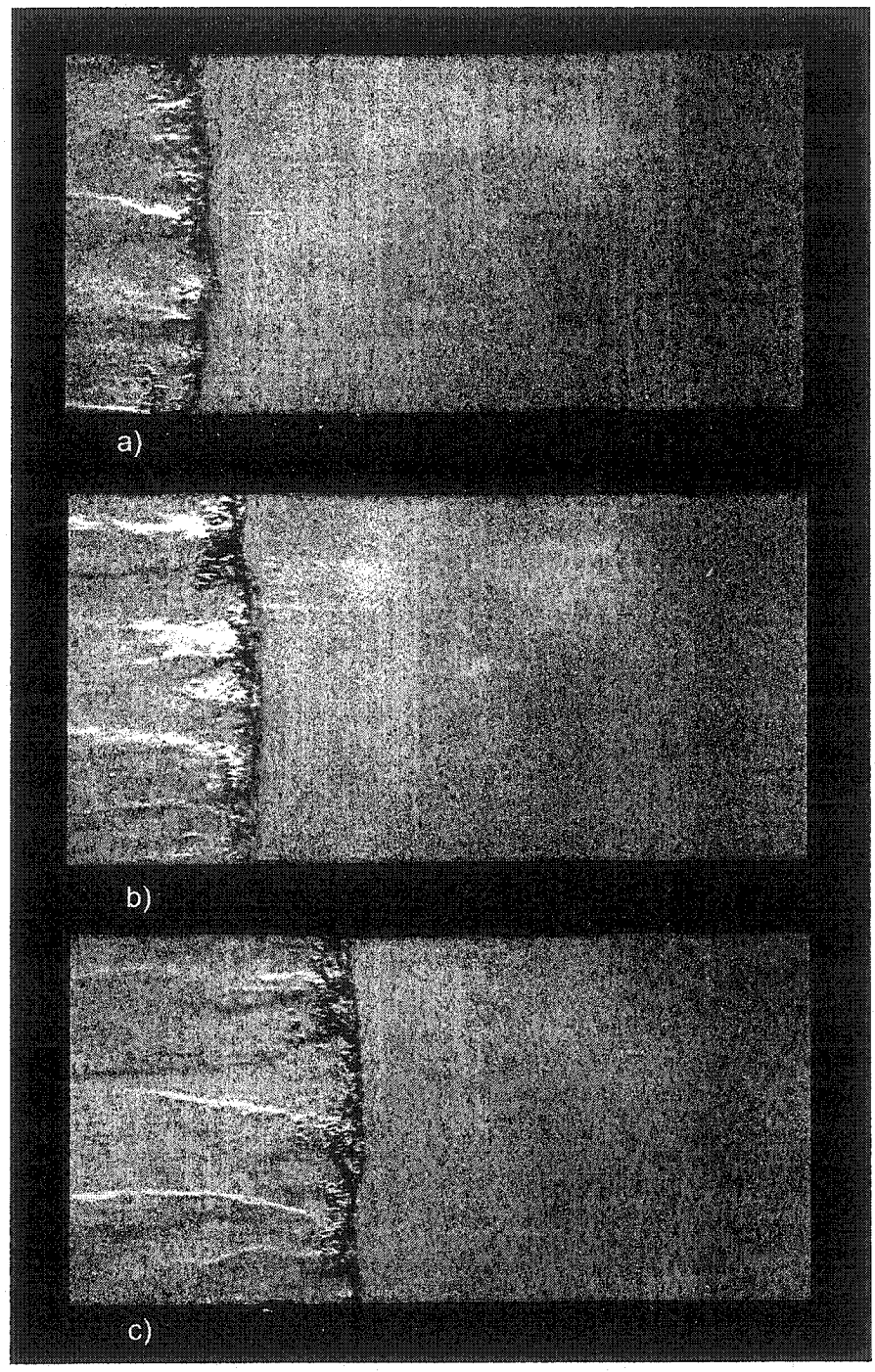

Fig. 3.14 Schlieren photographs in $C_3H_8 + 5O_2$ in the porous wall section of the channel, $P_o = 5.6$ kPa; left of the photograph corresponds to 1.5 channel heights downstream of the porous wall section entrance (see Fig. 3.15)

channel axis at $x \approx d$, the cells enlarge and new small scale triple points are re-

generated, which give rise to new transverse waves.

The photographs in Fig. 3.14 show the temporal evolution of the detonation front during this transient. Although the individual frames were taken from separate experiments, due to the reproducibility of the global features, they provide a time sequence of the important features of the flow field. Following the initial attenuation of the detonation wave and the first penetration of expansion waves, the frontal structure of the detonation wave becomes curved (Fig 3.14a). The reaction zone becomes thicker and the detonation bubbles extend further downstream. The attenuation due to the porous walls can be best seen at the bottom of Fig 3.14a, where, following the interaction of the triple point with the porous wall, un-reacted gas bubbles extends significantly further downstream. The thickening of the reaction zone near the triple point interactions is also visible on the top of Fig. 3.14b. However, following the initial attenuation of the detonation, the detonation structure is quickly re-established, as shown in Fig. 3.14c. The detonation frontal structure recovers part of its planarity due to the explosion of the un-reacted gas pockets, as indicated by the significant circular pressures waves observed in the wake of the detonation front. In conjunction with the smoke foils records (such Fig. 3.15), this clarifies the origin of new transverse waves in the detonation wave, following the attenuation at the porous walls. Owing to the instabilities at the reaction front, new pressure waves are generated from localized regions, which later coalesce and re-enforce the transverse wave

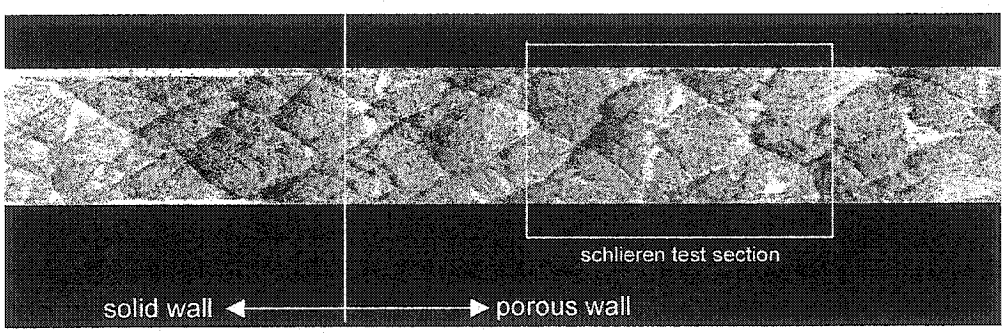

Fig. 3.15 Smoke foil obtained in $C_3H_8 + 5O_2$ detonations illustrating the flowfield corresponding to conditions in Figs. 3.14

spectrum. It is thus these small-scale instabilities in the reaction zone, which by generating new interacting pressure waves allow the detonation structure to be more robust, and thus overcome the losses to the porous walls.

Near criticality, the schlieren photographs indicate that the spotty reaction zone is further decoupled from the main front (Fig. 3.16). This is clearly evident in Figure 3.16c, where both at the top porous wall and at the bottom wall, the spotty reaction zone is decoupled from the main front due to the triple point reflections at the porous walls. The main transverse shocks are also damped, as they no longer appear in the wake of the detonation. The decoupling at these near limit conditions can thus be attributed to the increase in the rate of transverse waves attenuation at the wall. This leads to less turbulent interactions in the detonation structure, slower burning rates and hence detonation failure.

The conclusions that can be reached are that the reaction zone structure of highly irregular propane-oxygen detonations is highly turbulent and differs fundamentally from the piecewise laminar structure of previously studied regular structure mixtures such hydrogen-oxygen-argon. For the irregular turbulent detonations, the attenuation mechanism is due to the attenuation of the three-dimensional pressure waves, which are the means of the detonation wave to support gas ignition under more stringent conditions. The present experiments thus illustrate the important contribution of instabilities in the reaction zone to support a more robust mechanism of propagation.

3.5 Summary

The experiments conducted in the channel geometry permitted to clarify the flow fields and failure mechanisms of the different detonation systems studied. Two distinct behaviors were found. Mixtures that display a regular cell structure are attenuated gradually in the porous wall section. Re-initiation spots are seldom observed during the attenuation process and the transverse waves were found to be inconsequential in the damping limit, as two-dimensional and three-dimensional waves share the same limit, although the transverse wave density doubles from two to three dimensions. This indicates that the failure mechanism is by the global mass divergence generated by the porous walls.

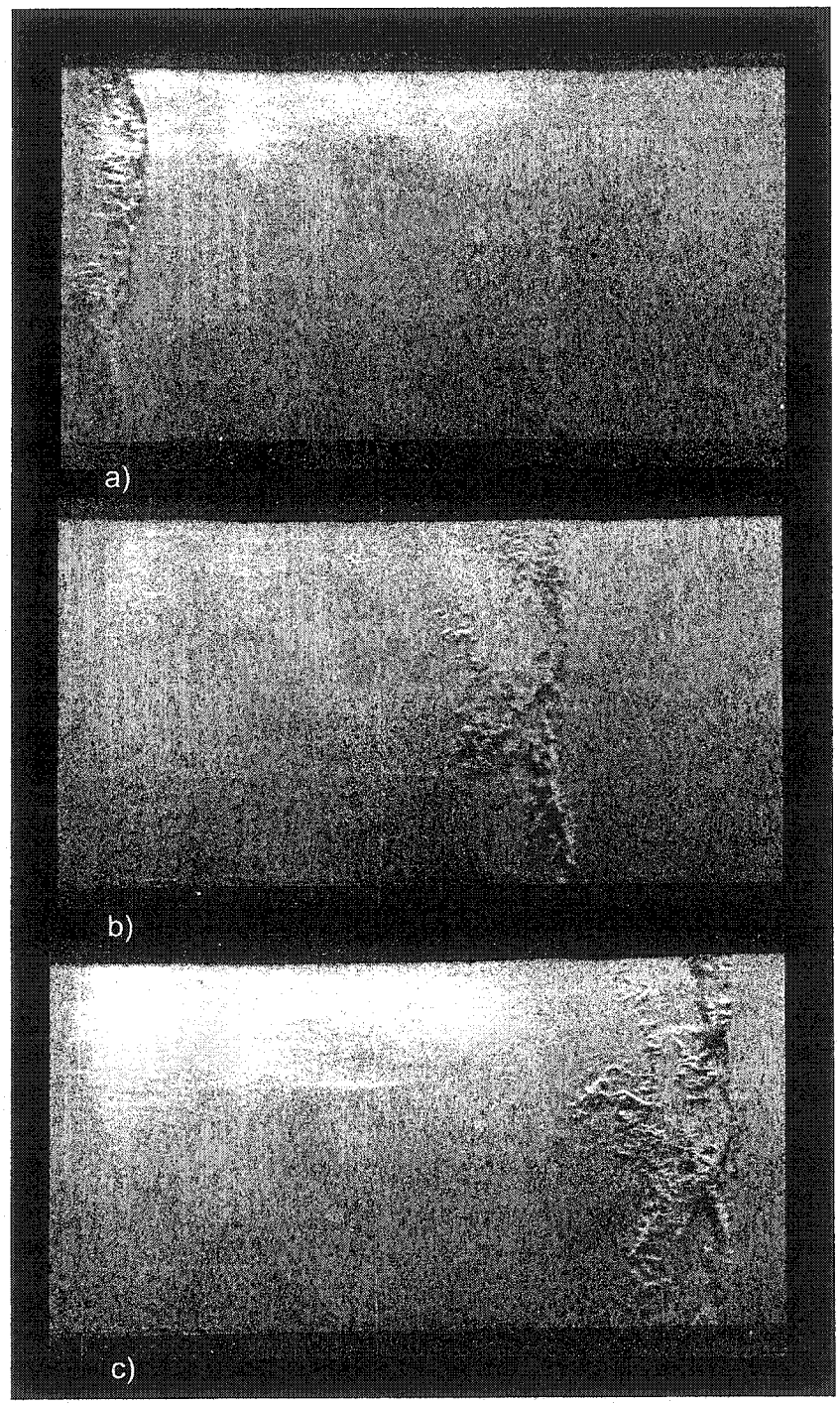

Fig. 3.16 Schlieren photographs illustrating marginal $C_3H_8 + 5O_2$ detonations in the porous wall section of the channel, P_o = 3.3 kPa; left of the photograph corresponds to 1.5 channel heights downstream of the porous wall section entrance (see Fig. 3.15)

On the other hand, mixtures exhibiting an irregular cell pattern,

characterized by a highly turbulent reaction zone, display the ability of flow re-organization during the attenuation process. New transverse waves are generated from local instabilities in the reaction zone. Although global mass divergence and transverse wave damping operate simultaneously, it appears that the failure limits is more closely governed by the competition between the local damping of these transverse waves at the porous walls and the regeneration of new transverse waves in the reaction zone.

Chapter 4 Limiting conditions for the existence of curved ZND detonations

4.1 Introduction

The experimental results obtained on the propagation and failure of gas detonations in porous wall tubes indicate that two distinct propagation and failure mechanisms operate in the mixtures investigated. The mixtures characterized by an irregular cell structure, such as the undiluted hydrocarbon-oxygen mixtures, rely on transverse wave re-generation to negate the losses to the porous walls. For these mixtures, a unique damping limit was found, namely $(d / \lambda)^* \approx 4$. On the other hand, for regular cell structure mixtures, the above criterion is not valid, nor was a universal criterion based on λ found. For these mixtures, transverse waves are found to be significantly weaker and the reaction zone takes on a piecewise laminar structure. The attenuation also appears to be independent of this (weak) three-dimensional structure. It thus appears profitable to attempt to model the latter mixtures by the one-dimensional ZND model (Fickett & Davis, 1979), which assumes that ignition is operated by adiabatic compression behind the leading shock, and neglects the influence of transport processes or transverse wave interactions. To model the present experiments, the one-dimensional model can be extended to include source terms, such a mass sink, to model the boundary conditions at the porous wall. The study of this model and comparison with experimental observations will permit further conclusions on the failure mechanism of the detonations investigated.

Significant work has been conducted on the critical conditions necessary for the existence of a quasi-steady ZND curved detonation waves (for review, see Klein, 1994). In the presence of mass divergence within the reaction zone, a competition exists between the chemical heat release rate which accelerates the flow to the sonic condition at the CJ plane and the diverging nozzle flow due to the lateral mass divergence, leading to a slowdown in the subsonic flow acceleration and exothermicity. Based on a quasi-steady weakly curved formulation and simplified one-step chemical kinetic model, it was found that a

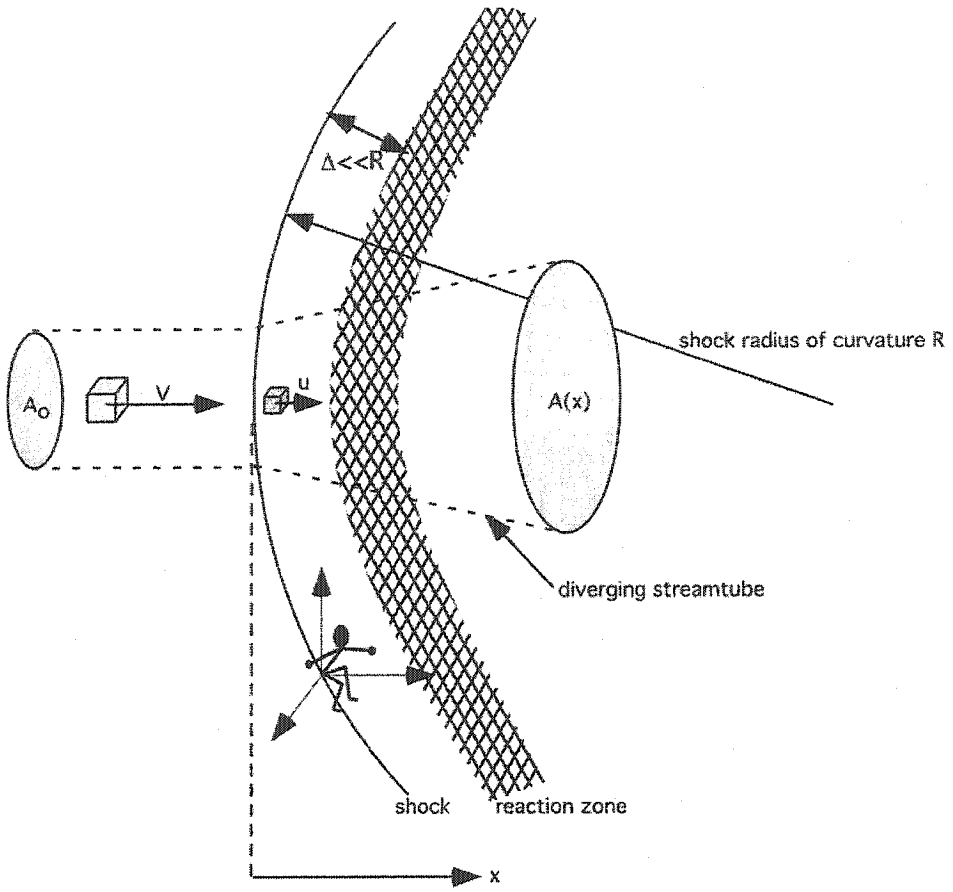

Fig. 4.1 Schematic illustrating the quasi-steady quasi-one-dimensional flowfield

limiting value of mass divergence exists that permits the existence of a self-supported detonation (He & Clavin, 1994, Klein et al., 1994, Yao & Stewart, 1995). For permissible values of mass divergence, the detonation exhibits a velocity deficit, which varies monotonically with the amount of mass divergence. So far, these previous analyses concentrated on simplified chemistry models with very few attempts involving more realistic chemistry (He, 1996, Klein et al., 1994), which were limited to hydrogen mixtures. It is thus worthwhile to extend the previous investigations by using realistic chemistry models, apply the formulation to the case of porous wall tubes (through suitable boundary conditions) and hence compare the theoretical predictions of detonations limits with those determined experimentally in the present study.

4.2 Formulation of the model

The formulation of the quasi-one-dimensional quasi-steady model presented below follows closely the work of Klein et al. (1994). In the presence of lateral mass divergence in a quasi-steady wave, the lateral mass losses can be modeled as source terms in the one-dimensional conservation equations of mass, momentum and energy (Fickett & Davis, 1979), written in a frame of reference fixed with the quasi-steady curved detonation (Fig. 4.1). For slightly divergent flow, the conservation laws of the quasi-one-dimensional flow with area change and chemical reactions can be written as:

$$\begin{aligned} &\frac{\mathrm{d}}{\mathrm{d}x}(\rho u A) = 0 \\ &\rho u \frac{\mathrm{d}u}{\mathrm{d}x} = -\frac{\mathrm{d}p}{\mathrm{d}x} \\ &\frac{\mathrm{d}}{\mathrm{d}x}\left(h + \frac{u^2}{2}\right) = 0 \\ &u\frac{\mathrm{d}y_i}{\mathrm{d}x} = \frac{W_i \dot{w}_i}{\rho} \quad (i = 1,\ldots,N_s) \end{aligned} \qquad 4.1$$

where u is the particle velocity and x is the distance behind the leading front (see Fig. 4.1). The net molar rate of creation of species i has been denoted $\dot{w}_i$, which can be computed once a chemical reaction mechanism and set of reaction rates for all N_s species have been specified. y_i is the mass fraction of specie i, W_i the molar mass of specie i, ρ is the mixture density, h the specific enthalpy, and p is the pressure.

For small-curvature quasi-steady waves the variation of the stream tube area $A(x)$ behind the leading shock is related to the wave frontal curvature κ or to the radial velocity transverse spatial derivative v_r by (Fickett & Davis, 1979)

$$\xi(x) = \frac{1}{A(x)}\frac{\mathrm{d}A(x)}{\mathrm{d}x} = \kappa\left(\frac{V}{u(x)} - 1\right) = \frac{j}{u(x)} v_r(x) \qquad 4.2$$

where V is the detonation velocity. The wave front curvature κ is given by

$$\kappa = \frac{j}{R} \qquad 4.3$$

where R is the front radius of curvature and j the geometric index (j =1, 2 for cylindrical or spherical waves respectively).

A more convenient form for integration of the governing equations (4.1) can be expressed in terms of the time coordinate t, which yields:

$$\begin{aligned}
\frac{1}{\rho u^2}\frac{dp}{dt} &= -\frac{(\dot{\sigma} - u\xi)}{1-M^2} \\
\frac{1}{\rho}\frac{d\rho}{dt} &= -\frac{(\dot{\sigma} - uM^2\xi)}{1-M^2} \\
\frac{1}{u}\frac{du}{dt} &= \frac{(\dot{\sigma} - u\xi)}{1-M^2} \\
\frac{dy_i}{dt} &= \frac{W_i \dot{w}_i}{\rho} \quad (i = 1, \ldots, N_s)
\end{aligned} \tag{4.4}$$

for which M is the particle Mach number ($M = u / c$, c is the local sound velocity) in the frame of reference of the leading shock and the exothermicity parameter $\dot{\sigma}$ is used to denote the non-dimensional chemical energy release rate:

$$\dot{\sigma} = \sum_{i=1}^{N_s} \left(\frac{W}{W_i} - \frac{h_i}{c_p T} \right) \frac{dy_i}{dt} \tag{4.5}$$

where W is the mean molar mass of the mixture, c_p is the mixture specific heat at constant pressure, and h_i is the specific enthalpy of specie i.

It can be seen that when the rate of mass divergence $u\xi$ is zero, the above equations reduce to the one-dimensional steady ZND formulation (Fickett & Davis, 1979). The RHS of the above ODE's give the rate of change of the various dependent variables, revealing explicitly the competing role of exothermicity and area divergence, i.e. between $\dot{\sigma}$ and $u\xi$. Since the flow velocity in the shock fixed frame is initially subsonic behind the leading shock, the exothermicity tends to accelerate the flow to the sonic condition, while area divergence tends to decelerate the flow.

The boundary conditions for the above system of equations must be imposed at the shock front and at the termination of the reaction zone. At the shock front ($t = 0$, $x = 0$), the field variables must satisfy the normal shock jump conditions given by the Rankine-Hugoniot equations for frozen chemistry (Fickett & Davis, 1979). The post shock state variables are a function of the detonation velocity V, so that the entire detonation structure will be parameterized by V. At

the rear of the reaction zone, the generalized Chapman-Jouguet criterion must be satisfied, where, for a regular solution free of singularities, both the top and bottom of the right hand side in (4.4) must simultaneously vanish. In words, a regularity condition corresponds to the conditions that:

a) when the flow is choked in the frame of reference of the leading shock, i.e.,

$$u = c \tag{4.6}$$

b) the rate of chemical energy release must balance the rate of mass divergence, i.e.,

$$\dot{\sigma} = u\xi \tag{4.7}$$

For a fixed value of wave curvature κ (or equivaluently $\xi(t = 0)$), the correct detonation velocity V is found by satisfying the regularity conditions (4.6) and (4.7). It can be noted that with $\xi = 0$, the regularity condition is the well-known Chapman-Jouguet criterion that requires the flow field to reach unity Mach number as the reactions come to completion ($\dot{\sigma} = 0$). The problem at hand is thus a two-point boundary value problem with a regularity condition at one end point that determines the eigenvalue solutions $V(\kappa)$. For realistic thermodynamic properties and reaction rate laws, the above system of equations is solved numerically. The numerical procedure to solve these equations is as follows. For a given initial gas state and a fixed value of wave curvature κ, the detonation velocity V is input as a guess. This permits to initialize the state variables at the Von Neumann state. The system of ODE's are then numerically integrated in time, until either of the conditions 4.6 and 4.7 is met. The correct initial guess for the detonation velocity is only achieved when both conditions 4.6 and 4.7 are met simultaneously. This shooting method was used in order to determine the correct $V(\kappa)$ relationship for a given mixture.

The system of equations were numerically integrated with a Fortran code initially developed by Shepherd for a one-dimensional ZND reaction zone structure (Shepherd, 1986), by including the modifications due to area divergence. The code is linked to the CHEMKIN II package (Kee et al., 1989) in order to compute the necessary thermodynamic data and different chemical kinetic rates.

Table 4.1 Summary of the detonation properties at the maximum permissible curvature of the front

Mixture	P_o [kPa]	V_{CJ} [m/s]	Δ_{CJ} [mm]	κ^* [cm^{-1}]	$\Delta_{CJ}\kappa^*$	$(V/V_{CJ})^*$	Δ^*/Δ_{CJ}
$2H_2+O_2$	23.5	2758	0.200	0.323	0.0065	0.87	3.4
$2H_2+O_2+2Ar$	24.25	1990	0.183	0.308	0.0056	0.83	4.4
$2H_2+O_2+N_2$	35.5	2361	0.174	0.320	0.0056	0.88	3.2
$C_2H_2+2.5O_2+10.5Ar$	26.5	1714	0.138	0.406	0.0056	0.84	4.2
$C_3H_8+5O_2$	11.5	2258	0.209	0.115	0.0024	0.92	3.2
CH_4+2O_2	34.5	2345	1.097	0.027	0.0029	0.94	2.6

4.3 $V(\kappa)$ laws for the mixtures investigated

Following the formulation presented above, we have integrated the governing equations coupled with the corresponding chemical kinetic models for the mixtures investigated. In all cases, the initial gas state of the mixtures corresponds to T_o = 298K and the initial pressure found critical in the 41mm porous tube experiments presented in Chapter 2. These parameters and results of the simulations are given in Table 4.1. The detonation velocity dependence on curvature (i.e. the $V(\kappa)$ relationship) was found for each of the mixtures. For the acetylene, propane and hydrogen mixtures, the San Diego kinetic mechanism was used due to its accuracy in predicting experimental shock tube ignition delays in these mixtures (Varatharajan & Williams, 2001, 2002). For methane detonations, this mechanism is not appropriate. For this reason, the kinetic mechanism developed by Lutz et al. (1988) was used instead. The integration of the reaction zone structure in undiluted oxy-acetylene mixtures did not yield accurate results in the re-combination zone, hence is omitted. The results are presented in graphical form in Figure 4.2. The eigenvalue detonation velocity $V(\kappa)$ is normalized by the Chapman Jouguet velocity obtained for zero curvature V_{CJ}. For all mixtures, the eigenvalue CJ velocity obtained by the iteration method outlined above corresponded to within 1% to the value computed with the CEA equilibrium code (Gordon & McBride, 1994).

The $(V(\kappa))$ / $V_{CJ})$ curves shown in Fig 4.2 for the various mixtures reveal the nonlinear dependence between wave curvature and detonation velocity. For

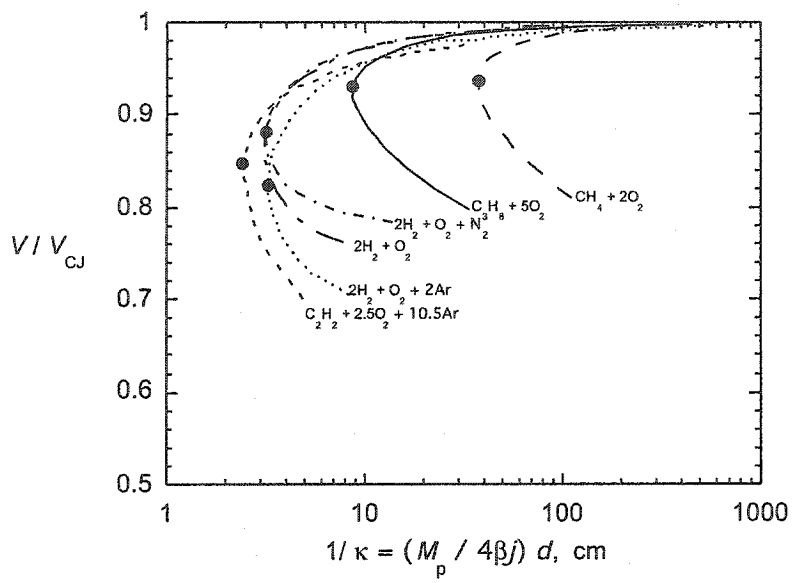

Fig. 4.2 The eigenvalue detonation velocity, normalized by the Chapman-Jouguet velocity of a planar detonation, in terms of wave curvature κ for the mixtures investigated; (●) indicates the turning point (maximum permissible curvature) below which the solution is not physical

increasing values of wave curvature, the detonation has a higher velocity deficit. These curves also display a turning point (κ*, *V**), corresponding to the maximum permissible curvature beyond which a sonic plane does not exist. Beyond this limit, the physical interpretation is that any disturbance behind the detonation wave can catch up to it and quench it, hence not permitting the existence of a self-sustained detonation. The lower branch of the curve is unstable (Klein, 1994) so only the top branch has a physical meaning.

An example of the ZND detonation wave structure in the absence of losses and at the maximum curvature condition is shown in Fig. 4.3 for the $C_2H_2 + 2.5O_2$ + 75%Ar mixture. The temperature and exothermicity profiles in the reaction zone are shown. As a result of the lower detonation velocity in the curved detonation, the shock temperature is lower. The combined effects of lower temperatures and smaller particle accelerations in the induction stage lead to

larger induction zone lengths. The induction zone length, Δ^* is approximately 4 times larger than the induction zone length in the planar CJ wave, Δ_{CJ} (the induction zone length has the usual definition as the distance between the shock to the maximum in exothermicity). Due to the mass divergence and lower temperatures in the reaction zone, the rate dependent exothermic rates are also reduced and the exothermicity drops, delaying the total energy release. Similar profiles were obtained for the other mixtures. It can thus be concluded that the effect of area divergence is manifested in both the induction and reaction zone of the ZND reaction zone structure.

4.4 Comparison with experimental limits

From the nonlinear detonation velocity dependence on curvature $V(\kappa)$ showed in Fig. 4.2, one can define the limiting values of wave curvature κ^* and velocity deficit $(V/V_{CJ})^* \equiv V/V_{CJ}(\kappa^*)$ corresponding to each turning point. These

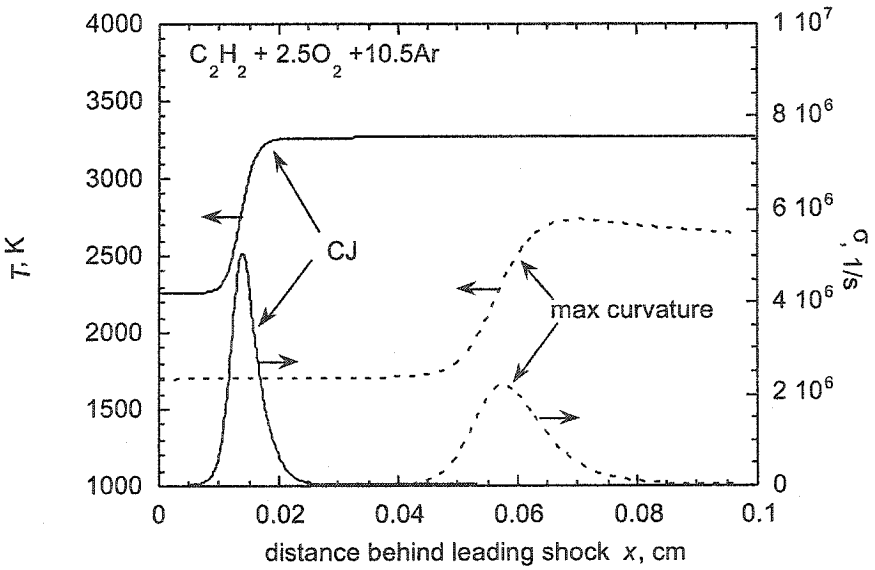

Fig. 4.3 The ideal ZND reaction zone structure (temperature and exothermicity) in C_2H_2 + 2.5 O_2 + 75%Ar; full lines are for the planar detonation, broken lines at the maximum curvature condition

values are tabulated in Table 4.1. Since all the simulations were conducted for the initial pressures corresponding to the critical damping limit in a porous wall tube of *constant* diameter (d = 41mm), it is worthwhile comparing the critical velocity deficit $(V / V_{CJ})^*$ and the length scale characterizing the critical curvature $(1/\kappa)^*$ between *a*) the various mixtures and *b*) between numerical results and experimental observations.

From Table 4.1, it can be seen that for the hydrogen-oxygen mixtures and for the acetylene-oxygen mixture diluted with 75% argon, approximately the same value of curvature is obtained, ~ 0.3 - 0.4 cm^{-1}. Since the simulations were conducted for mixtures exhibiting the same experimental damping limit (same porous tube diameter and material), this observation suggests that curvature dictates the limit for these mixtures in the experiments. The predicted velocity deficits computed for these regular structure mixtures $(V / V_{CJ})^* \approx 0.85$ are also in very good agreement with the experimental values of ~0.8-0.85. Furthermore, at criticality, the induction zone length Δ^* increases by a factor of ~3-4 at the maximum curvature condition with respect to the induction zone in the undisturbed region Δ_{CJ} (see Table 4.1). If one accepts the one-to-one correspondence between induction zone length and cell size for a given mixture, as established phenomenologically in previous studies (Lee, 1984, Gavrikov et al., 2000), then the theoretical result is consistent with the experimental observation that cells increase by a factor of approximately 3 at the critical conditions for failure (e.g., Fig. 3.5) for the mixtures characterized by a regular cellular structure. These observations indicate that the failure mechanism in the experiments is consistent with the limits of weakly curved ZND detonations, where the influence of the transverse wave structure is a priori neglected.

For propane and methane mixtures, the critical wave curvatures κ^*'s predicted (see Table 4.1) do not agree neither between the two mixtures (order of magnitude differences) nor with the other regular cell mixtures. Furthermore, the predicted limiting values of detonation velocity deficit of 5 to 10% are significantly different than observed experimentally, i.e. ~30%. The experimental velocity deficit being significantly higher than the value predicted indicates that

these irregular structure mixtures can propagate under conditions where regular structure detonations would fail. This indicates the inadequacy of the steady ZND model to capture the failure mechanism in these mixtures, as was already observed from the visualization experiments.

In order to quantitatively compare the experimentally determined limits with the critical curvature predictions based on quasi-one-dimensional ZND detonations, it is necessary to estimate the dependence between wave curvature κ and mass divergence into the permeable walls of the porous wall tubes used in the experiments. The boundary condition at the porous tube walls can be approximated as a mass sink to the pores of the tube. In the quasi-one-dimensional formulation used, the curvature κ (or area divergence) at the front can be expressed in terms of the rate of mass divergence given by equation (4.2). The transverse velocity derivative v_r can be estimated directly. Since the average pressure within the detonation reaction zone is usually higher than ambient by a factor of ~20, the flow velocity into the pores of the steel mesh wall is choked, propagating radially at local sonic velocities. Due to the finite porosity of the wall, only part of the gas will escape at sonic velocity c, the other facing the impermeable parts of the wall. Taking into account the open area ratio of the mesh wall used in the present experiments ($\beta = 0.3$), the radial velocity at the walls becomes

$$v(d/2) \cong \beta c \qquad 4.8$$

Expanding the radial velocity in a Taylor's expansion and noting that both the radial velocity and its derivative vanish at the tube (or channel) axis, to leading order we have

$$v(r) \propto r^2 \qquad 4.9$$

At the walls (i.e., $r = d / 2$), where the maximum curvature is expected in the experiments, the lateral derivative v_r thus becomes:

$$v_r = \frac{4\beta c}{d} \qquad 4.10$$

where c is the local sonic velocity in the reaction zone and d the tube diameter (or channel height). Making use of equation 4.2, the curvature κ can thus be expressed in terms of the tube diameter d:

$$\frac{j}{\kappa} = \left(\frac{V-u}{c}\right)\frac{d}{4\beta} \equiv \frac{M_p}{4\beta}d \qquad 4.11$$

where M_p, the particle Mach number in the laboratory frame of reference is evaluated at the Von Neumann state. Typical values of M_p for the mixtures investigated are tabulated in Table 4.2, as computed with the CEA code for frozen chemistry across a shock moving at CJ velocity. Expression 4.11 thus provides the link between wave curvature and porous tube diameter in terms of the wall porosity β. It also should be noted that expression (4.11) shows explicitly the link between the limiting tube diameter or channel height d. In the circular tube experiments, the mass divergence is three-dimensional and the frontal curvature is spherical ($j = 2$). Alternatively, for channel experiments, the mass divergence is two-dimensional and the frontal curvature is cylindrical ($j = 1$). Hence, from (4.11), for a given mixture characterized by an unique critical curvature κ^*, the limiting tube diameter $d^*_{j=2}$, is two times larger than the critical channel height $d^*_{j=1}$:

$$d^*_{j=2} = 2d^*_{j=1} \qquad 4.12$$

As noted in the previous chapter, this agrees with the experimental observation that the failure limit obtained in the tube geometry for the acetylene-oxygen-argon (dilutions above 70% argon) are approximately twice more severe than in the channel experiments (i.e. $d^*_{\text{tube}} = 2d^*_{\text{channel}}$), as shown in Fig. 3.9. This further suggests that failure in these regular structure mixtures is well approximated by the global mass divergence mechanism. For the undiluted hydrocarbon-oxygen mixtures, which are characterized by irregular structures and turbulent reaction zones, condition (4.12) is not verified. Instead, the failure limit is identical in the channel and tube experiments. It is also worthy to stress out that a global area divergence formalism, even derived on a statistical average basis, could not reproduce this experimental result. For example, when the global area divergence is approximated from a hydrodynamic averaged form of the reaction zone

structure in cellular detonations (Murray and Lee, 1986), relation (4.12) still holds theoretically, but does not reproduce the present experimental results. It can thus be concluded that the mass divergence mechanism is not applicable to the irregular structure mixtures, where the local details of transverse wave interactions need to be taken into account.

Using equation 4.11 and the critical values of wave curvature determined numerically (see Table 4.1), we can thus compare the predicted critical porous wall tube diameter d_{model} with the actual experimental value in which the experiments were performed ($d_{\text{exp}} = 41\text{mm}$). The meaning of d_{model} is simply the porous wall tube diameter where the given mixture is *expected* to fail, i.e., the critical tube diameter that permits the existence of a quasi-one-dimensional ZND detonation wave. The results are tabulated in Table 4.2. As can be seen, the agreement between the experimental value and the predicted value is excellent for the hydrogen mixtures and for the acetylene mixture diluted with argon. These mixtures are characterized by *regular* cellular structures. This indicates that the mass divergence failure mechanism is appropriate for describing the detonation limits in porous walls tubes for regular cell structure mixtures, where three-dimensional effects are rather weak.

On the other hand, for propane and methane detonations, the predicted porous tube diameter d_{model} is found to be well in excess of the experimental values. For methane-oxygen mixtures, d_{model} is larger than the experimental value by an order of magnitude. Among the mixtures studied, oxy-methane detonations

Table 4.2 Comparison between the theoretical damping limit based on quasi-one-dimensional limiting ZND detonations and experimental values

Mixture	*Cell regularity*	M_p	$d_{\text{model}} = \frac{4\beta j}{\kappa^* M_P}$, mm	d_{exp}, mm
$2H_2 + O_2$	Good	1.82	**41**	41
$2H_2 + O_2 + 2Ar$	Excellent	1.62	**48**	41
$2H_2 + O_2 + N_2$	Fair	1.82	**41**	41
$C_2H_2 + 2.5O_2 + 10.5Ar$	Good	1.61	**37**	41
$C_3H_8 + 5O_2$	Poor	2.87	**73**	41
$CH_4 + 2O_2$	Very poor	2.51	**360**	41

are also the mixtures displaying the most irregular cell structures. These large over-predictions in the failure limit indicate that in the experiments, the detonations propagate well beyond the one-dimensional curvature limit, in porous tubes of much smaller diameter. This is consistent with the experimental observations that in these mixtures, transverse wave interactions and turbulent ignition play a significant role in sustaining the detonation propagation, and the limit is more closely governed by the rate of transverse wave damping at the porous walls.

4.5 Comparison with previous diffraction experiments

The present treatment could be easily extended to the detonation diffraction problem, provided the attenuation in the diffraction problem is quasi-steady, i.e. occurs on long time scales under which the quasi-steady assumption of the above model is valid. For regular structure mixtures such the acetylene-oxygen mixture diluted with a significant amount of argon, the diffraction experiments revealed that the attenuation process operates on very long length scales with respect to the tube diameter (Lee, 1996, see Chapter 1), hence the quasi-steady approximation is valid. For the diffraction process, the characteristic velocity of mass divergence during the expansion process is the sonic velocity in the products. For this reason, the model developed above can be directly applied by setting

$$\beta_{CT} \approx 1 \qquad 4.13$$

By virtue of (4.11), we thus expect that the critical tube diameter for diffraction be larger than the critical porous wall tube diameter used in the present study ($\beta = 0.3$) by a factor of 3 for the same mixture (same κ^*). This is in good agreement with experiment. For diffraction from tubes in regular structure mixtures, Desbordes et al. (1993) empirically found that $(d / \lambda)^* \approx 26$ for oxy-acetylene mixtures diluted with 81% argon. This value is higher that the present value found in porous wall tubes of $(d / \lambda)^* \approx 11$ in the same mixture by a factor of 2.4. Similarly, from the diffraction in two-dimensional channels shown in Fig. 1.2 (Lee, 1996), we deduce that $(d / \lambda)^* \approx 18$, higher than the experimental value

found in the two-dimensional porous wall channels (i.e., $(d/\lambda)^* \approx 5.5$) by a factor of 3.3. Since the present quasi-one-dimensional theory was found to predict very well the limits in the porous wall tubes in these mixtures, it thus follows that the extension to the diffraction experiments in regular structure mixtures is equally valid.

For the irregular structure mixtures, the curvature formalism is not applicable to the diffraction problem for the same reasons why it is not applicable to the porous walled tubes experiments, as described above. For example, by applying the model to the diffraction problem in these mixtures, an order of magnitude difference between experimental and theoretical limits is obtained in methane-oxygen detonations. Furthermore, a global curvature formalism, for which inevitably relation (4.12) is obtained, is in direct contradiction with experiment. Liu et al. (1984) determined that the limit in wide two-dimensional channels is approximately $d^* \cong 3\lambda$, while in the circular tube, the limit is approximately $d^* \cong 13\lambda$ in a wide range or irregular structure mixtures (Lee, 1984). This departure from the factor of two expected theoretically was in fact the first quantitative indication that three-dimensional effects (transverse waves) need to be considered when describing detonation limits in irregular structure mixtures.

4.6 Summary

Comparison between the quasi-1D ZND predictions and the present experiments in porous wall tubes provides a means to interpret the experimental observations in mixtures displaying regular cell structures and weak transverse waves. This indicates that the ZND model is adequate to capture the essential physical processes in real detonations for which the reaction zone is piecewise laminar. Although transverse wave structures are observed in the experiments, it appears that models devoid of any transverse wave structures, based on the one-dimensional ZND model, may provide useful approximations for these detonations. In comparing the limits observed experimentally with the predicted values, very good agreement was found. However, it was found that mixtures

characterized by strong transverse waves and irregular structures cannot be approximated by the curved ZND model.

Chapter 5 Discussion

5.1 The failure and propagation mechanisms of regular and irregular detonations

The results of the experiments conducted in porous wall tubes and channels have revealed two distinct failure mechanisms. Mixtures characterized by regular cellular structures and weak transverse waves, such as oxy-hydrogen or oxy-acetylene diluted with large amounts of argon, were found to fail by the global mass divergence mechanism. The experiments also showed that the existence of weak transverse waves in these mixtures was inconsequential.

Visual observations of the reaction zone structure in these mixtures revealed a piecewise laminar structure, as postulated in the ZND model (Fickett & Davis, 1979). Independent observations (Shepherd et al., 2002) of the OH radical distribution in the reaction zone structure of hydrogen-oxygen detonations by the PLIF technique revealed that indeed ignition was operated mainly behind the leading shocks, with no significant contribution from the weak transverse waves.

In conclusion, the propagation mechanism of these detonations is well approximated by the classical ZND model: a leading shock compresses the gas to high enough temperature permitting auto-ignition. The driving mechanism of such a ZND detonation wave is by the gasdynamic expansions of the detonation products, which by expanding do work and thus sustain the leading shock. The above detonations are henceforth called *piece-wise laminar*, since the propagation mechanism postulated in the ZND model appears valid in describing their propagation and limits.

On the other hand, the reaction zone structure of irregular-cell detonations revealed that large three-dimensional instabilities appear in the form of discrete exothermic centers forming a turbulent fine scale reaction structure. It can be speculated that due to these instabilities, the detonation structure develops an irregular structure of transverse waves of significant strength, as observed experimentally on smoke foils and from pressure recordings. In the failure experiments, the detonations propagated well beyond the one-dimensional limit

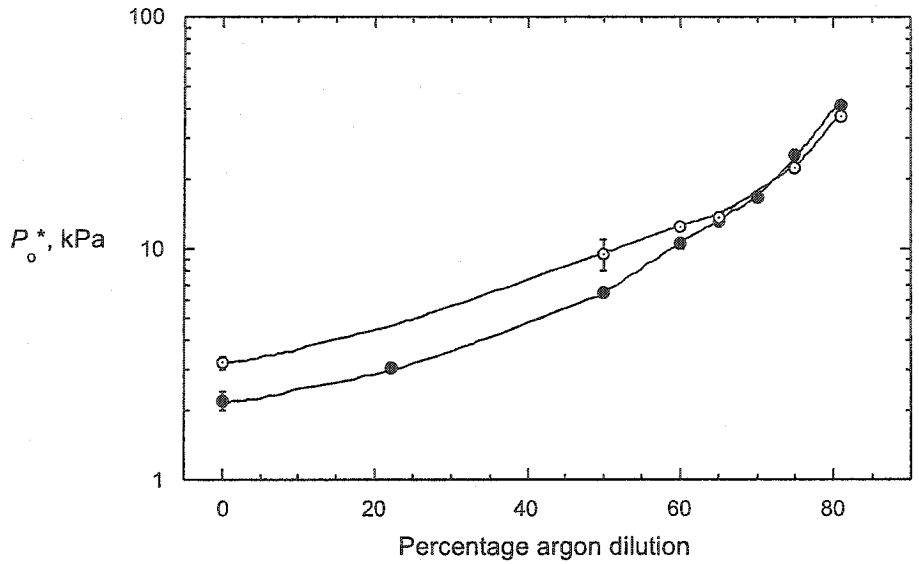

Fig. 5.1 Variation of the critical pressures P_o* in the (d = 41 mm) porous walled tube experiments (●) and in the (d = 25.4 mm, w = 4 mm) porous walled channel experiments (⊙) in C_2H_2 + 2.5 O_2 + %Ar

predicted via the ZND model. We attribute this finding to the three-dimensional instabilities observed, which permit detonation self-sustenance where compression by the leading shock alone in one dimension (longitudinally) is insufficient.

The conclusions that can be reached is that the propagation and failure mechanism in the irregular structure mixtures is fundamentally different than the mixtures characterized by piece-wise laminar reaction zone structures, for which the ZND model was adequate. We thus label these detonations as *turbulent*, to bring out the fact that their reaction zone structure is highly unstable, the reaction zone is turbulent and the propagation mechanism is no longer well approximated by the classical ZND mechanism. The propagation mechanism of these detonations is further examined in the remainder of the discussions and the role played by hydrodynamic compressible turbulence is explored.

5.2 The transitional behavior of failure mechanism from regular to irregular structures

The results obtained experimentally on the failure mechanisms in regular and irregular structure detonations point out the existence of an abrupt transition between the failure limits. The results supporting this observation have been presented in Chapters 2 and 3, and summarized graphically in Fig 3.9. Fig 3.9 shows the $(d / \lambda)^*$ limits obtained in the tube and channel experiments as a function of argon dilution in acetylene-oxygen mixtures. A discontinuous bifurcation can be observed on this graph at approximately 60% argon dilution. Above this dilution, the limits in the tubes are twice more severe than in the channel experiments, suggesting that the global failure mechanism is by the global mass divergence (see Chapter 4 for discussion). Below 60% argon, the limits in the tube and channels are identical but different from the high argon dilution case, suggesting that the transverse wave mechanism governs the failure limit (see Chapter 3 for discussion). This result suggests that the failure mechanism undergoes a change at approximately 60% argon dilution. As was already noted, this critical value of argon dilution corresponds very well with the value reported in previous studies on cell regularity (Shepherd, et al. 1986, Vandermeiren & Van Tiggelen, 1984) for the transition between regular to irregular cellular structures.

Nonetheless, the variation of the critical pressure in the tube and channel experiments (shown in Fig. 5.1), from which Fig. 3.9 was obtained, indicates a smooth change in limits as the argon dilution is varied. This important observation indicates that the switchover in failure mechanism is likely to be more gradual.

To reconcile the observation that the change in failure mechanism is gradual (when looking at P_o^*) as a function of argon dilution and abrupt when the limit $(d / \lambda)^*$ is considered, we investigated two possible explanations: *a*) abrupt changes in the chemical kinetics with increasing argon dilution, or *b*), abrupt changes in the detonation dynamics for smooth changes in the chemical kinetics. Detailed chemical kinetic simulations of the ZND reaction zone structure revealed

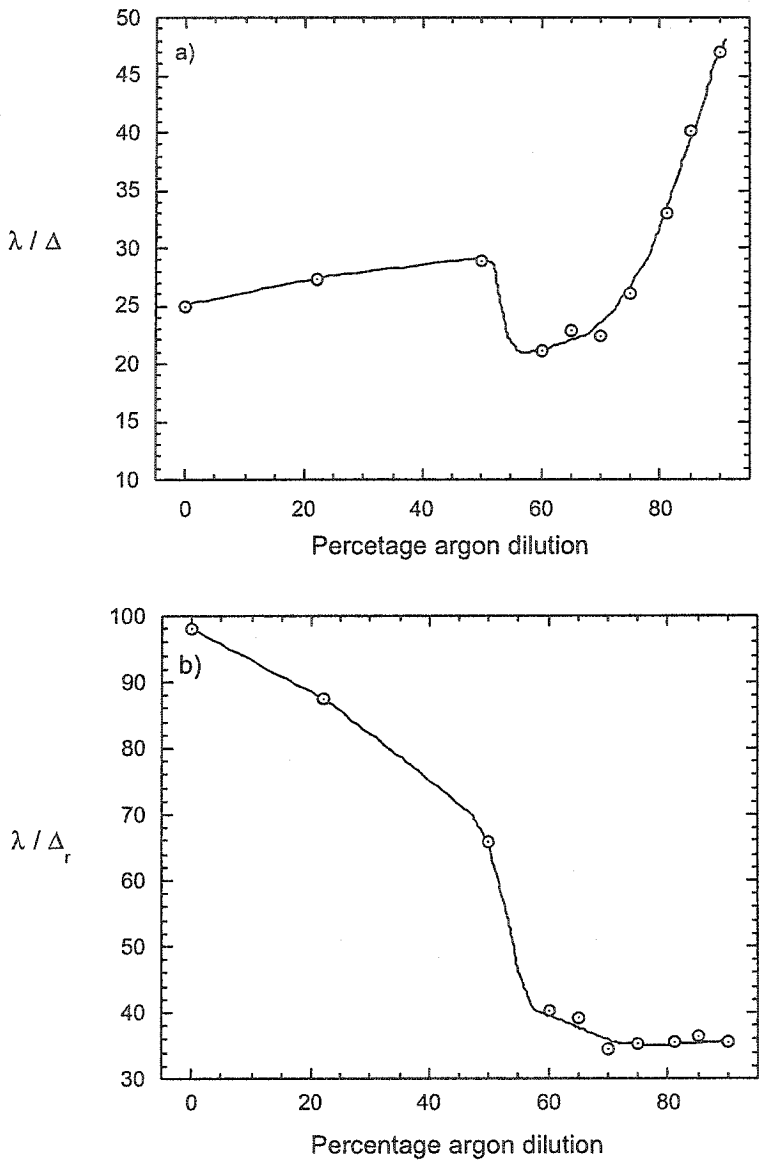

Fig 5.2 Variation of the cell size λ with a), induction length Δ, and b), with reaction length Δ_r as a fuction or argon dilution in $C_2H_2 + 2.5O_2 + \%Ar$

that all quantities (detonation velocity, shock temperature and pressure, induction and reaction lengths, activation energies, heat release, specific heat ratios...) vary smoothly with increasing argon dilution (see Radulescu et al, 2002). Hence only the second possibility could account for this abrupt change in the limits.

To investigate the change in detonation dynamics length scales with varying argon dilution, the relationship between the characteristic transverse wave spacing λ was systematically compared to the characteristic induction and reaction length scales, respectively Δ and Δ_r, computed from the steady ZND profiles (obtained as outlined in Chapter 4). The induction length Δ is taken as the distance from the shock to the point of maximum exothermicity $\dot{\sigma}_{max}$, and the reaction length is defined as

$$\Delta_r \equiv \frac{u_{\dot{\sigma}=\dot{\sigma}_{max}}}{\dot{\sigma}_{max}} \qquad 5.1$$

where $u_{\dot{\sigma}=\dot{\sigma}_{max}}$ is the particle velocity in the shock fixed reference frame at the point where exothermicity is maximum and $1/\dot{\sigma}_{max}$ is the characteristic time for the chemical energy release (see Appendix 2). The variation of cell size λ with these two length scales is shown in Figure 5.2, as computed for the initial pressures P_o* obtained in the tube experiments (Fig. 5.1). Separate experiments were conducted to measure the cell size at 85% argon dilution and 90% argon dilution (see below). Both the variations of (λ / Δ) and (λ / Δ_r) display a strong discontinuity at approximately 60% argon dilution. This indicates that the dynamics of the detonation wave undergo a bifurcation-like transition at this critical value of argon dilution, thus clarifying the bifurcation of the failure limit (d / λ)* observed experimentally. The variations of the (λ / Δ) and (λ / Δ_r) with argon dilution are also quite instructive. It appears that for dilution above 60%, (λ / Δ_r) is a constant, indicating that the length of the exothermic region controls the cell spacing for regular structure detonations. This is consistent with Strehlow's observations that for regular structure detonations, the long reaction length is a more appropriate length scale (Strehlow and Engel, 1969). For dilutions below 60% argon, the cell size appears to be better controlled by the induction length, as is usually assumed (Gavrikov et al., 2000).

5.3 The origins of the cellular structure in regular and irregular structures

At present, the origins of the cellular structures in gaseous detonations are still unresolved. However, the results of the present study suggest that detonations characterized by regular structures are well approximated by the ZND model in terms of their failure limits. For this reason, it appears worthwhile to study the transient behavior of unsteady ZND detonations and hence clarify the

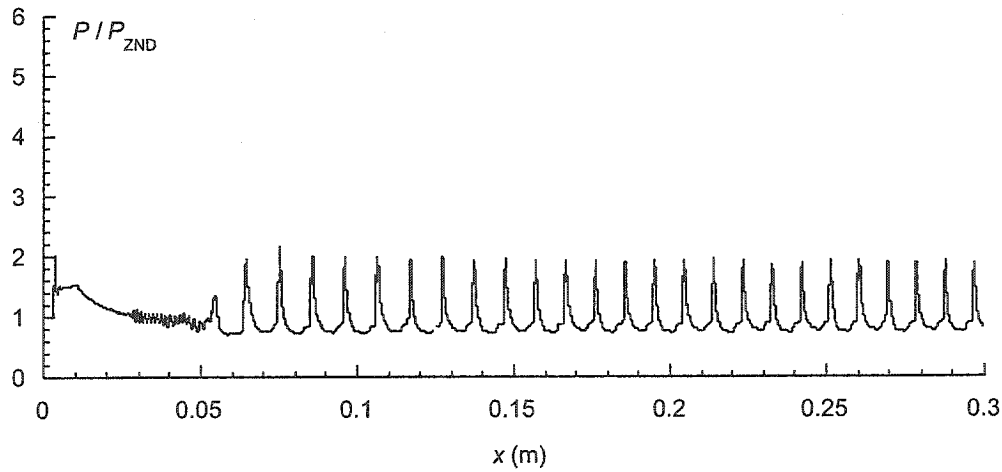

Fig. 5.3 Leading shock pressure oscillations (P / P_{ZND}) in terms of shock position in $C_2H_2 + 2.5O_2 + 90\%Ar$, $P_o = 100kPa$, $T_o = 298K$ (from Radulescu et al, 2002)

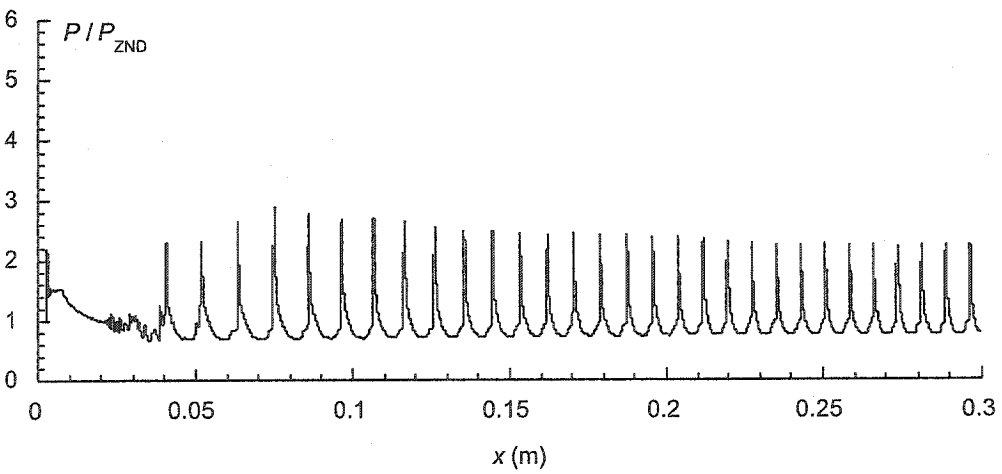

Fig. 5.4 Leading shock pressure oscillations (P / P_{ZND}) in terms of shock position in $C_2H_2 + 2.5O_2 + 85\%Ar$, $P_o = 60kPa$, $T_o = 298K$ (from Radulescu et al, 2002)

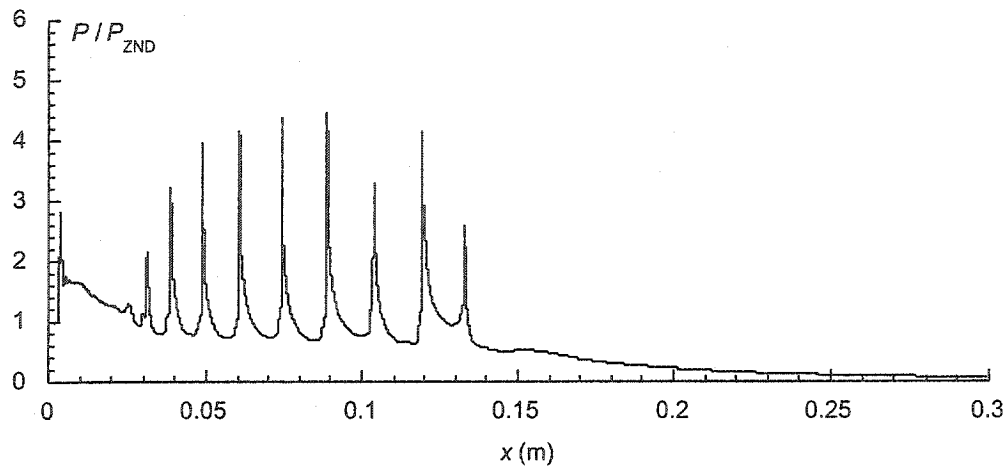

Fig. 5.5 Leading shock pressure oscillations (P / P_{ZND}) in terms of shock position in C_2H_2 + 2.5O_2 + 70%Ar, P_o = 16.3 kPa, T_o = 298K (from Radulescu et al, 2002)

origin of the weak transversal structure in these mixtures and the changes in the detonation wave dynamics as the argon dilution is decreased, as outlined in the previous section.

We hence performed numerical simulations of Eulerian acetylene-oxygen-argon detonations in one-dimension with realistic chemistry. The details of the simulations can be found in (Radulescu et al., 2002). The results of the simulations are shown in Figures 5.3 to 5.5. For sufficiently high argon dilution (85% and 90% argon), the detonation propagates in a periodic oscillatory mode with leading shock pulsations of weak amplitude (Fig. 5.3 and 5.4). For decreasing argon dilutions, the amplitude of the pressure pulsations increase, revealing the role of argon dilution on the stability of ZND detonations. However, when the argon dilution was decreased below 70%Ar (Fig. 5.5), a self-supported oscillatory detonation was not possible.

The numerical results obtained are in good agreement with experimental observations, which indicate that cells become highly regular with weak transverse waves for increasing argon dilutions. Typical experimental smoke foils obtained for 85% and 90% argon dilution are shown in Fig. 5.6, where highly regular cells can be observed with weak transverse waves interactions. At

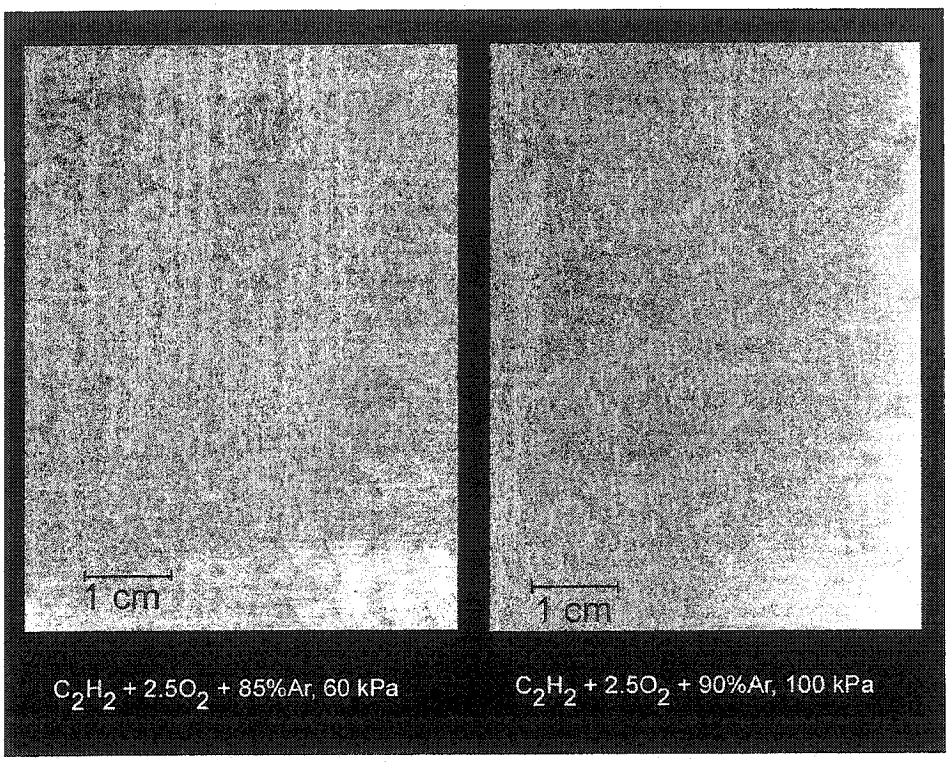

Fig. 5.6 Experimental soot foils obtained across a 20 cm-diameter tube revealing the cellular structure of $C_2H_2 + 2.5O_2$ diluted with *a*) 85%Ar, and *b*), 90%Ar, for the same initial conditions as the numerical computations (courtesy of P. Pinard)

90% argon dilution, the cell pattern indicates very weak markings on the foil, suggesting the very weak strength of the triple point shears, thus of transverse waves. These smoke foils are to be compared with the records of the cellular structure obtained in the experiments with undiluted acetylene-oxygen (e.g., Fig. 3.3), which display much stronger and much more irregular transverse waves.

In Table 5.1 we compare the length of the one-dimensional pulsations in the 85 and 90% dilutions with the experimentally determined cell length. Very

Table 5.1 Comparison of experimental cell lengths with 1D oscillation lengths

	1D pulsation length, mm	Experimental cell length, mm
$C_2H_2 + 2.5O_2 + 90\%Ar$ $P_o = 100$ kPa	9.0	10.7
$C_2H_2 + 2.5O_2 + 85\%Ar$, $P_o = 60$ kPa	7.5	8

good agreement is found between the two. This good agreement suggests that the regular cells observed experimentally in these highly diluted mixtures could be a result of the one-dimensional instability mechanism only. The multi-dimensional weak transverse wave structure observed experimentally can thus be borne out from portions of the wave oscillating out of phase with others, setting in a resonant system of oscillations in the transverse directions which propagate at sonic velocity in the products. In this scenario, the transverse waves strength is a direct function of the one-dimensional oscillation amplitudes, since the transverse waves result from the out of phase pressure oscillations. This scenario however remains to be confirmed through more extensive numerical calculations in one and multi-dimensions.

However, with increasing magnitude of pulsations, the leading shock eventually decays to temperatures lower than permitted to self-sustain sufficiently fast reactions and the one-dimensional detonation fails (Fig. 5.5). For acetylene-oxygen-argon detonations, this limit was at ~70% argon dilution for the range of pressures investigated. Below this critical value one-dimensional pulsating detonations cannot be self-sustained. The failure scenario was associated with the increase in the pulsations of the leading shock. The minimum temperature that the shock could decay to was found close to the chain-branching crossover temperature, thus confirming the detonation failure scenario analyzed by Short & Quirk (1997) for simplified chemistry three-step chain-branching model of detonations.

The inability of a one-dimensional detonation to propagate below the critical argon dilution of approximately 70% corresponds closely to the switchover in detonation dynamics determined experimentally. The failure of the one-dimensional detonation raises the question of the exact mechanism by which cellular detonations propagate below this limit. In a one-dimensional Eulerian detonation, ignition can only be achieved via adiabatic shock heating behind the leading shock. Therefore with increasing instability and large amplitude oscillations, the leading shock attained a critical sub-CJ auto-ignition limit and the reactions are effectively quenched. In one-dimensional detonations there are no

other mechanisms to effect ignition. However in two or three-dimensional detonations, ignition behind the strong transverse shocks, by transverse wave interactions and turbulent mixing can provide alternate means to effect auto-ignition and thus maintain the detonation propagation. Three-dimensional cellular detonations are commonly observed for acetylene-oxygen mixtures even for no argon dilution (e.g., Fig 3.3). The conclusion is that the role of transverse waves thus becomes essential to sustain the detonation propagation for irregular structure detonations.

5.4 Comparison with Oppenheim's criterion for stability for shock ignition

The present experimental results revealed that the onset of instability is manifested by small-scale instabilities behind the pulsating leading shocks of the detonations: for regular structure mixtures, the ignition was found uniform behind the leading shock, forming a piecewise-laminar reaction structure, while for the irregular mixtures such propane-oxygen, the reaction zone is spotty and turbulent.

The differences between these two regimes are very similar to the two regimes of ignition observed experimentally in shock-tube studies. Soloukhin and Oppenheim noted that the ignition behind a shock could either be uniformly distributed (the *strong* regime) or originating from discrete exothermic spots (the *mild* regime) (Meyer & Oppenheim, 1971*a*, Vermeer et al, 1972, Voyevodsky and Soloukhin, 1965). For the case of detonations, the mild regime corresponds to turbulent detonations where the ignition is spotty, while the strong corresponds to regular structure detonations, where uniform ignition is achieved behind the causal leading shock. Hence the stability in the reaction zone of gas detonations may be linked to the regime of ignition behind shock waves, as already noted by Takai et al., (1974).

Following Oppenheim's work, the requirement of stability in the reaction structure can be formulated on the requirement that neighboring particles, shocked initially at slightly different shock strengths, would release their chemical energy with similar time delays, so that the power pulses can overlap, or be "coherent" in time and space as to give rise to a single global gasdynamic effect

Table 5.2 Stability parameters of the gas detonations investigated, cell regularity and the failure mechanism observed experimentally in the porous wall tubes experiments

	Reduced activation energy, ε	Induction to reaction time ratio, Λ	$\chi = \varepsilon\Lambda$	Cell regularity	Failure Mechanism
$CH_4 + 2O_2$	10.9	32.1	350	Highly irregular	TWD
$C_3H_8+5O_2$	9.8	6.5	64	Highly irregular	TWD
$C_2H_2+2.5O_2$	5.3	7.9	42	Irregular	TWD
$C_2H_2+2.5O_2+22\%Ar$	5.1	6.1	31	Irregular	TWD
$C_2H_2+2.5O_2+50\%Ar$	5.1	3.7	19	Fair	TWD
$C_2H_2+2.5O_2+60\%Ar$	5.1	2.9	15	Fair	Transition
$C_2H_2+2.5O_2+65\%Ar$	5.1	2.5	13	Fair	Transition
$C_2H_2+2.5O_2+70\%Ar$	5.1	2.2	11	Good	Transition
$C_2H_2+2.5O_2+75\%Ar$	5.1	1.7	8.8	Good	GMD
$2H_2+O_2+25\%N_2$	5.2	1.4	7.5	Fair	GMD
$C_2H_2+2.5O_2+81\%Ar$	5.1	1.4	7.2	Good	GMD
$2H_2+O_2$	4.9	1.4	7.0	Good	GMD
$C_2H_2+2.5O_2+85\%Ar$	5.2	1.1	5.9	Excellent	GMD
$2H_2+O_2+40\%Ar$	4.2	0.6	2.7	Excellent	GMD

free of small scale gasdynamic instabilities (Meyer & Oppenheim, 1971*b*, Oppenheim, 1985, Lutz et al., 1988). Clearly, to meet this requirement, the sensitivity of the chemical induction time (time delay to maximum exothermicity) to changes of shock temperature needs to be small. For gases, the induction time has the usual Arrhenius from

$$\tau_i \propto \exp\left(\frac{Ea}{RT}\right) \qquad 5.2$$

where T is the initial gas temperature and (Ea/R) the global activation energy describing the thermally neutral chemical induction process. A requirement for stability is thus that

$$\left[\left(\frac{T}{\tau_i}\right)\left(\frac{\partial \tau_i}{\partial T}\right)\right] = \frac{Ea}{RT} \equiv \varepsilon \qquad 5.3$$

be small, i.e., small activation energy ε. However, the characteristic times for energy deposition τ_r also plays an important role, since relatively long times for energy release (broad power pulses) will still lead to quasi-simultaneous energy deposition and coherence in time and space even if the changes of induction times are important. This concept is shown schematically in Fig. 5.6. Thus, as first pointed out by Soloukhin in a comment to Meyer and Oppenheim's work (Meyer & Oppenheim, 1971*a*), stability is more accurately described by the sensitivity to temperature fluctuations of the characteristic induction time *relative* to the characteristic exothermic reaction times. Mathematically, we can thus define a stability parameter of the form:

$$\chi \equiv \left[\left(\frac{T}{\tau_r}\right)\left(\frac{\partial \tau_i}{\partial T}\right)\right] = \frac{Ea}{RT}\frac{\tau_i}{\tau_r} = \frac{Ea}{RT}\tau_i \dot{\sigma}_{max} = \varepsilon \Lambda \qquad 5.4$$

where the time scale for the duration of the exothermic power pulse τ_r is simply the inverse of the maximum exothermicity $\dot{\sigma}_{max}$, as defined by (4.5) (see also Appendix 2). For small values of χ, we expect that power pulses originating from neighboring particles will overlap, thus leading to a coherent phenomenon in time and space, as shown schematically in Fig. 5.7. On the other hand, if this parameter is large, the power pulses will not be coherent and their discreteness can lead to the three-dimensional gasdynamic instabilities in the reaction zone structure.

Although the above parameter is qualitative and does not predict when the stability will be lost, it can permit comparison of the relative stability between different mixtures. We hence computed this parameter for the various mixtures investigated from the detailed chemical kinetic mechanisms (see Appendix 2). The variations of the stability parameters ε, Λ, and χ are shown in Table 5.2, as

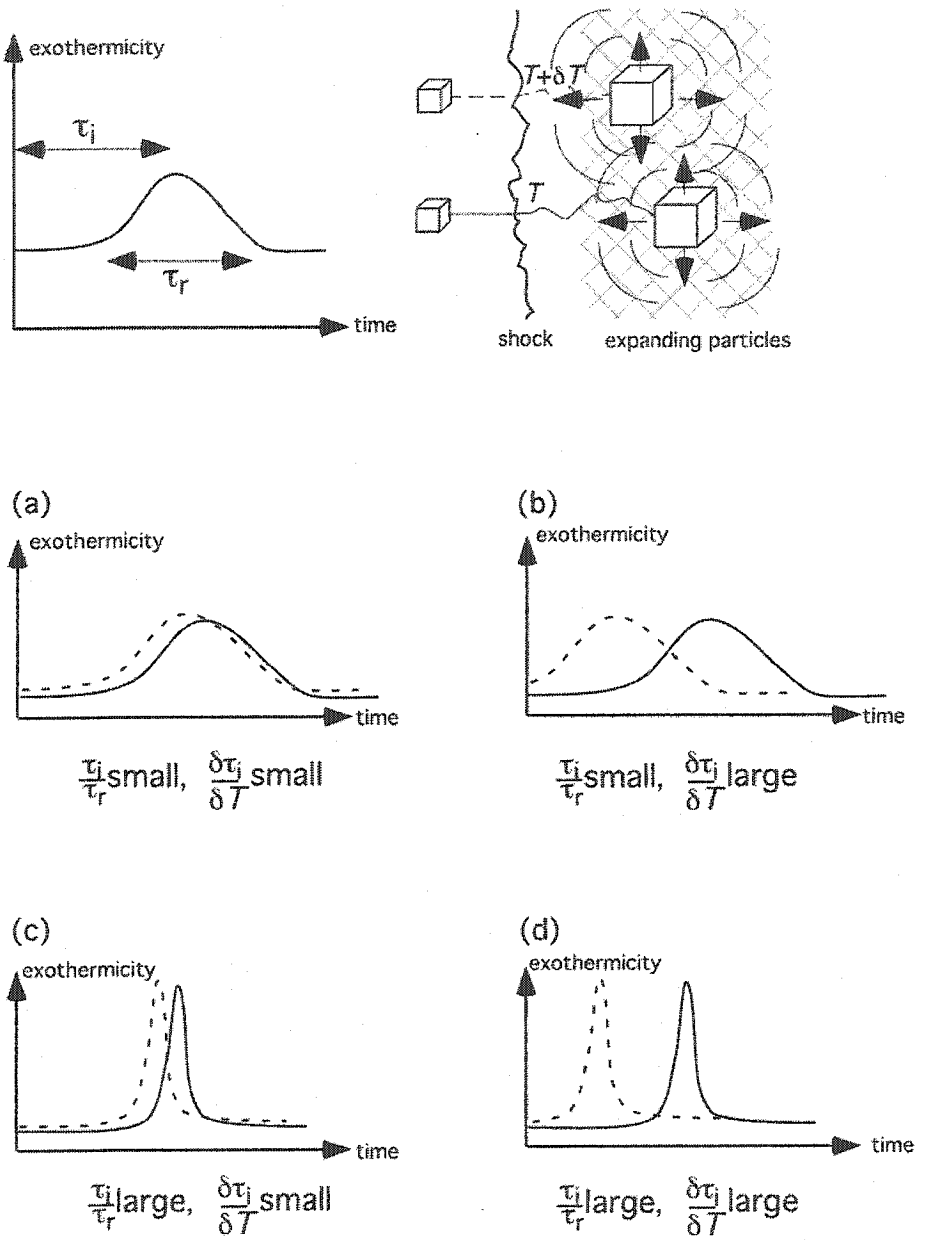

Fig 5.6 Illustration of the coherence concept between neighboring power pulses, given by the exothermicity profiles for two neighboring gas elements at an initial shock state differing by δT: *a*) small activation energy and small relative exothermicity, *b*) large activation energy, small exothermicity, *c*) small activation energy, large exothermicity, and *d*) large activation energy and large exothermicity

computed at the initial conditions corresponding to the shocked state in the critical damping of detonations in the 41-mm porous wall tube experiments. The results

are presented in order of decreasing χ, i.e., in order of increasing stability. Also tabulated are the qualitative assessment of the cell regularity and the failure mechanism, as observed experimentally in the present study ("TWD" stands for transverse wave damping and "GMD" stands for the global mass divergence mechanism).

As can be observed from Table 5.2, the cell regularity correlates very well with the failure mechanism observed in the experiments. Furthermore, the coherence criterion χ provides a very good correlation in classifying both the cell regularity effects and the demarcation between the two modes of failure in the porous wall tube experiments. Also to be noted is that activation energy alone (as is usually assumed) cannot solely account for the stability in these mixtures. The transitional value between the two failure mechanisms in porous walled tubes is found at approximately

$$\chi \approx 10 \qquad 5.5$$

This is an empirical estimate. For a quantitative assessment of stability, as was performed in Radulescu et al. (2002) for C_2H_2-O_2-Ar detonations, the entire chemical kinetics coupling to the hydrodynamic equations is required, including the variation of activation energy and exothermicity with the varying shock temperature, which are specific for each mixture and initial thermodynamic state. This is however beyond the scope of the present discussion, which only seeks to determine the mechanism by which the detonations lose their stability and their structure becomes highly unstable. The very good agreement between experiments and the coherence stability parameter supports the scenario that the incoherence in the exothermicity of the gas leads to gasdynamic instabilities in the reaction zone, as observed experimentally. It should be noted that a similar stability parameter can be derived from Short's stability analysis of the amplitude of oscillations in self-supported ZND detonations (Short, 2001). However, Oppenheim's treatment is more general, since it can be extended to turbulent detonations alike.

5.5 The role of instabilities in the propagation mechanism of turbulent detonations

The experiments performed in porous wall tubes revealed that irregular structure mixtures rely on their three-dimensional interacting transverse waves for successful propagation. The reaction zone in such detonations was turbulent. When the transverse waves were damped out, the detonations failed. Thus the answer to the original question "*Why do detonations display such a complicated three-dimensional structure*" is that these three-dimensional effects and turbulence offer a more efficient propagation mechanism.

The choice of the word *turbulent* needs further clarification, since it is usually associated with notions acquired from incompressible hydrodynamic turbulence, where vorticity is generated via hydrodynamic instabilities (e.g., Frisch, 1995) and an energy cascade operates between the large scales, at which energy is injected, to small scales where energy is dissipated. In detonation waves, the nature of turbulence is different due to two fundamental differences. First, compressibility effects play a significant role, as evidenced by the interactions of shock waves and density gradients in the reaction zone structure. However, these interactions create vorticity, thus approaching the usual definition of turbulence. Second, chemical reactions take place, which provide energy in maintaining these turbulent fluctuations on all scales.

A speculative scenario of the turbulent mechanism in gas detonations can be formulated based on present and past experimental observations. Unlike the classical turbulence mechanism, detonations may display a double energy cascade, one from small scales up, the second from the large scales (cellular structure) downwards. The upward cascade can be viewed as originating from the spatial and temporal non-uniformities in exothermicity. The spotty nature of the reactions observed experimentally in irregular structure detonations suggests that chemical instabilities set-in at scales comparable to the characteristic time of energy deposition, which in general is two orders of magnitude smaller than the characteristic period of the large scale cellular structure. Hence, the mechanism postulated by Oppenheim for instabilities in the reaction zone can be considered

as the source term that gives rise to the turbulent state. Resulting from the high frequency spectrum of chemical instabilities, high frequency pressure waves are formed through the explosion of the various exothermic spots. Through the mutual interactions of these pressure waves and interactions with neighboring exothermic regions, these pressure waves can coalesce and amplify, giving rise to less numerous, larger amplitude and lower frequency pressure oscillations. Hence the postulated inverse energy cascade consists of energy transfer from the small-scale instabilities to the large integral scale cellular pulsations. However, the large-scale pulsations (cellular structure) could not amplify indefinitely, and will stop amplifying when its wavelength λ is larger than the global length of the turbulent reaction zone. Indeed, experiments revealed that the length of the turbulent chemical reaction zone is on the order of the cell size λ itself (Subbotin, 1976).

The competing cascade is the Kolmogorov-like downward cascade, which serves to dissipate the energy of the large-scale cellular pulsations and turbulent fluctuations, by the usual vorticity producing mechanisms and dissipation. As pointed out by Lee, (1988, 1991, 2001) shock-shock interactions lead to vorticity production along the shear layers via Kelvin-Hemoltz instability. Shock interactions with vortices leads to shock scattering, randomization of the kinetic energy and finer scale vorticity. Shock interactions with misaligned density interfaces (due to chemical reactions) result in vorticity production via the baroclinic torque mechanism between pressure and density gradients (Meshkov instability). All these mechanisms are likely to operate simultaneously, hence generating a tremendous amount of vorticity. This is the classical Kolmogorov energy cascade for turbulence from large to small scales (Frisch, 1995), although in the present case turbulence occurs in highly compressible flow.

The presence of chemical reactions is likely to affect all scales of this turbulent spectrum. Since the detonation is a supersonic combustion wave (by definition), the pressure waves generated within the reaction zone cannot outrun the detonation front and hence are "trapped" within the detonation structure. These pressure waves are thus in phase with the chemical energy release, and

hence amplify while traveling through the spotty reaction zone. Since gradients of mixture reactivity are likely to be formed, spontaneous reaction waves are likely to be amplified in a three-dimensional stochastic version of the SWACER mechanism (Lee and Moen, 1980). Simultaneously, since these transverse pressure waves can amplify to form finite strength shocks (Edwards et al., 1976) of non-negligible strength, they offer supplementary means to increase the burning rates by supplementary localized compression of the gases shocked by the leading front. In fact, this supplementary compression by transverse waves was long recognized in irregular structure detonations (e.g., Lee et al., 1969).

The postulated turbulent mechanism of ignition involves only non-uniform exothermicity for turbulence generation (Oppenheim's mechanism). Since viscosity is not required to generate this turbulence, it is unclear at present if molecular mixing (hence transport terms in the governing equations) is required in the description of turbulent detonations. The amplification of the turbulent pressure spectrum via the inverse cascade mechanism appears a priori sufficient to account for the reaction zone structure observed experimentally.

Nonetheless, turbulent mixing cannot be ruled out as a possible source of ignition. Due to the presence of the significant amount of vorticity, the mixing rates also increase. It is possible that the fine scale mixing of the gas, which is at different stages of its oxidation process, occurring in the turbulent reaction zone structure can enhance the burning rates. Thus, similar to the deflagration ignition mechanism which relies solely on transport (Schelkin & Troshin, 1965), turbulent diffusion of active radicals and heat may ease the ignition process in detonations alike. In this scenario, as first noted by Lee (1988), it appears that the propagation mechanism of turbulent detonations could no longer be clearly differentiated from that of turbulent deflagrations, in that both shock compression and turbulent transport from fine scale vorticity may both contribute to the gas ignition mechanism.

A further indication that transport properties are likely to play a role is the comparison of the behavior of detonations waves that share the same kinetic properties but different transport properties. For example, propane-oxygen

detonations diluted with 60% argon share the same chemical-kinetic and thermodynamic properties (hence same detonation Mach number, shock temperature and kinetic rates) as propane-oxygen detonations diluted with 60% helium, since the two diluents are inert. Yet the helium mixture does not permit galloping detonations, while the argon mixture does (Haloua et al., 2000). To reconcile these observations, it is possible that the increase in the transport coefficients in the helium mixture (due to the effective increase in thermal speed and sound speed) suppresses the fine scale instabilities required for the galloping phenomenon by increased dissipation.

There is further experimental evidence that turbulent mixing can operate in detonations, and should be included in a theoretical account of the detonation structure. In experiments on supersonic deflagrations in obstacle-filled tubes (e.g., Teodorczyk et al., 1990, Chao & Lee, 2003), steady waves were observed with average shock velocities of approximately 1000m/s. Although the temperature behind the shock for these conditions (~800K) is too low to allow rapid auto-ignition by shock compression, rapid ignition was still achieved from the interactions of the obstacle-generated pressure waves, giving rise to significant vorticity and mixing. These studies showed that indeed very rapid burning rates could be generated through sufficiently high levels of compressible turbulence and mixing. These conclusions can readily be extended to self-supported unstable detonations, where the necessary turbulence is not provided from an external means. Instead, through the Oppenheim incoherence of ignition, self-generated turbulence is driven and maintained by the energy release in the chemical reactions occurring within the detonation structure.

Although a (statistically) stationary distribution of the various state variables fields is likely to be established in self-sustained turbulent detonation waves for large χ, very little is presently known, due to the difficulty in conducting accurate measurements or well-resolved realistic DNS studies of such turbulent detonations. It is hoped however that the present discussion will motivate future studies in this direction.

In closing, for irregular structure detonations such the undiluted hydrocarbon–oxygen mixtures, the experiments in the porous wall tubes revealed that the global mass divergence and attenuation of transverse waves at the porous walls are overcome by the re-amplification of new transverse waves from local instabilities in the reaction zone. The detonation limits were found identical for these mixtures, yielding $(d / \lambda)^* \approx 4$, similar to the conclusions reached by Dupré et al. (1986) and Guo et al. (2002). The fact that the limit is identical in the various studies, where different porous walls were used, it suggests that this value is independent of the wall porosity, as long as transverse waves are successfully damped. A possible explanation for this constant failure limit is given by Radulescu & Lee (2002), derived phenomenologically in terms of the competition of transverse wave damping at the wall and the regeneration rate of new transverse waves from local instabilities.

The constant correlation with the characteristic transverse wave spacing λ suggests the importance of the detonation transverse wave structure in irregular structure turbulent detonations. Similar conclusions can be deduced from the constant correlations with λ in direct initiation experiments (Lee, 1984, Radulescu et al., 2000), diffraction limits (Lee, 1984) or successful deflagration-to-detonation transition (DDT) criteria (Dorofeev et al., 2000) in irregular structure mixtures. In conclusion, it appears that the integral scale λ, and hence the detonation transverse wave structure, play a universal role in the detonation propagation and limits. For this reason, the author's opinion is that progress in the field could only be achieved by investigating how the transverse waves are generated in turbulent detonations, since the competing roles of generation of transverse waves from chemical instabilities and damping of transverse waves due to boundary conditions in experiments could elucidate the failure limits of detonations. It is likely that a statistical description could be more profitable to describe detonation waves, instead of the classical ZND model or weak perturbations of the ZND structure. In this sense, stochastic simulations based on Oppenheim's instability mechanism for large values of χ could lead to the elucidation of the basic scaling laws governing turbulent detonations.

Chapter 6 Summary and conclusions

6.1 Summary

The present thesis showed the existence of two different failure mechanisms for detonations propagating in porous wall tubes. For regular structure mixtures, the global mass divergence to the porous walls dictates the failure limit. These mixtures were found to be well approximated by the laminar ZND model for the detonation structure. Likewise, the limits were in very good agreement with the limiting form of ZND detonations subjected to lateral mass divergence.

In mixtures characterized by an irregular structure with strong transverse waves, the transverse wave re-generation from local instabilities in the reaction structure permitted to overcome the mass divergence and the attenuation of transverse waves at the porous walls and hence sustain the detonation propagation well beyond the predictions based on the curved ZND model.

The fundamental difference in the failure mechanism between the two classes of mixtures was shown to have severe implications on the propagation mechanism of detonations. While the regular structure mixtures are well approximated by the ignition mechanism postulated in the ZND model, i.e. ignition by bulk thermal compression behind the leading shock, the irregular mixtures also rely on compression by transverse waves and turbulent interactions to permit sufficiently high burning rates.

6.2 Conclusions

In conclusion, only a very special class of detonations can be well approximated by the classical ZND model, i.e., mixtures characterized by regular cellular structures and weak transverse waves. For common hydrocarbon detonations characterized by irregular cell structures and turbulent reaction zones, the ignition mechanism relies on both shock compressions and compressible turbulence interactions for maintaining the sufficiently high burning rates necessary for the wave self-sustenance.

Contributions to original knowledge

The present thesis clarified the failure mechanism of detonations propagating in porous wall tubes. Regular structure mixtures characterized by weak transverse waves and piece-wise laminar reaction zone structures fail due to the global mass divergence to the porous walls. Their limit agrees very well with the limit derived from curved ZND detonations. Irregular structure mixtures characterized by strong transverse waves and turbulent reaction zones fail from the attenuation of their strong transverse waves.

The present thesis thus clearly showed that only a very special class of detonations can be well approximated by the classical ZND model, i.e., mixtures characterized by regular cellular structures and weak transverse waves. The ignition mechanism in common detonations, characterized by irregular cellular structures, relies on both shock compressions and compressible turbulence interactions for maintaining the sufficiently high burning rates necessary for the wave self-sustenance.

References

1. Barthel, H. O., Predicted spacings in hydrogen-oxygen-argon detonations. *Physics of Fluids*17:1547-1553 (1974).
2. Bdzil, J. B., and Stewart, D. S., Time-dependent two-dimensional detonation: the interaction of edge rarefactions with finite-length reaction zones. *Journal of Fluid Mechanics* 171:1-26 (1986).
3. Chao, J., and Lee, J. H. S, The propagation mechanism of high speed turbulent deflagrations. *Shock Waves* 12:277-289 (2003).
4. Dabora, E. K., and Broda J.-C., Oblique detonation waves in a laboratory setting. In *Shock Waves @ Marseille IV: Shock structure and Kinematics, Blast Waves and Detonations* (R. Brun and L. Z. Dumitrescu, Eds.) Springer, pp. 431-436, 1993.
5. Dabora, E. K., Nicholls, J. A., and Morrison, R. B., The influence of a compressible boundary on the propagation of gaseous detonations. *Proceedings of the Combustion Institute* 10:817 (1965).
6. Desbordes, D., and Vachon, M., Critical diameter of diffraction for strong plane detonations. *Progress in Astronautics and Aeronautics* 106:131-143 (1986).
7. Desbordes, D., Guerraud, C., Hamada, L., and Presles, H. N., Failure of the classical dynamic parameters relationships in highly regular cellular detonation systems. *Progress in Astronautics and Aeronautics* 153:347-359 (1993).
8. Desbordes, D., Transmission of overdriven plane detonations: critical diameter as a function of cell regularity and size. *Progress in Astronautics and Aeronautics* 114:170-185 (1988).
9. Dorofeev, S. B., Sidorov, V. P., Kuznetsov, M. S., Matsukov, I. D., Alekseev, V. I., Effect of scale on the onset of detonations. *Shock Waves*10:137-149 (2000).
10. Dupré, G., Knystautas, R., and Lee, J.H., Near-limit propagation of detonation in tubes. *Progress in Astronautics and Aeronautics* 106:244-259 (1986)
11. Dupré, G., Péraldi, O., Joannon, J., Lee, J. H. S., and Knystautas, R., Limit criterion of detonation in circular tubes. *Progress in Astronautics and Aeronautics* 133:156-169 (1991).
12. Dupré, G., Péraldi, O., Lee, J. H., and Knystautas, R., Propagation of detonation waves in an acoustic absorbing walled tube. *Progress in Astronautics and Aeronautics* 114:248-263 (1988).
13. Edwards, D. H., Hooper, G., Morgan, J. M., and Thomas, G. O., The quasi-steady regime in critically initiated detonation waves. *Journal of Physics D: Applied Physics* 11:2103-2117 (1978).

14. Edwards, D. H., Jones, A. T., Phillips, D. E., Location of Chapman-Jouguet surface in a multiheaded detonation-wave. *Journal of Physics D: Applied Physics* 9:1331-1342 (1976).

15. Edwards, D. H., Thomas, G. O., and Nettleton, M. A., The diffraction of a planar detonation wave at an abrupt area change. *Journal of Fluid Mechanics*, 95:79-96 (1979).

16. Edwards, D. H., and Morgan, J. M., Instabilities in detonation waves near the limits of propagation. *Journal of Physics D: Applied Physics* 10:2377-2387 (1977).

17. Fay, J. A., Two-dimensional gaseous detonations: velocity deficit. *Physics of Fluids* 2:283-289 (1959).

18. Fickett, W., and Davis, W. C., *Detonation: theory and experiment*, University of California Press, Berkley, 1979.

19. Frisch, U., *Turbulence: the Legacy of A. N. Kolmogorov*. Cambridge University Press, 1995.

20. Gavrikov, A. I., Efimenko, A. A., and Dorofeev, S. B., A model for detonation cell size prediction from chemical kinetics. *Combustion and Flame* 120:19-33 (2000).

21. Gordon, S., and McBride, B. J., *NASA RP-1311*, 1994.

22. Guo, C., Thomas, G., Li, J., and Zhang, D., Experimental study of gaseous detonation propagation over acoustically absorbing walls. *Shock Waves* 11:353-359 (2002).

23. Haloua, F., Brouillette, M., Lienhart, V., and Dupré, G., Characteristics of unstable detonations near extinction limits. *Combustion and Flame* 122:422-438 (2000).

24. He, L. T., and Clavin, P., On the direct initiation of gaseous detonations by an energy source. *Journal of Fluid Mechanics* 277: 227-248 (1994).

25. He, L., Theoretical determination of the critical conditions for the direct initiation of detonations in hydrogen-oxygen mixtures. *Combustion and Flame* 104:401-418 (1996).

26. Kaneshige, M. J., *Gaseous Detonation Initiation and Stabilization by Hypervelocity Projectiles*. PhD thesis, California Institute of Technology,1999.

27. Kee, R. J., Rupley, F. M., and Miller, J. A., Chemkin-II: a Fortran chemical kinetics package for the analysis of gas-phase chemical kinetics. Sandia National Laboratories Report SAND89-8009, 1989.

28. Klein, R., Curved detonations in explosive gas mixtures with high temperature sensitivity. Proceedings of the Zel'dovich Memorial, Moscow, Russia, September 12, 1994, pp. 288-315.

29. Klein, R., Krok, J. C., and Shepherd, J. E., Investigation of curved quasisteady detonations using asymptotic analysis and detailed chemical kinetics. Preprint, (1994).

30. Knystautas, R., Lee, J. H., and Guirao, C. M., The critical tube diameter for detonation failure in hydrocarbon-air mixtures. *Combustion and Flame* 48: 63-83 (1982).

31. Kobayashi, S., Adachi, T., and Suzuki, T., Regular reflection of a shock wave over a porous layer: theory and experiment. In *Shock Waves @ Marseille IV: Shock structure and Kinematics, Blast Waves and Detonations* (R. Brun and L. Z. Dumitrescu Eds.) Springer, pp. 175-180, 1993.

32. Laberge, S., Knystautas, R., and Lee, J.H.S., Propagation and extinction of detonation waves in tube bundles. *Progress in Astronautics and Aeronautics* 153: 381-396 (1993).

33. Lee, J. H. S., On the universal role of turbulence in the propagation of deflagrations and detonations. In *Computational Fluid Dynamics and Reacting Gas Flows* (B. Engquist, M. Luskin and A. Majda, Eds.), Springer-Verlag, New York, 1988, pp. 169-193.

34. Lee, J. H., Dynamic structure of gaseous detonation. In *Dynamic Structure of Detonation in Gaseous and Dispersed Media* (A. A. Borisov, Ed.), Fluid Mechanics and its Applications v. 5, Kluwer Academic Publishers, Netherlands, 1991, pp. 1-26.

35. Lee, J. H. S., and Moen, I. O., The mechanism of transition from deflagration to detonation in vapor cloud explosions, Progress in Energy and Combustion Science, 6:359-389 (1980).

36. Lee, J. H., Soloukhin, R. I., and Oppenheim, A. K., Current views on gaseous detonation. *Astronautica Acta* 14:565-584 (1969).

37. Lee, J. J., Dupré, G., Knystautas, R., and Lee, J. H., Doppler interferometry study of unstable detonations. *Shock Waves* 5:175-181 (1995).

38. Lee, J. H. S., Detonation waves in gaseous explosives. In Handbook of Shock Waves, Volume 3, (G. Ben-Dor, O. Igra, and T., Elperin Eds.), Academic Press, pp. 309-415, 2001.

39. Lee, J. H. S., Dynamic parameters of gaseous detonations. *Annual Review of Fluid Mechanics* 16:311-336 (1984).

40. Lee, J. H. S., On the critical tube diameter, in *Dynamics of Exothermicity* (J. R. Bowen Ed.), Gordon and Breech Publishers, Netherlands, 321-336, 1996.

41. Liu, Y. K., Lee, J. H., and Knystautas, R., Effect of geometry on the transmission of detonation through an orifice, *Combustion and Flame*, 56: 215-225 (1984).

42. Lutz, A. E., Kee, R. J., Miller, J. A., Dwyer, H. A., and Oppenheim, A. K., Dynamic effects of autoignition centers for hydrogen and C1,2-hydrocarbon fuels. *Proceedings of the Combustion Institute* 22:1683-1693 (1988).

43. Manson, N., Brochet, C., Brossard, J., and Pujol, Y., Vibratory phenomena and instability of self-sustained detonations in gases. *Proceedings of the Combustion Institute* 9:461-469 (1963).

44. Manzhalei, V. I., Detonation regimes of gases in capillaries. *Combustion, Explosion and Shock Waves*, 28:296-302 (1992).

45. Manzhalei, V. I., Mitrofanov, V. V., and Subbotin, V. A., Measurement of inhomogeneities of a detonation front in gas mixtures at elevated pressures. *Combustion, Explosion and Shock Waves* 10:89-95 (1974).

46. Meyer, J. W., and Oppenheim, A. K., Coherence theory of the strong ignition limit. *Combustion and Flame* 17:65-68 (1971 *b*).

47. Meyer, J. W., and Oppenheim, A. K., On the shock-induced ignition of explosive gases. *Proceedings of the Combustion Institute* 13:1153-1164 (1971 *a*).

48. Mitrofanov, V. V., and Soloukhin, R. I., The diffraction of multifront detonations. *Soviet Physics - Doklady* 9(12):1055-1058 (1965).

49. Moen, I. O, Sulmistras, A., Thomas, G. O., Bjerketvedt, D., and Thibault, P. A., Influence of cellular regularity on the behavior of gaseous detonations. *Progress in Astronautics and Aeronautics* 106:133:220-243 (1986).

50. Murray, S. B., and Lee, J. H., The influence of physical boundaries on gaseous detonation waves. *Progress in Astronautics and Aeronautics* 106:329-355 (1986).

51. Murray, S. B., and Lee, J. H., The influence of yielding confinement on large-scale ethylene-air detonations. *Progress in Astronautics and Aeronautics* 94:80-103 (1984).

52. Oppenheim, A. K., Dynamic features of combustion. *Philosophical Transactions of the Royal Society of London A* 315:471-508 (1985).

53. Oran, E. S., Weber, J. W., Stefaniw, E. I., Lefebvre, M. H., and Anderson, J. D. A numerical study of a two-dimensional H_2-O_2-Ar detonation using a detailed chemical reaction model. *Combustion and Flame* 113:147-163 (1998).

54. Pedley, M. D., Bishop, C. V., Benz, F. J., Bennett, C. A., McClenagan, R. D., Fenton, D.L., Knystautas, R., Lee, J.H., Peraldi O., Dupré, G., and Shepherd, J.E., Hydrazine vapor detonations. *Progress in Astronautics and Aeronautics* 114:45-63 (1988).

55. Radulescu, M. I., Higgins A. J., Lee, J. H. S., and Murray, S. B., On the explosion length invariance in direct initiation of detonation. *Proceedings of the Combustion Institute* 28: 637-644 (2000).

56. Radulescu, M. I., Higgins, A. J., Murray, S. B., and Lee, J. H. S., An experimental investigation of the direct initiation of cylindrical detonations. *Journal of Fluid Mechanics*, in press (2003).

57. Radulescu, M.I., and Lee, J. H. S., The failure mechanism of gaseous detonations: experiments in porous wall tubes, *Combustion and Flame*, 131:29-46 (2002).

58. Radulescu, M. I., Ng, H. D., Lee, J. H. S., and Varatharajan, B., The effect of argon dilution on the stability of acetylene/oxygen detonations. *Proceedings of the Combustion Institute* 29, in press (2002).

59. Saint-Cloud, J. P., Guerraud, C., Brochet, C., and Manson, N., Quelques particularités des détonations très instables dans les mélanges gazeux. *Astronautica Acta* 17:487-498 (1972)

60. Schelkin, K. I., and Troshin, Ya. K., *Gasdynamics of combustion*, Mono Book Corp., Baltimore, 1965.

61. Settles, G. S., *Schlieren and shadowgraph techniques*. Springer-Verlag, Berlin Heidelberg New York, 2001.

62. Shepherd, J. E., Chemical kinetics of hydrogen-air-diluent mixtures. *Progress in Astronautics and Aeronautics* 106:263-293 (1986).

63. Shepherd, J. E., Moen, I., Murray, S., and Thibault, P., Analyses of the cellular structure of detonations. *Proceedings of the Combustion Institute* 21:1649-1658 (1986).

64. Short, M., A nonlinear evolution equation for pulsating Chapman-Jouguet detonations with chain-branching kinetics. *Journal of Fluid Mechanics* 430: 381-400 (2001).

65. Short, M., and Quirk, J. J., On the nonlinear stability and detonability limit of a detonation wave for a model three-step chain-branching reaction. *Journal of Fluid Mechanics*339: 89-119 (1997).

66. Shepherd, J. E., Pintgen, F., Austin, J. M., and Eckett, C. A., The structure of the detonation front in gases. AIAA Paper 2002-0773 (2002).

67. Strehlow, R. A., and Biller, J. R., On the strength of transverse waves in gaseous detonations. *Combustion and Flame* 13:577-582 (1969).

68. Strehlow, R. A., and Salm, R. J., The failure of marginal detonations in expanding channels. *Acta Astronautica* 3:983-994 (1976).

69. Strehlow, R. A., and Engel, C. D., Transverse waves in detonation II: structure and spacing in H_2-O_2, C_2H_2-O_2, C_2H_4-O_2, and CH_4-O_2 systems. AIAA Journal 7:492-496 (1969).

70. Strehlow, R. A., Gas phase detonations: recent developments. *Combustion and Flame* 12:81-101 (1968).

71. Strehlow, R. A., Liangminas, R., Watson, R. H., and Eyman, J. R., Transverse wave structure in detonations. *Proceedings of the Combustion Institute* 11:683-692 (1967).

72. Strehlow, R. A., The nature of transverse waves in detonations. *Astronautica Acta* 14:539-548 (1969).

73. Subbotin, V. A., Two kinds of transverse wave structures in multifront detonation. *Combustion, Explosion and Shock Waves* 11:96-102 (1976).

74. Takai, R., Yoneda, K., and Hikita, T., Study of detonation wave structure. *Proceedings of the Combustion Institute* 15:69-78 (1974).

75. Teodorczyk, A., and Lee, J. H. S., Detonation attenuation by foams and wire meshes lining the walls. *Shock Waves* 4:225-236 (1995).

76. Teodorczyk, A., Lee, J. H. S., and Knystautas, R., The structure of fast turbulkent falmes in very rough, obstacle-filled channels. *Proceedings of the Combustion Institute* 23:735-741 (1990).

77. Vandermeiren, M., and Van Tiggelen, P. J., Cellular structure in detonation of acetylene-oxygen mixture. *Progress in Astronautics and Aeronautics* 94:104-117 (1984).

78. Varatharajan, B. and Williams, F. A, http://maeweb.ucsd.edu/combustion/cermech/sandiego20021001.mec (2002).

79. Varatharajan, B. and Williams, F. A., Chemical-kinetic descriptions of high-temperature ignition and detonation of acetylene-oxygen-diluent systems. *Combustion and Flame*, 124: 624-645 (2001).

80. Vasil'ev, A. A., Gavrilenko, T. P., and Topchian, M. E., On the Chapman-Jouguet surface in multi-headed gaseous detonations. *Astronautica Acta* 17:499-502 (1972).

81. Vasil'ev, A. A., Near-limiting detonation in channels with porous walls. *Combustion, Explosion and Shock Waves*, 30(1):101-106 (1994).

82. Vermeer, D. J., Meyer, J. W., and Oppenheim, A. K., Auto-ignition of hydrocarbons behind reflected shock waves. *Combustion and Flame* 18:327-336 (1972)

83. Voitsekhovskii, B. V., Kotov, B. E., Mitrofanov, V. V., and Topchyian, Optical studies of transverse detonation waves. *Izv. Sibirsk. Otd. Akad. Nauk SSSR* 9:44 (1958).

84. Voyevodsky V. V., and Soloukhin, R. I., On the mechanism and explosion limits of hydrogen-oxygen chain self-ignition in shock waves. *Proceedings of the Combustion Institute* 10:279-283 (1965).

85. White, D. R., Turbulent structure of gaseous detonation. *Physics of Fluids* 4:465-480 (1961).

86. Yao, J., and Stewart, D. S., On the normal detonation shock velocity – curvature relationship for materials with large activation – energy. *Combustion and Flame* 100:519-528 (1995).

Appendix 1 Boundary layer losses versus mass divergence to porous walls in the channel experiments

In the present appendix we derive the relative importance of mass divergence to the boundary layers developing on a solid wall to the mass divergence due to the porous walls in rectangular channels made of two solid walls spaced by w and two porous walls spaced by d.

A1.1 Curvature due to mass divergence to porous walls

From the results derived in Chapter 4, the curvature κ_p due to porous walls of porosity β arising between two porous walls spaced by d becomes

$$\kappa_p \cong \frac{4\beta c_{VN}}{V - u_{VN}}\left(\frac{1}{d}\right) \qquad \text{A1.1}$$

where V is the detonation wave velocity, u_{VN} the particle velocity in a shock frame of reference at the Von Neumann(VN) state and c_{VN} is the sound velocity at the VN state.

A1.2 Curvature due to wall boundary layers

The negative mass displacement thickness δ_b due to wall boundary layers behind an incident shock (Fay, 1959) can be expressed

$$\delta_b \cong 0.22x^{0.8}\left(\frac{\mu}{\rho u}\right)^{0.2} \qquad \text{A1.2}$$

where x is the distance behind the leading shock, μ the gas viscosity, ρ the density, and u the gas velocity in the shock frame of reference. The corresponding wave curvature can be readily found from the relation between the stream tube area increase and the front curvature (4.2), reproduced here for completeness

$$\frac{1}{A}\frac{dA}{dx} = \kappa\left(\frac{V}{u} - 1\right) \qquad \text{A1.3}$$

Noting that the effective cross-sectional stream tube area between two walls separated by w becomes ($A = w + 2\,\delta_b$), and since (w / δ_b)>>1, the wave curvature κ_b due to the boundary layers can be obtained by combining (A1.2) and (A1.3)

$$\kappa_b \cong 0.352 \mathrm{Re}_{x_c,\mathrm{VN}}^{-0.2} \left(\frac{1}{V_{\mathrm{VN}} / u_{\mathrm{VN}} - 1} \right) \left(\frac{1}{w} \right) \qquad \text{A1.4}$$

where $\mathrm{Re}_{x_c,\mathrm{VN}}$ is the Reynolds number whose properties are evaluated at the VN state and x_c is a characteristic scale for the length of nozzle flow (typically the chemical reaction induction length, Δ_i).

A1.3 The relative importance of mass loss to boundary layers and mass loss to porous wall tubes

The ratio ζ between the wave curvature κ_b due to the mass divergence to the boundary layers and the wave curvature κ_p due to mass divergence to the porous walls in a channel geometry of aspect ration (w / d) is readily obtained from (A1.1) and (A1.4). It yields

$$\zeta \equiv \frac{\kappa_b}{\kappa_p} \cong \frac{0.088}{\beta} \mathrm{Re}_{x_c,\mathrm{VN}}^{-0.2} M_{\mathrm{VN}} \left(\frac{w}{d} \right)^{-1} \qquad \text{A1.5}$$

We estimated the variation of $\zeta(w/d)$ for the experiments conducted in $C_2H_2 + 2.5O_2$ + 75%Ar and C_2H_2 + $2.5O_2$ mixtures in Chapter 3. The thermodynamic properties were evaluated with the CEA equilibrium code (Gordon and McBride, 1994) for characteristic initial states corresponding to the experiments (see Table 3.1). These parameters are shown in Table A1.1. The length scale x_c for which the effect of mass divergence was considered is the characteristic induction zone length, computed as outlined in Appendix 2.

With the parameters in Table A1.1, we obtain a unique correlation for

Table A.1Parameters for estimation of boundary layer effects on the propagation of detonations in porous wall channels

	P_o kPa	Δ_I mm	M_{VN}	u_{VN} m/s	μ_{VN} kg/m*s (*10^5)	ρ_{VN} kg/m^3	$\mathrm{Re}_{\Delta i,\,VN}$
C_2H_2+2.5O_2	3.3	0.21	0.34	272	6.6	0.33	286
C_2H_2+2.5O_2+75%Ar	22.5	0.16	0.43	360	9.1	1.63	1031

$\zeta(w/d)$ valid for both mixtures

$$\zeta \cong 1 + 0.03\left(\frac{w}{d}\right)^{-1} \tag{A1.6}$$

A1.4 The effective limit in the channel experiments

From simple geometric arguments, the effective curvature κ_{eff} that the detonation will be subjected to in the porous wall channel experiments of finite aspect ratio (w/d) is simply the algebraic sum of the curvatures developed in the two orthogonal directions, i.e., κ_p and κ_b. Using (A1.6), the effective curvature becomes

$$\kappa_{eff} \cong \left(1 + 0.03\left(\frac{w}{d}\right)^{-1}\right)\kappa_p \tag{A1.7}$$

Since the critical curvature for a given mixture is simply the inverse of a characteristic length representing the sensitivity of a mixture (Chapter 4), it can be replaced without loss of generality by the inverse of the cell size λ (or any length scale that varies in the same proportion as $1 / \kappa^*$) (Kleine et al., 1985). Hence we can re-write (A1.7) as

$$\left(\frac{d}{\lambda^*_{eff}}\right) \cong \left(1 + 0.03\left(\frac{w}{d}\right)^{-1}\right)\left(\frac{d}{\lambda^*_{porouswalllossesonly}}\right) \tag{A1.8}$$

Expression (A1.8) thus provides the explicit relation between the observable, effective $(d / \lambda)^*$ limit and the limit observed when the channel aspect ratio is large and only the porous wall curvature operates. This expression is compared with the limits observed experimentally in Chapter 3 in porous wall channels. In comparing with the experimental results, we have assumed ***a priori*** that ***the limit observed for large (w/d) in the experiments is governed by the curvature mechanism***, hence fixing the value of $(d/\lambda)^*_{(w/d)\to\infty}$ to the observed limit. The results are shown in Figures A1.1 and A1.2 for the experiments in the C_2H_2 + $2.5O_2$ + 75%Ar and $C_2H_2 + 2.5O_2$.

The conclusions that can be reached from Fig A1.1 is that the variation of the limit with channel aspect ratio in $C_2H_2 + 2.5O_2$ + 75%Ar detonations is in

excellent agreement with the theoretical prediction. Since the theoretical critical curvature due to porous walls alone was in excellent agreement with the experiments (Chapter 4), it follows that the experiments in this mixture agree fully with the theoretical predictions.

However, as can be observed in Fig. A1.2, the variation in the limit in $C_2H_2 + 2.5O_2$ is inconsistent with the assumed mechanism of curvature affecting the limits. As shown in Chapter 3, the limit in this mixture is due to transverse wave damping at the porous walls.

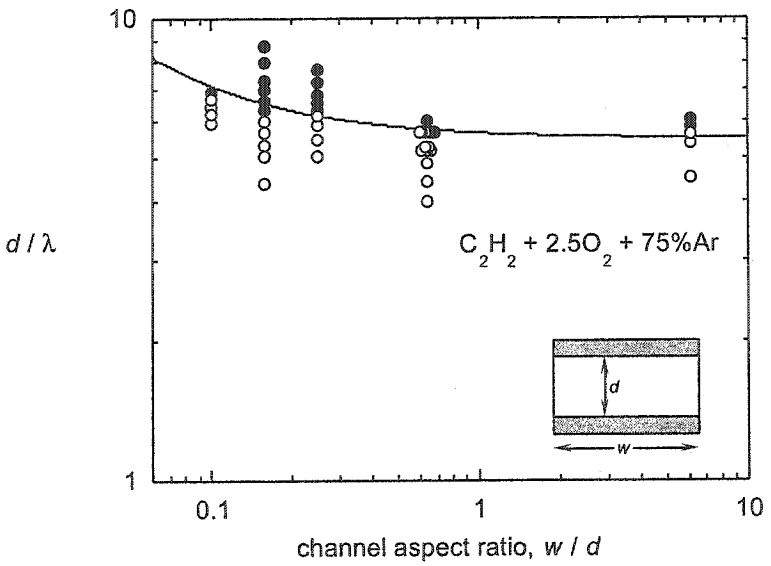

Fig. A1.1 Same as Fig. 3.6; line given by (A1.8)

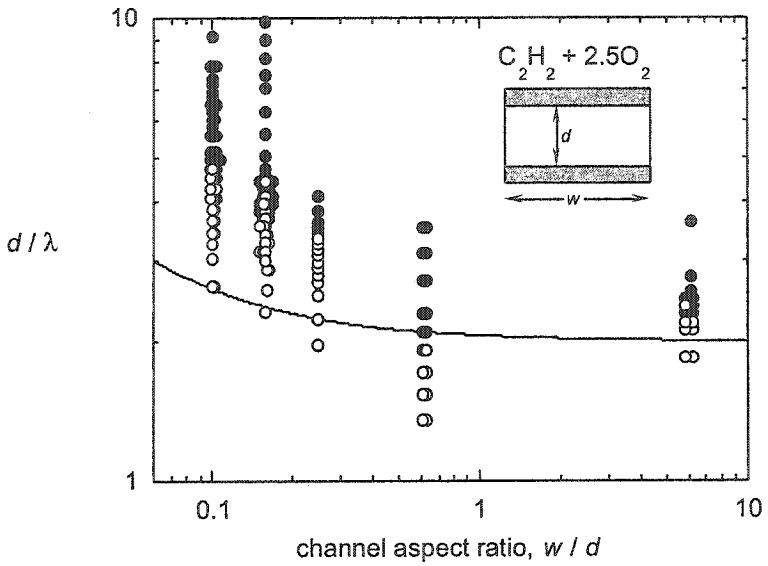

Fig. A1.2 Same as Fig. 3.7; line given by (A1.8)

Appendix 2 Determination of the detonation kinetic parameters

A2.1 Induction and reaction times

The induction and reaction times were obtained from the ZND structure of the detonations. The ZND reaction zone structure was obtained as outlined in Chapter 4. The induction time τ_i was defined as the time elapsed from the shock to the point where the fluid particle reaches its maximum rate of heat release, i.e., maximum exothermicity $\dot{\sigma}_{max}$. The characteristic time for the heat release was taken as the inverse of the maximum rate of heat release, i.e. $1/\dot{\sigma}_{max}$.

Examples of the ZND reaction structures and the corresponding induction and reaction times are shown in Figs. A2.1 - A2.4 for some of the mixtures investigated. The kinetic mechanism of Varatharajan & Williams (2001, 2002) was used for all mixtures except for the methane mixtures, where we used the mechanism given by Lutz et al. (1988).

A2.2 Effective activation energies

Assuming that the induction time has an Arrhenius form, i.e.,

$$\tau_i = A\rho^n \exp\left(\frac{Ea}{RT}\right) \qquad \text{A2.1}$$

the activation temperature Ea/R can be found from a linear regression of the form

$$\log \tau_i = \log(A\rho^n) + \frac{Ea}{R}\left(\frac{1}{T}\right) \qquad \text{A2.2}$$

if the dependence of induction time is known for variations of temperature at fixed density. The induction time was computed from constant volume simulations using a FORTRAN code (Shepherd, 1996). The initial density in the simulations was kept constant at the post shock Von-Neumann (VN) value and only the temperature was varied. The Von Neumann density and temperature at which (Ea/RT_{VN}) were estimated correspond to the VN condition of the detonations investigated in the experiments of Chapter 2. The initial thermodynamic states for the calculations are given in Table A2.1. The

dependence of induction time with varying temperature for the various gases investigated is shown in Fig. A2.5. The activation temperature (Ea / R) was determined by linear regressions in the log-normal plots around the VN point, bracketing the VN temperature by approximately 200K.

Table A2.1 Initial* and Von Neumann gas states and the corresponding effective activation energies

	P_o kPa	γ_{VN}	ρ_{VN} kg/m^3	T_{VN} K	Ea/R K	Ea/RT_{VN}	Ea/RT_o
$2H_2+O_2$	23.5	1.32	0.626	1689	8352	4.94	28
$2H_2+O_2+2Ar$	24.3	1.4	1.084	1888	7961	4.22	26.7
$2H_2+O_2+N_2$	35.5	1.32	1.259	1653	8607	5.21	28.9
$C_2H_2+2.5O_2+75\%Ar$	26.5	1.41	1.918	2257	11492	5.09	38.6
$C_3H_8+5O_2$	11.5	1.14	1.669	1816	17873	9.84	60
CH_4+2O_2	34.5	1.18	3.184	1853	20260	10.9	68
$C_2H_2+2.5O_2$	2.2	1.2	0.221	1961	10346	5.28	34.7

*T_o = 298 K for all

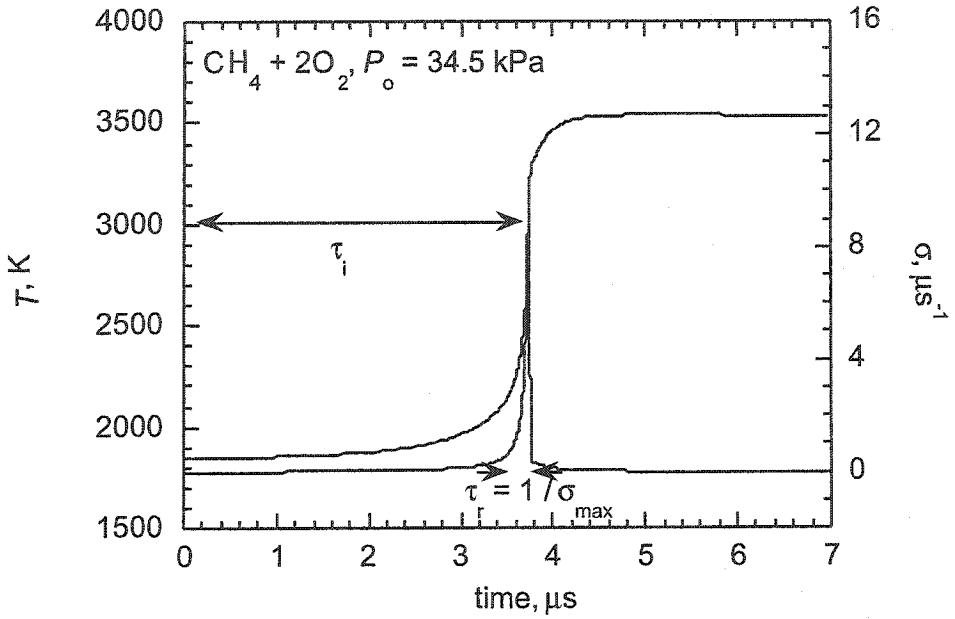

Fig. A2.1 ZND reaction zone structure in $CH_4 + 2O_2$, $P_o = 34.5$ kPa, $T_o = 298$ K

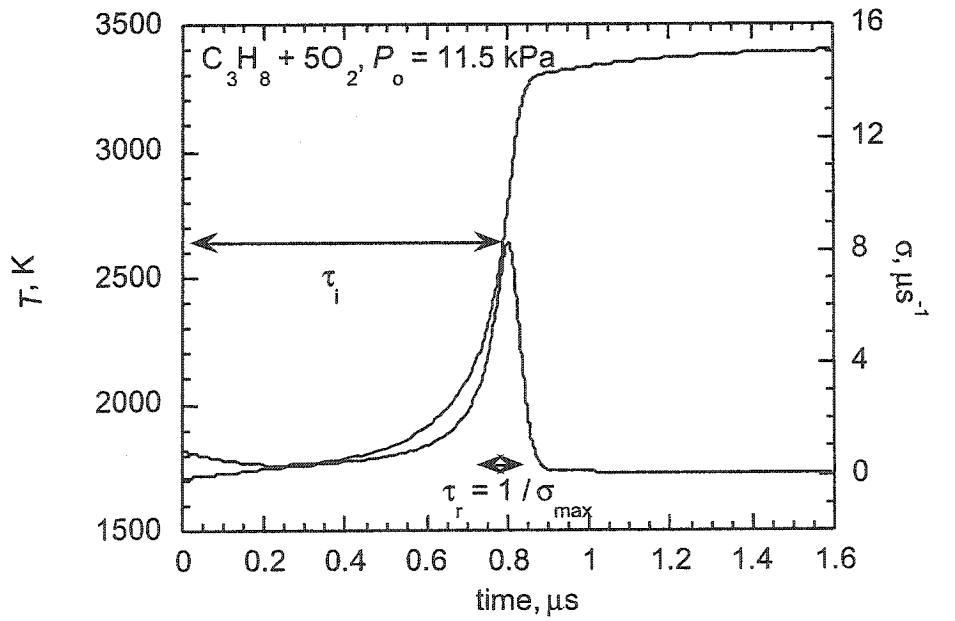

Fig. A2.2 ZND reaction zone structure in $C_3H_8 + 5O_2$, $P_o = 11.5$ kPa, $T_o = 298$ K

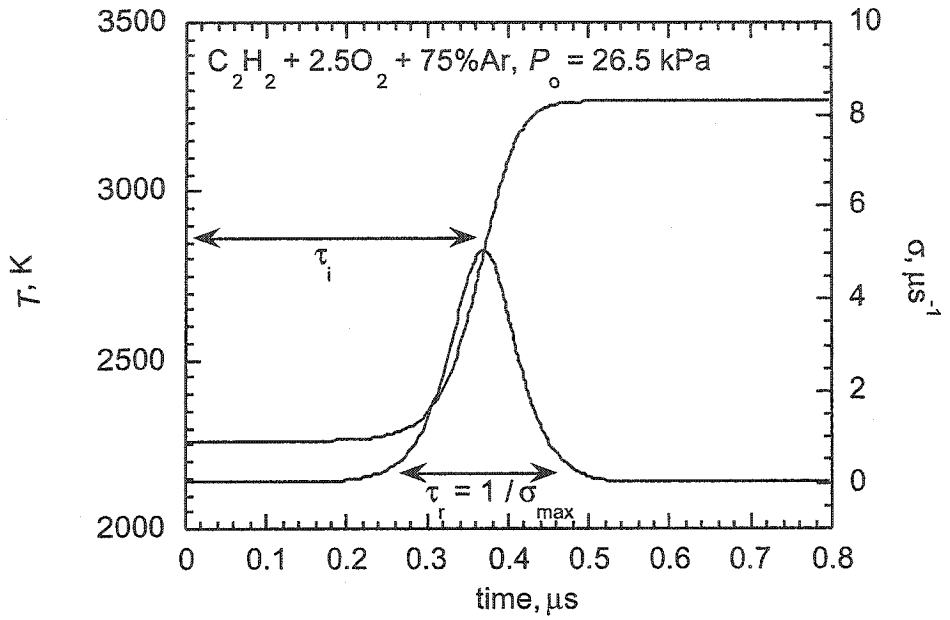

Fig. A2.3 ZND reaction zone structure in $C_2H_2 + 2.5O_2 + 75\%Ar$, $P_o = 26.5$ kPa, $T_o = 298$ K

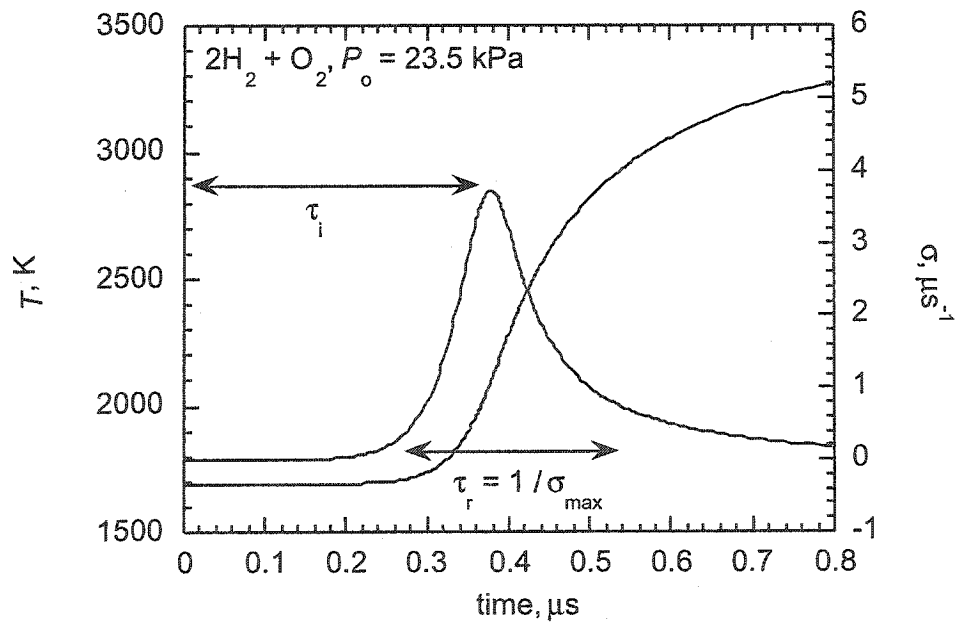

Fig. A2.4 ZND reaction zone structure in $2H_2 + O_2$, $P_o = 23.5$ kPa, $T_o = 298$ K

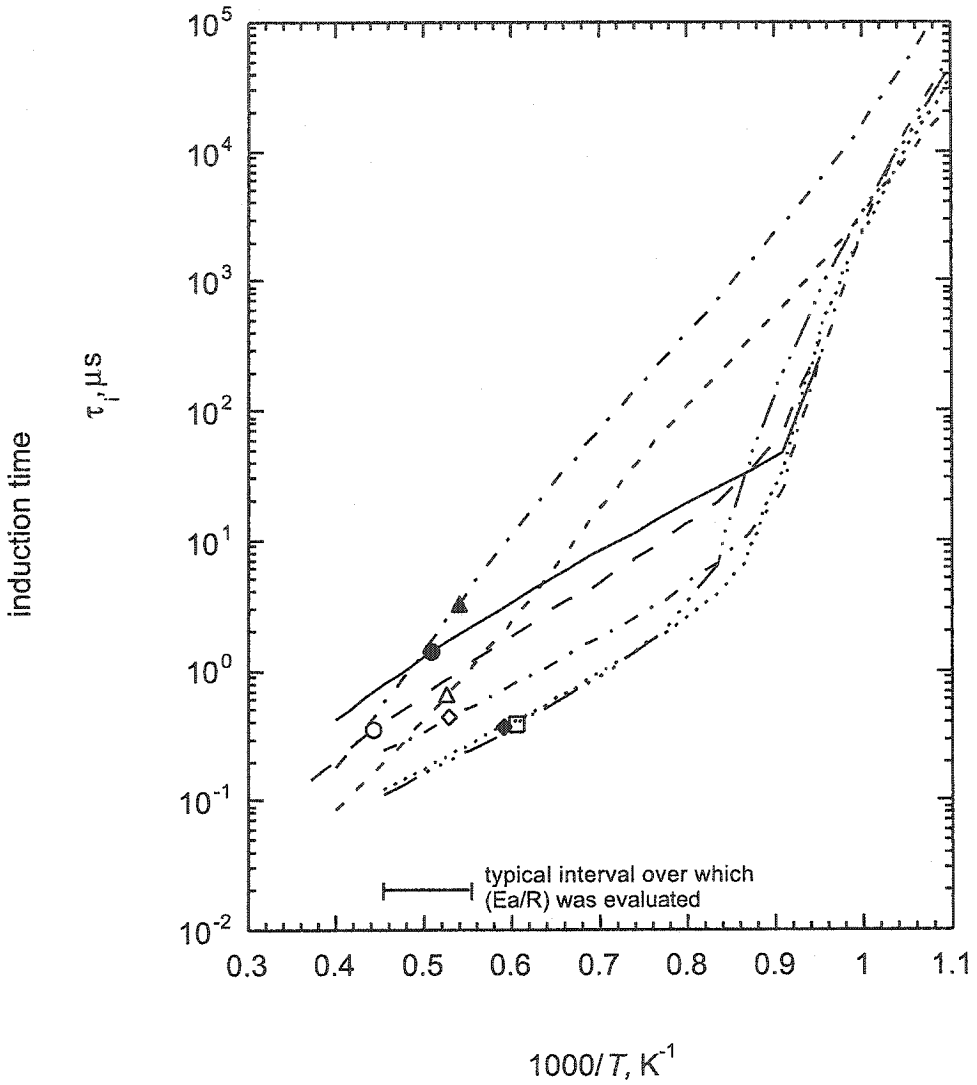

Fig. A2.5 Induction times estimated by constant density simulations for $2H_2 + O_2$ (◆), $2H_2 + O_2 + 2Ar$ (◇), $2H_2 + O_2 + N_2$ (□), $C_2H_2 + 2.5O_2$ (●), $C_2H_2 + 2.5O_2 + 75\%Ar$ (○), $C_3H_8 + 5O_2$ (△), and CH4 + 2O2 (▲); all calculations used the kinetic mechanism of Varatharajan & Williams (2001, 2002) except for CH_4 mixtures mechanism of Lutz et al., 1988); initial conditions correspond to constant density (ρ_{VN}) behind a shock moving at CJ velocity in a gas at initial state given in Table A2.1, T is varied; symbols represent the VN point